TUM

Technische Universität München
Ingenieurfakultät Bau Geo Umwelt

Lehrstuhl für Wasserbau und Wasserwirtschaft

Rolling stones
Modelling sediment in gravel bed rivers

Markus Andreas Reisenbüchler

Vollständiger Abdruck der von der Ingenieurfakultät Bau Geo Umwelt der Technischen Universität München zur Erlangung des akademischen Grades eines

Doktor-Ingenieurs

genehmigten Dissertation.

Vorsitzender:	Prof. Dr. Kurosch Thuro
Prüfer der Dissertation:	1. Prof. Dr.sc.tech. Peter Rutschmann
	2. Prof. Dr. Helmut Habersack
	3. Prof. Dr.-Ing. Dr.h.c. mult. Franz Nestmann

Die Dissertation wurde am 10.06.2020 bei der Technischen Universität München eingereicht und durch die Ingenieurfakultät Bau Geo Umwelt am 08.10.2020 angenommen.

Dies ist eine kumulative Dissertation basierend auf Veröffentlichungen in internationalen Fachzeitschriften.

Acknowledgement

First and foremost, I would like to thank my Mentor Dr.-Ing. Minh Duc Bui and Supervisor Prof. Dr. Peter Rutschmann for the offer and opportunity to do a dissertation. During the study, they supported me with guidance, mentoring, and encouragement. Special gratitude goes to Dr.-Ing. Daniel Skublics, whose expertise on the study site helped me a lot during this work. I am also grateful to my colleagues and staff members at the Chair of Hydraulic and Water Resources Engineering, for their help in my research but also for the common activities besides the work.

Finally, I'm deeply grateful to my family and my girlfriend Isabella for supporting me during this intensive and valuable time.

Markus Andreas Reisenbüchler

Email: markus.reisenbuechler@tum.de

Abstract

The precise description of our environment is highly important, as our civilisation is very sensitive to changes in natural systems. We are very much affected by meteorological phenomena and extreme events like thunderstorms, flash floods or, conversely, droughts and heat waves. Computational models are widely used to describe natural processes and make predictions about the future or estimate the impact of planned measures. However, some processes in nature are too complex to describe in terms of their physics or to measure adequately and are thus neglected or only represented in simplified models.

In this thesis, the focus is on riverine processes, in particular on sediment transport in gravel-bed rivers - an underestimated phenomenon. The heterogeneity in the composition of the riverbed, the different transport phenomena and the difficulty of measuring these in quality and quantity, make the precise description of sediment transport challenging. For instance, no comprehensive formula so far exists for sediment transport; there are only empirical parametrised transport equations, derived from small scale laboratory experiments. There is therefore a clear demand for improvements in this field, as sedimentation and erosion can lead to severe problems. For instance, it is estimated that sedimentation causes an annual loss in worldwide reservoirs of around 0.5-1%, which will finally result in a loss of around 1/4 of the world's dams in the next 25 to 50 years. Moreover, floodings and inundations are affected by sediment transport processes. For example deposition of sediments can cause riverbed levels to rise in critical sections and thus led to inundation and damages to households. On the other hand, riverbed erosion as a consequence of sediment deficit, can led to groundwater level reduction and thus have negative ecological consequences.

This thesis investigates approaches to overcoming limitations in existing modelling methodologies, caused by data scarcity and uncertainty, as well as computational limitations. A real world study area, the Saalach River in south Germany, is selected to study existing methodologies and develop new approaches and make improvements. The work is structured as follows: (I) Improvements to the sediment calculation methodology in the numerical solver *TELEMAC-SISYPHE*, (II) Impact assessment of sediment transport on inundations and flood risk, (III) Development of an approach to precisely quantify sediment loads at the location of interest, (IV) Investigation of the suitability and possibilities of numerical modelling to re-establish sediment continuity at a hydropower plant, and (V) Proposing alternative sediment modelling approaches. This chain of steps were developed at the Chair of Hydraulic and Water Resources Engineering at the Technical University of Munich to provide tools for authorities and consultants who have to deal with sediments.

By studying the 2013 flood event at the Saalach River, it becomes evident that rivers

are not only water. Long lasting and heavy rainfall caused an extreme discharge, which led to enormous inundations and damage. Due to sedimentation, the riverbed was at this time, unfortunately, much higher than a few years earlier. The analysis performed, using an improved numerical model, showed that in previous years this discharge would have passed through this region more or less harmlessly. This clearly demonstrates that we should consider the morphology in the assessment of flood risk and possible damage. Furthermore, the processes observed during such a flood event can only be explained and reproduced with an integrative hydro-morphological model as opposed to a hydrodynamic alone.

Moreover, it was shown that sediment loads at a specific location in the river can be estimated precisely and reliably by using a sediment budget approach. This information was used as boundary condition for numerical models. The proposed methodology efficiently allowed accurate calibration and validation of a numerical hydromorphological model over a period of multiple years. In addition, the approach also enabled the sediment loads to be evaluated directly at the domain of interest, thus reducing computational load as well as computation time.

The model was developed to offer a more sustainable sediment management strategy based on reservoir flushing at an existing run-of-river hydro power plant at the Saalach river (Germany). The simulation results showed that a more balanced sediment regime could be achieved than before, and yielded fresh insights into important factors for flushing, such as effective intensity and duration. Overall, the developed model and insights gained might serve as a reference case for other domains.

Finally, an alternative modelling approach was studied using artificial neural networks (ANN) to predict morphological developments for rivers. An ANN can in theory learn very complex patterns or correlations between different data sets. Combining this approach with data derived from conventional numerical modelling might provide innovative tools for sediment management. The results obtained show, for instance, that a well trained ANN can efficiently predict the total volume of sediment mobilised by reservoir flushing. In addition, a more complex structure deploying several ANNs shows promising results for the prediction of the temporal development of the riverbed along a certain river stretch. This last section concludes with possible avenues for future research on river sediment transport and management.

Kurzzusammenfassung

Die genaue Beschreibung unserer Umwelt ist für unsere Gesellschaft von großer Bedeutung, da wir sehr anfällig für Änderungen in diesem System sind. Wir spüren unmittelbar die Auswirkungen verschiedener meteorologischer Phänomene wie Gewitter und Sturzfluten, aber gleichzeitig auch Dürren und Hitzewellen. Weitverbreitet sind deswegen computergestützte Modelle, um die Natur und ihre Prozesse zu beschreiben sowie Vorhersagen zu geben oder die Auswirkungen von Maßnahmen zu bewerten. Jedoch gibt es auch Prozesse, die sich auf Grund ihrer Komplexität kaum beschreiben oder messen lassen. Diese Prozesse werden oftmals vernachlässigt oder nur sehr vereinfacht dargestellt.

In dieser Arbeit geht es um die Prozesse, die in Flüssen ablaufen, genauer gesagt um Sedimenttransport - ein unterschätztes Thema. Die Heterogenität in der Zusammensetzung der Gewässersohle, die verschiedenen Transportphänomene sowie die Schwierigkeit, diese zu messen, macht eine genaue mathematische Beschreibung zu einer Herausforderung. So existiert aktuell keine einheitliche Transportformel für Sediment, sondern nur empirische Beziehungen, abgeleitet aus kleinskaligen Laborversuchen. Es bedarf hier verschiedenster Verbesserungen, da Sedimentation und Erosion große Probleme verursachen können. So wird beispielsweise geschätzt, dass allein durch Sedimentation weltweit das Volumen von Reservoirs um 0.5-1% zurückgeht. Das bedeutet, dass in den nächsten 25 bis 50 Jahren rund ein Viertel aller aktueller Sperren verloren sind. Darüber hinaus werden auch Hochwasser und Überschwemmungen von Sedimenten beeinflusst. Beispielsweise kann Sedimentation in ungünstigen Stellen im Fluss zu verstärkten Ausuferungen führen, welche ein großes Schadenspotential haben. Andererseits kann eine starke Erosion der Gewässersohle als Konsequenz eines Sedimentdefizits zum Absinken der Grundwasserstände führen, was wiederum negative Folgen auf die Ökologie hat.

Entsprechend der aufgeführten Probleme, werden in dieser Dissertation Möglichkeiten studiert, um bestehende Grenzen und Limitierungen in der Modellierung zu überwinden. Diese Grenzen ergeben sich neben dem Mangel an Messdaten auch aus Limitierungen der Modellsoftware oder Hardware. In der Arbeit wird ein real existierenden Flussabschnitt als Pilotgebiet bearbeitet, um neue Ansätze zu entwickeln und zu testen. Dabei handelt es sich um die Saalach, ein voralpiner Fluss an der Deutsch-Österreichischen Grenze. Die folgende Arbeit gliedert sich wie folgt: (I) Überarbeitung des Sedimentmoduls des numerischen Gleichungslösers *TELEMAC-SISYPHE*, (II) Bewertung der Auswirkungen von Sedimenttransport auf Hochwasser, (III) Entwicklung eines Ansatzes zur präzisen und verlässlichen Definition von Sedimentfrachten im Untersuchungsgebiet, (IV) Untersuchung der Möglichkeiten mittels numerischer Modellierung, ein Sedimentgleichgewicht an einem Kraftwerk wieder zu etablieren, (V) Aufzeigen von alternativen Ansätzen zur

Sedimentmodellierung. Diese Reihe an Aufgaben wurden am Lehrstuhl für Wasserbau und Wasserwirtschaft der Technischen Universität München durchgeführt, um Werkzeuge für Behörden und Berater zu liefern, die sich mit Sedimentprozessen beschäftigen.

Dass Flüsse nicht nur aus Wasser bestehen, wird spätestens klar, wenn wir das Juni-Hochwasser 2013 an der Saalach betrachten. Andauernde und schwere Niederschläge führten zu einer extremen Abflussspitze, welche letztlich zu großflächigen Überschwemmungen und enormen Schäden führte. Infolge von Sedimenttransport war die Gewässersohle zu diesem Zeitpunkt deutlich höher als nur wenige Jahre zuvor. Die durchgeführte Untersuchung mit Hilfe des verbesserten numerischen Modells zeigte, dass damals das gleiche Hochwasser noch weitgehend schadlos vorbeigeflossen wäre. Dieses Beispiel führt eindrucksvoll auf, dass morphologische Prozesse bei der Bewertung von Hochwasser und Hochwasserrisiko berücksichtigt werden sollten. Darüber hinaus können die beobachteten Prozesse nur mit einem numerischen hydro-morphologischen Modell korrekt erklärt und dargestellt werden. Ein rein hydrodynamisches Modell reicht hierzu nicht aus.

Ferner wurde gezeigt, dass mittels einer Sedimentbilanz die Sedimentfrachten entlang des Flusses präzise und konsistent beschrieben werden können. Diese Information kann eingesetzt werden, um Randbedingungen für die numerische Modellierung zu bestimmen. Die Verknüpfung der Sedimentbilanz mit dem numerischen Modell gibt ein konsistentes Paket, mit dem ein Fluss über mehrere Jahre genau simuliert werden kann.

Das entwickelte und kalibrierte Modell wurde herangezogen, um ein nachhaltiges Sedimentmanagementkonzept an einem Laufwasserkraftwerk in der Saalach zu entwickeln. Das Konzept basiert hierbei auf Stauraumspülungen bei größeren Abflüssen. Die Ergebnisse zeigten, dass mit Änderungen in den Spülungen ein ausgeglicheneres Sedimentregime erzielt werden kann. Ebenso etabliert sich so ein niedrigeres Hochwasserrisiko, da die Gewässersohle stabiler und tiefer liegt. Das entwickelte Modellkonzept mit der verbesserten Software kann als Referenz für andere Studiengebiete dienen.

Im letzten Schritt dieser Arbeit wurde eine alternative Modellierungsmethode basierend auf künstlichen neuronalen Netzen (ANN). Ein gut trainiertes ANN kann in der Theorie komplexe Muster oder Beziehungen zwischen verschiedenen Daten erkennen. Eine Verknüpfung dieses Ansatzes mit den Daten aus der klassischen Numerik könnte innovative Werkzeuge für ein Sedimentmanagement liefern. Die erzielten Resultate zeigen beispielsweise, dass ein entsprechend konzipiertes ANN sehr effizient das Sedimentvolumen bei einer Stauraumspülung vorhersagen kann. Zusätzlich zeigt ein anderes ANN vielversprechende Ergebnisse bei der zeitlichen Vorhersage der Sohlentwicklung entlang eines Flussabschnittes. Letztlich gibt dieser Abschnitt der Arbeit einen Ausblick auf mögliche Richtungen und Aspekte bei der Sedimentforschung.

Preface

This thesis is based on the following conference and journal papers:

(I) Reisenbüchler, M.; Bui, M.D.; Rutschmann, P. Implementation of a new layer-subroutine for fractional sediment transport in Sisype. Proceedings of the XXIIIrd Telemac-Mascaret User Conference; Bourban, S., Ed.; HR Wallingford Ltd: Wallingford, England, 2016; pp. 215–220

(II) Reisenbüchler, M.; Bui, M.D.; Skublics, D.; Rutschmann, P. An integrated approach for investigating the correlation between floods and river morphology: A case study of the Saalach River, Germany. *Science of The Total Environment* **2019**, *647*, 814–826, doi:10.1016/j.scitotenv.2018.08.018

(III) Reisenbüchler, M.; Bui, M.D.; Skublics, D.; Rutschmann, P. Enhancement of a numerical model system for reliably predicting morphological development in the Saalach River. *International Journal of River Basin Management* **2019**, pp. 1–13, doi:10.1080/15715124.2019.1628034

(IV) Reisenbüchler, M.; Bui, M.D.; Skublics, D.; Rutschmann, P. Sediment Management at Run-of-River Reservoirs Using Numerical Modelling. *Water* **2020**, *12*, 249, doi:10.3390/w12010249

(V) Reisenbüchler, M.; Bui, M.D.; Rutschmann, P. Development of an ANN-based tool for sediment management at run-of-river reservoirs. 11th River, Coastal and Estuarine Morphodynamics Symposium RCEM 2019; Friedrich, H.; Bryan, K., Eds., 2019, p. 112

In the introduction chapter I defined the state of the art and research gaps. Based on these research gaps, I selected and justified the used methods. At the end, I concluded the overall contribution of the study. The introduction section also contains a summary of the above mentioned publications along with a declaration of consent of authors and their contributions.

Contents

List of Figures

List of Tables

Chapter 1

Introduction

1.1 Research background

Flow in rivers is commonly described in mathematical models by purely hydrodynamic approaches, thus neglecting sediment transport. The reasons for this are, for instance, the complexity of the morphological processes, scarcity of morphological data and computational limitations. However, sediment transport in rivers may greatly alter the shape and characteristics of the river course, and thus requires a different approach to river management. In the following, the importance of numerical sediment transport modelling and necessary developments are described in detail:

1.1.1 TELEMAC-SISYPHE

Fluvial processes can be numerically described by a set of mathematical equations derived from physical laws and empirical observations. These governing equations are solved iteratively on a time and space discretised domain. In the literature a broad range of different programs can be found, for instance *HYDRO_AS*, *MIKE*, *BASEMENT*, and *TELEMAC* (which is used in this thesis). The *TELEMAC* open-source modelling suite consists of several modules, in particular the flow solver *TELEMAC2D* and *TELEMAC3D* and the main morphological package *SISYPHE* (Version 6.3). The open-source character of the software makes it preferable for research as the source code is freely available and additional features can be integrated.

The hydrodynamic solver calculates the flow quantities, e.g. velocity, water depth, and turbulence. The three-dimensional solver *TELEMAC3D* is based on the Reynolds-Averaged-Navier-Stokes equations (RANS). The averaging of the original Navier-Stokes equations (NSE) by the Reynolds number smoothes the turbulent chaotic behavior of the fluid. This treatment simplifies the equations and thus makes computation faster compared to a direct numerical solution (DNS) of the NSE. The second available flow-module, *TELEMAC2D*, consists of another set of equations: the depth-averaged shallow-water-equations (SWEs). These equations simplify the NSEs by averaging them over the

vertical water depth. This assumption is valid in the case of rivers where the length (L) and width (W) is significantly greater than the depth (H) (L,W»H), and vertical velocities are negligible ($v_z \approx 0$) [7, 8]. Both flow modules are wel-established and frequently applied in research and project work [9, 10, 11, 12, 13, 14].

The morphological module *SISYPHE* can be coupled to one of the above-mentioned flow modules. The coupling is conducted using a quasi-steady-state approach assuming a constant flow field (i.e. velocity and water depth) during the morphological calculation, and mutatis mutandis, a constant morphology (i.e. riverbed and roughness) during the flow calculation. This assumption allows the equations of both modules to be solved independently and not simultaneously. In general, depending on the present flow and morphological conditions, *SISYPHE* calculates the transport rates of sediment and the concentration of particles in motion. This information determines the future riverbed elevation and composition resulting from sedimentation and erosion. So far, no unique equation exists to describe sediment transport in a comprehensive way. However, several researchers have obtained different semi-empirical relations between the flow and the morphology - which are applicable under specific conditions - from laboratory experiments and field observations (e.g. [15, 16, 17, 18]). *SISYPHE* thus includes several formulas and parameters to model different aspects of sediment transport processes such as slope effect or hiding-exposure [19, 8].

One outstanding feature of *TELEMAC* is that it has two simulation modes, namely scalar and parallel mode. Whereby the first uses one computational core to solve the equations on the domain, the second uses the parallel mode multiple cores. In theory, the speed-up in parallel mode is linear, meaning that the use of two cores decreases the computational time required by 50% compared to one core, and so on. Since *TELEMAC* shows good scalability and performance in the parallel mode up to dozens of cores, it can be used on high-performance-computational (HPC) systems [20, 21, 22]. For domains with a larger number of numerical elements and for long simulation times, this mode is unavoidable and necessary.

However, in *SISYPHE*, the updating of the riverbed is prone to errors for fractional sediment transport, i.e. if more than one-grain class is available in the river, and for long term simulations. This is a critical issue, which limits the suitability of the software for complex and real study cases.

1.1.2   Flood risk assessment

River floods happen when the discharge, and thus the corresponding water level, exceeds the embankments. In our densely populated world, many cities and settlements are lo-

cated close to rivers and, therefore, must be protected from such inundation. In Bavaria, Germany, the administration together with the municipalities are responsible for ensuring flood safety up to a design discharge, which corresponds to the statistical 100-year discharge [23, 24, 25, 26]. Flood protection measures such as dykes, levees or flood retention basins are constructed around the cities according to this design value. Such technical structures can be designed, optimised or evaluated using numerical methods. In recent years, two-dimensional, depth-averaged hydrodynamic models have been widely applied to predict the water level in rivers and the extension of floods [25, 26]. However, such purely hydrodynamic models represent only a static state of the topography and the riverbed, and cannot not take into account temporal and spatial changes. This limits their usefulness, as rivers are more than just water.

Morphology and sediments can have a great impact on the characteristics and development of a river, especially on the riverbed elevation. This impact becomes clear when comparing a historical river with its present state [27]. But rivers can also change over shorter periods. Especially in mountainous regions, huge amounts of coarse gravel, the bedload, are transported by the river, which can rapidly lift or lower the riverbed significantly. In addition to natural variability and changes, anthropogenic river training (i.e. straightening, channeling) and engineering structures in rivers (e.g dams, weirs and ramps) can radically unbalance the natural sediment regime. The consequences of this might be erosion and sedimentation in an unexpected and unwanted intensity. These morphological processes can have a great influence on flood risk and inundation intensities. An issue which the public are generally not aware of.

Developing tools that describe hydromorphological processes in more detail and more comprehensively, therefore, is an ongoing research aim. Various stakeholders are interested in applying such tools: municipal authorities, as they have to ensure the flood safety in a cost-efficient way; insurance companies, who benefit from such developments as it enables them to calculate risk more precisely; hydropower plant owners, who want to operate in a sustainable and efficient way.

1.1.3 Sediment management strategies

As highlighted above, sediment transport should be considered as part of a comprehensive flood risk assessment for river sections or systems. Despite this, the structure and composition of sediments in rivers have additional functions: they form and determine the riverbed and the morphology, they structure biological habitats, regulate groundwater infiltration and contribute to nutrient transport. The bed condition in respect of sediment processes can be separated into three categories: sedimentation, erosion and equilibrium:

One of the biggest reasons for unnatural sedimentation is the interruption of the river continuity and so the sediment flux caused by dams and barrages across the channel. The damming causes a deceleration of the flow and reduces shear stresses, which are the driving force for sediment transport. As a consequence, the material starts to deposit, on the ground, raising riverbed levels. If this process goes on, it leads finally to a reduction of the retention space of the reservoir and so limits the efficiency and purpose of the structure. Worldwide, sedimentation causes a loss of reservoir volume of around 0.5-1% per year, an amount which cannot be compensated by newly build dams. This includes storage dams but also run-of-river hydropower plants. Such unintended sedimentation has to be taken into account in the operation of the reservoir. Several management possibilities exists in theory, but their implementation is challenging and requires detailed knowledge of the site-specific characteristics [6].

Erosion, on the other hand, is a result of a sediment deficit, due, for instance, to excavation of sediment for industrial purposes or the retention of sediments in upstream dams and reservoirs, which are then missing downstream. Straightening of the river can also cause erosion, as the slope of the river has to be increased and the flow resistance decreases due to the uniformly straight shape. Both effects lead to higher velocities and thus a higher sediment transport potential. As a result, the river takes material from the bed, which can destabilise the river embankments or, finally, lead to lower groundwater levels in the surroundings with a negative impact on ecosystems. Figure 1.1 shows the influence of a dam on upstream and downstream sections of a river.
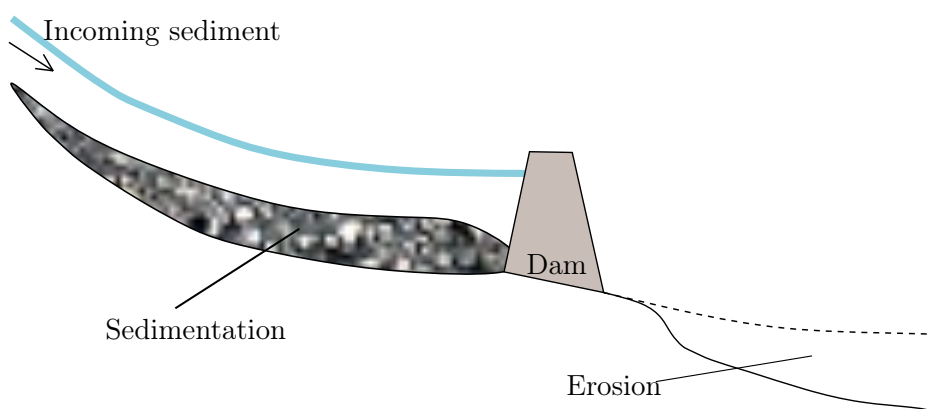

Figure 1.1: Sedimentation and erosion due to damming. Adapted from [6].

When erosion and sedimentation alternate and balance out over time, we can speak of an equilibrium condition. However, this balance might not be directly visible, since such morphological processes have a long response time of several years. The aim of man-

agement strategies is the establishment of a balanced system, which fits the needs and conditions of the system. This goal can be achieved by technical measures, river restoration, different operation modes of hydropower plants or integrative solutions, taking into account all catchment processes (e.g. sediment yield and land use). What all strategies have in common are the challenge that each hydrological year is unique and generally the morphological processes are difficult to describe on account of their complexity. In addition, the response time of a river system to some morphological measures can be quite long (>10 years), which requires modelling tools suitable for long periods.

Numerical models offer be a valuable and efficient option to develop such strategies, as they can be used to predict future developments and to test multiple scenarios flexibly. The challenge is here the lack of data for the models, which are needed for model generation, calibration, and validation. Furthermore, high uncertainty attaches to the evaluation of the quantity and quality of sediment load entering a particular river section. However, this information is necessary to obtain reliable boundary conditions. Moreover, computational resources limit the applicability of some numerical models for long-term predictions over several years. Research must address these points if the suitability of numerical modelling for sediment management is to be improved.

1.2   Study area

For this thesis, a real-world study area was selected to apply new developments under real conditions and obtain new insights on sediment transport and management. The selected area is located in southeastern Germany, close to the Austrian border.

Figure 1.2 provides an overview of the study region. Starting at the Kibling Dam at river kilometre x=20.6 km the Saalach river passes at x=8.0 km an unregulated weir, which stabilises the riverbed. Following its straight course, a step-pool ramp is passed, as well as a railway bridge, until the run-of-river hydropower plant Rott at x=2.4 km is reached. Finally, the river contributes to the bigger Salzach river. The Saalach is an important supplier of coarse sediment for the Salzach to stabilise the riverbed.

The Alpine Saalach river is, in the lower section, the natural border between Austria and Germany. This particularity has made the river historically important. Originally, the Saalach formed a meandering, braided river network, which did not provide a clear border between the two countries, as after each flood event new branches occurred and old disappeared. Therefore, in 1820, the river was straightened and a fixed straight channel excavated, now clearly demarcating each side of the border. One additional objective was to generate benefits for flood protection and gain land for agriculture. Moreover, several engineering structures (e.g. dams, weirs, ramps) were constructed along the river,
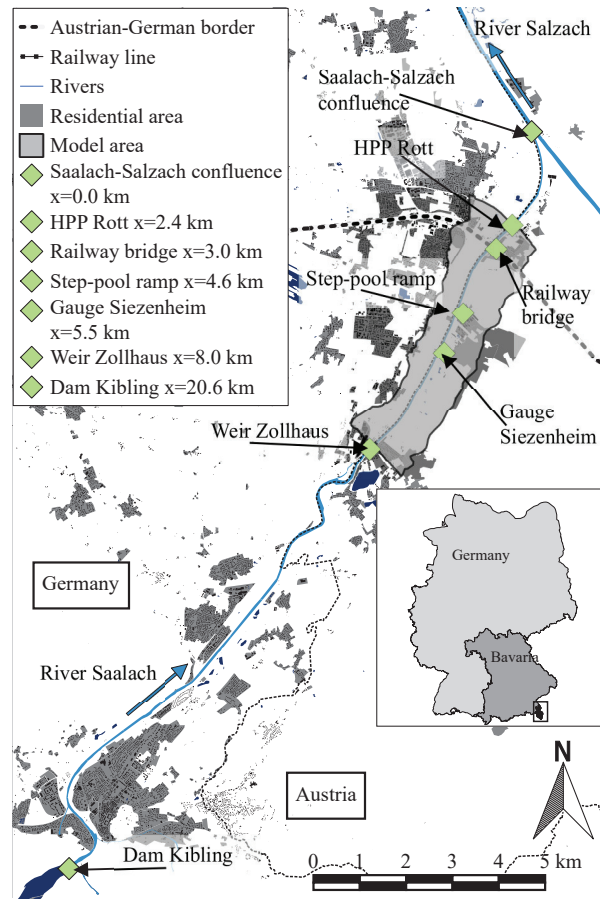
Figure 1.2: Overview of the study site (Adapted from [2]).

to produce energy, to regulate the water level or lower the ongoing riverbed deepening. The combination of all these engineering measures has led to critical riverbed deepening of 4.5 m in the last 80 years, measured 600 m upstream of the confluence to the Salzach (Figure 1.3).

Furthermore, in 2013, a flood event on the scale of the statistically one-hundred-year event HQ$_{100}$ occurred, and, despite the regulations, led to enormous inundations and damage in this region, especially in the city of Freilassing. That this was possible also surprised the responsible authorities. Figure 1.4 shows the official flood inundation for the region. In the area of Freilassing, where the Saalach meets the Salzach, it was predicted that a flood of the size of HQ$_{100}$ should have passed the region without harmlessly as no inundation is depicted. It is only in further downstream regions that inundation should occur (colored blue). The reasons why this was not the case are unknown and therefore addressed in this research.

This short overview illustrates that the river is greatly impacted by humanity and various serious problems exist. This makes the lower Saalach river an ideal study area for

Figure 1.3: Riverbed erosion of the Saalach 600 m upstream of the confluence with the Salzach.
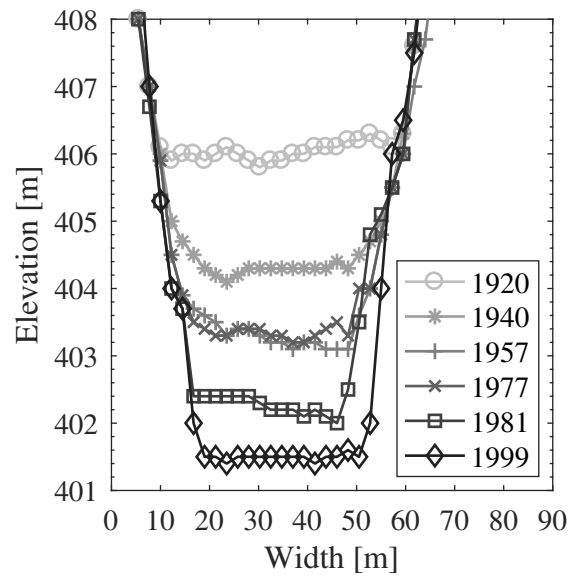
this research. The changes led to severe problems, which are described, investigated and solutions offered in the following chapters.
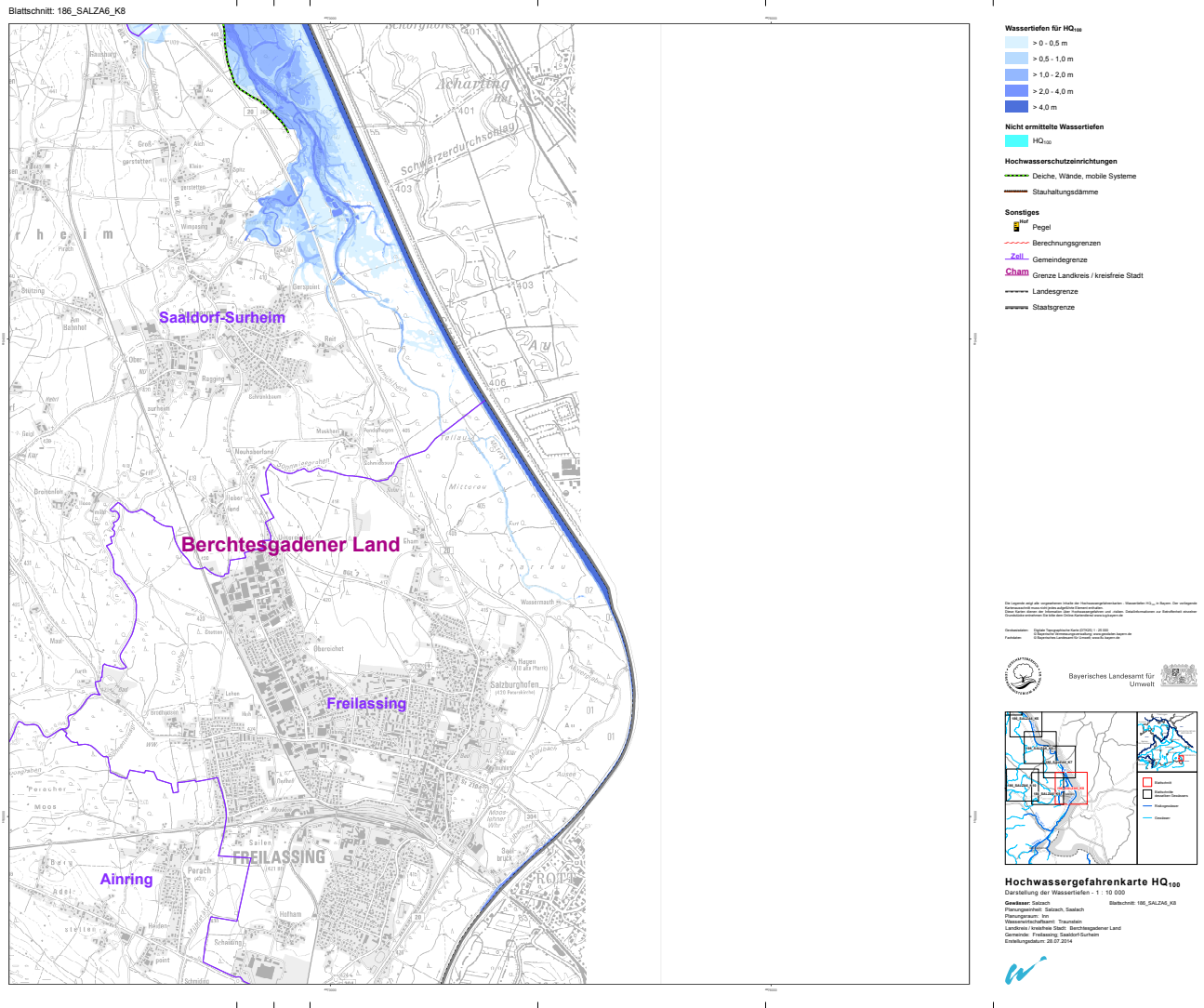
Figure 1.4: Inundation map of a HQ_{100} for the region of Freilassing.

1.3 Research objectives

Sediment modelling is not yet a state-of-the-art methodology for engineering companies and authorities. However, the demand and necessity are obviously there. The following five specific objectives are investigated in this dissertation:

- Improving a numerical hydromorphodynamic modelling suite, to be able to investigate real world river engineering topics

- Assessing the impact of morphological developments on flood events

- Developing a reliable and accurate method to determine morphological boundary conditions at a site of interest

- Investigating the potential of reservoir flushing as part of a sustainable sediment management strategy

- Assessing the applicability of data driven methods such as artificial neural networks (ANNs) in combination with conventional numerical modelling for sediment problems in the study area

1.4 Research methodology

The stated objectives and research gaps are addressed by the following consecutive steps:

(I) Improvement of *TELEMAC-SISYPHE*: The development of an integrative model for a real world study site requires specific capabilities in the numerical solver. These include high stability, good accuracy and the flexibility to adapt site-specific conditions. The *TELEMAC-SISPHYE* environment (v6.3) has the main requirements for hydromorphodynamic modelling, but is prone to errors for multi-grain or fractional sediment transport. Therefore, important parts of *SISYPHEs* source code are replaced or rewritten, and requisite new functions added. The functionality and accuracy of the developments is accomplished by comparing simulations with laboratory data.

(II) Comparative analysis between hydrodynamic and integrative hydro-morphodynamic model: To highlight the importance of an integrative hydro-morphological modelling approach, the 2013 flood event in the Saalach is investigated comparatively with a classical hydrodynamic approach.

(III) The concept of a sediment balance is a promising tool to evaluate the boundary
      conditions for a consecutive numerical hydromorphological model in regions with
      limited data. The concept is applied to the Saalach and finally used to calibrate
      and validate a numerical model over multiple years using water level and riverbed
      readings.

(IV) An existing hydropower plant in the Saalach is a bottleneck for the sediment con-
      tinuity in the river. A numerical model should help to develop a more sustainable
      solution for the operation of the hydropower plant and indicate the important pa-
      rameters for effective sediment flushing.

 (V) The suitability and applicability of ANNs for sediment related issues in the study
      area is addressed by implementing two different approaches: First, a time indepen-
      dent ANN is developed to predict sediment processes, and second a time dependent
      one.

1.5   Structure of dissertation and authors contribution

The dissertation is based on peer-reviewed published articles on sediment modelling in
gravel-bed rivers using numerical and data driven methods, conducted at the Chair of
Hydraulic and Water Resources Engineering, at the Technical University of Munich. A
brief summary of each publication along with the author contributions is given below.

1.5.1   Implementation of a new Layer-Subroutine for fractional sediment transport in SISYPHE

In the following the main findings of the publication "Implementation of a new Layer-
Subroutine for fractional sediment transport in SISYPHE" are briefly summarised. The
article was published in the proceedings of the $23^{th}\,Telemac-Mascaret\,User\,Conference$
in 2016 [1]:

Main results: The Layer subroutine in *SISYPHE* is responsible for updating the
riverbed at every time step of the numerical solver and is therefore one of the most
important subroutines for sediment transport modelling. However, the application of the
original code to a real case domain was not possible due to inconsistencies in the code
and numerical errors, which ultimately led to an abort of the simulation.

   Therefore, the subroutine and dependent codes were completely rewritten to increase
stability, accuracy and to make the code applicable to real locations. In addition, a
clear separation between erodible and non-erodible parts of the river was implemented,

which made the post- and pre-processing more flexible. Also, the two empirical bedload transport formulas after Hunziker [17] and Wu [15] were newly implemented.

A comparative analysis based on the well-known laboratory experiment according to Günter [28] shows the effectiveness and the benefits of the developments compared to the original code. Finally, the modelling suite can now be used in real case applications.

Authors' contribution: The work was carried out by Markus Reisenbüchler under the guidance of Minh Duc Bui and Peter Rutschmann. The fundamental concept of the major subroutine was developed by Minh Duc Bui, further modifications and and the integration of the new codes in the whole modelling suite by Markus Reisenbüchler. Markus Reisenbüchler wrote the manuscript with the support of Minh Duc Bui.

1.5.2   An integrated approach for investigating the correlation between floods and river morphology: A case study of the Saalach River, Germany

The peer-reviewed journal publication "An integrated approach for investigating the correlation between floods and river morphology: A case study of the Saalach River, Germany" includes the following main findings. The work was published in the international journal *Science of the Total Environment* in 2019 [2]

Main results: The 2013 flood event in the Saalach River in Germany caused the most severe flooding in this region for decades. The flow discharge slightly exceeded the statistical 100-year return period design value, a situation which had not been previously observed. Moreover, the magnitude of the inundation in this region was not expected, as man-made structures along the river should have ensured flood safeness up to the design discharge.

We found out that sediment transport greatly changes the elevation of the riverbed in this region, and it was for this reason that the designed protection systems did not work. A comparative analysis of the 2013 flood event using numerical modelling tools shows that for a lower riverbed than in 2013, e.g. the riverbed in 2002, a flood of this size would have passed the region almost harmlessly. Furthermore, using an integrative hydromorphological model to study this event in more detail leads to more accurate and realistic results than a conventional hydrodynamic model.

The developed model was accurately able to reproduce measured data as well qualitatively observed processes such as sedimentation at a step-pool ramp and flushing of sediments in a reservoir.

Authors' contribution: Peter Rutschmann initiated this research. The model setup was performed by Markus Reisenbüchler while discussing approaches with Daniel Skublics and Minh Duc Bui. Markus Reisenbüchler conducted the simulations and the preprocessing. The contact to the regional authorities was supported by Daniel Skublics. The manuscript was prepared by Markus Reisenbüchler supported by Minh Duc Bui and Daniel Skublics.

1.5.3   Enhancement of a numerical model system for reliably predicting morphological development in the Saalach River

The peer-reviewed paper "Enhancement of a numerical model system for reliably predicting morphological development in the Saalach River" was published in the *International Journal of River Basin Management* in 2019 [3].

Main results: One of the biggest challenges in modelling of sediments in rivers is the definition of correct boundary conditions, especially close to the region of interest. Without this information, the applicability of a numerical model is very limited and obtained results generally doubtful.

To overcome this issue, a quantitative approach, namely sediment balances or budgets, is combined with a qualitative method, a numerical hydromorphological model. This combination proposes a consistent and accurate modelling concept for a region with sparse morphological data. First, the sediment balance for a certain stretch of the river delivers the amount of transported sediments over a specific time. This information serves as input or boundary condition for a consecutive, numerical model located downstream. At the Saalach river, the sediment balance and the material load over eight years close to the model domain was accurately assessed. Using this input, the numerical model was accurately able to reproduce observed water levels and riverbed evolution over a period of eight years. This allowed the model to a make reliable prediction of future riverbed development and provide insights for more sustainable management.

The proposed concept might serve as a reference for other studies where data from sediment transport is also rare.

Authors' contribution: Markus Reisenbüchler had the idea of combining both approaches. Peter Rutschmann and Minh Duc Bui supported this work at all stages. Daniel Skublics provided the necessary data and expertise on the study area. Markus Reisenbüchler and Minh Duc Bui performed the volumetrical analysis. The numerical simulation were conducted by Markus Reisenbüchler. The results were interpreted together. The manuscript was prepared by Minh Duc Bui and Markus Reisenbüchler.

1.5.4   Sediment management at run-of-river reservoirs using numerical modelling

The peer-reviewed paper "Sediment management at run-of-river reservoirs using numerical modelling" was published in the MDPI-Journal *Water* in 2020 [4].

Main results: At run-of-river hydropower plants the river is dammed up and an artificial reservoir is created. The deceleration of the flow led to the accumulation of sediment in the reservoir and thus higher bed levels. This became critical during floods as higher water levels result. Efficient management strategies are therefore crucial for hydropower plant owners and responsible authorities. Drawdown flushing in particular seems a promising solution it uses the power of the river and no expensive excavation or construction measures are necessary.

At the Rott hydropower plant on the Saalach river, several operational schemes for different flow conditions were investigated using a well-calibrated numerical model to arrive at an efficient and effective sediment flushing approach. The simulation results indicated that there must be a sufficiently high discharge as otherwise the forces on the riverbed are too low. Moreover, the flushing time drastically influences the amount of sediment mobilised. An early opening before a flood event and a longer opening afterwards generates lower riverbed levels. Only then does the material from the upstream section have enough time to be transported through the whole reservoir.

Applying the results to a period of eight years led to clearly lower bed levels in total, higher sediment outputs and requires only 0.5% more time. In addition, benefits for flood protection were generated as well.

Authors' contribution: Markus Reisenbüchler together with Minh Duc Bui and Daniel Skublics selected the cases. The simulations were conducted and analysed by Markus Reisenbüchler. Peter Rutschmann coordinated the collaboration with the hydropower plant owner. The manuscript was written by Markus Reisenbüchler with support from the co-authors.

1.5.5   Development of an ANN-based tool for sediment management at run-of-river reservoirs

The first aspects of the work with artificial neural networks and sediment modelling were presented at the 11th Conference on River, Coastal, and Estuary Morphodynamics (RCEM) entitled "Development of an ANN-based tool for sediment management at run-of-river reservoirs" in 2019 [5]. This work was continued after the conference to address the topic in a comprehensive way.

Main results: Conventional numerical models can precisely represent sediment transport and morphological processes. However, their applicability is limited due to computational requirements and runtime. Other modelling concepts, such as artificial neural networks (ANNs) seems to offer a promising alternative. In an initial phase, the combination of numerical models, or rather the data derived from these models and ANNs were studied.

The results obtained indicate that an ANN can accurately represent the total amount of sediment flushed only based on discrete input data such as peak discharge or flushing intensity. Furthermore, a more complex and nested ANN structure shows promising results in the prediction of water level, discharge and riverbed development along a river reach.

Authors' contribution: Markus Reisenbüchler together with Minh Duc Bui designed the methodology of the study. Peter Rutschmann guided the work. The extended abstract was written by Markus Reisenbüchler and Minh Duc Bui. The oral presentation at the conference was prepared and delivered by Markus Reisenbüchler.

Chapter 2

Implementation of a new Layer-Subroutine for fractional sediment transport in SISYPHE

Implementation of a new Layer-Subroutine for fractional sediment transport in SISYPHE

Markus Reisenbüchler

Chair of Hydraulic Engineering and
Water Resources Management
Technical University of Munich
Arcisstr. 21, 80333 Munich,
Germany
markus.reisenbuechler@tum.de

Minh Duc Bui

Chair of Hydraulic Engineering and
Water Resources Management
Technical University of Munich
Arcisstr. 21, 80333 Munich,
Germany
bui@tum.de

Peter Rutschmann

Chair of Hydraulic Engineering and
Water Resources Management
Technical University of Munich
Arcisstr. 21, 80333 Munich,
Germany
peter.rutschmann@tum.de

Abstract—**One of the most critical issues in the modelling of graded sediment transport is the vertical discretization of the bed into different layers and their interaction, particularly between the active layer and active stratum. By applying the TELEMAC - SISYPHE system to study the influence of an open stone ramp on flood events of a river stretch in Germany we had often faced challenges related to unphysical simulation and numerical instability. To improve the sediment transport module SISYPHE concerning this matter, some parts of the FAST computer code (developed by KIT and TUM) are adapted into the TELEMAC environment. The present paper shows the fundamentals of a new layer subroutine and modifications required for the SISYPHE environment. Special treatments for nonerodible grid points are also presented. The calculated results of the developed model are compared with laboratory measurements conducted by Günter (1971) to analyse the behaviour of new implementation.**

I. INTRODUCTION

Modelling of graded sediment transport is quite a challenging task. The mixing of different soil layers with different sediment classes below the surface is not trivial. The module SISYPHE, part of the TELEMAC-MASCARET modelling environment, includes an algorithm for this task - the *layer.f*-subroutine. Applying this code to a fractionized sediment model some instabilities and errors are observed. Therefore, at the Chair of Hydraulic Research and Water Resources Management, Technical University of Munich (TUM) is a new version for SISYPHE implemented. The main idea is to adapt the *layer.f* and related subroutines based on the FAST computer code, which has been developed at the Institute for Hydromechanics, University of Karlsruhe, Germany (KIT) and TUM. As usual for graded sediment transport models a so called size-fraction method is used, in which the bed is divided into different layers and size-fractions, each characterised by a certain diameter and volumetric percentage of occurrence in the river bed. The effect of fractional sediment transport leads to an exchange of grains between the layers, and so a grain sorting process can be approached. A special treatment of nonerodible parts within a calculation domain comes up during the code development. Nonerodible regions, like concrete walls, bridge piers or large stone settings are typical structures in river engineering cases. In the present paper the structure for vertical layer discretization, fractional grain exchange within layers and nonerodible treatment is presented. Almost all variables in the new version remain the same as ones used before in the SISYPHE source code. The new approach is validated by modelling two of the well documented laboratory experiments performed in 1971 by Günter at the Laboratory of Hydraulics, Hydrology and Glaciology, Eidgenössischen Technischen Hochschule (ETH) Zürich, Switzerland [2]. Finally, brief remarks of the model application for a real case study are also given.

II. SISYPHE

A. Background and theoretical aspects

The existing and the new codes are both based on the so-called size-fraction method, where bed material is divided into a certain number of grain classes, which are different in size and percentage of occurrence. Furthermore, the bed is discretised in vertical direction into several layers. The first one is the active layer, which is directly exposed to the flow. Below this one are several subsurface layers, which are only in exchange with the surrounding layers. Due to evolution of the river bed, the thickness of the layers changes as well as the available percentages of each grain-class in each layer [4].

The bed-level change due to a fraction i is calculated from a mass-balance (1):

$$(1\text{-}p)\frac{\partial Z_{b,i}}{\partial t} + \nabla \overrightarrow{Q_{b,i}} = 0 \qquad (1)$$

using p = porosity of the bed material; and $\overrightarrow{Q_{b,i}}$ = fractional bed load flux, determined by an empirical transport function. The total bed deformation is then determined in the following equation:

$$\frac{\partial Z_b}{\partial t} = \sum_{i=1}^{NSICLA} \frac{\partial Z_{b,i}}{\partial t} \qquad (2)$$

using NSICLA = number of all size classes [1].

B. River bed representation in the numerical model

In the TELEMAC-MASCARET modelling environment the calculation domain is represented by a grid consisting of nodes connected to unstructured triangular elements. To

perform a simulation it is necessary to provide initial conditions all over the domain for each node. For the morphologic simulation information about the bottom (e.g. the river bed level ZF and the rigid bed elevation ZR, with ZF ≥ ZR) is necessary. Furthermore, the initial composition of the river bed has to be specified by the number of vertical soil layers NOMBLAY, the number of grain size classes NSICLA, the availability of each class i within the layer k $AVAIL_{k,i}$, and the thickness of each layer ES_k [4].

III. NEW IMPLEMENTATION

By applying the SISYPHE modelling environment from version v6p3 to a large, complex real river application in Germany some errors and numerical problems arouse. A common error message after several time steps was "Error in layer" and the simulation stopped. Using the newer release version v7p0 it was not even possible to start the simulations. From the User-Forum of TELEMAC it seems that many users face these problems. In order to solve this issue, the layer concept from FAST was adapted and integrated into SISYPHE. In the following parts, another treatment of the interaction of the layers to each other and of a nonerodible part is presented. Furthermore, the existing bedload formula after Hunziker [3] is modified and the transport function after Wu [5] is implemented in *qsform.f* subroutine. The new code was initially developed for the version v6p3r2 of the TELEMAC-SISYPHE system, but it is also integrated in the newer releases.

C. Treatment of nonerodible nodes

Modelling nonerodible parts in a calculation domain is a quite common task in river engineering problems. The river bed is commonly very thick until bedrock is reached, however, in some locations (e.g. stone ramps, concrete walls at embankment structures or at weirs, etc.) the river bed is nonmovable. In numerical models, a node is classified as nonerodible when the thickness of its layers is zero $ES_k = 0$. However, it should be noted, that during the simulation period deposition can occur at these places and the deposited materials can be eroded depending on the local hydromorphological conditions. This process should be considered in the numerical model. Furthermore, the condition

$$\sum_{i=1}^{NSICLA} AVAIL_{k,i} = 1 \qquad (3)$$

has to be fulfilled in any case, to avoid mass inconsistencies and division by zero.

The new developed code includes an additional size class in addition to the actual available ones to represent nonerodible structures. So that a high stability, consistency and flexibility of the model could be achieved. This additional size class is independent per se from the defined bed grain sizes, as the transport rate of this additional class is defined to be zero and it is excluded from most of the internal calculations. This additional grain class occurs only at nonerodible layers. Following equations can be formulated for any layer k:

$$\text{if } ES_k = 0 \text{ then } \begin{cases} AVAIL_{k,NSICLA} = 1 \\ \sum_{i=1}^{NSICLA-1} AVAIL_{k,i} = 0 \end{cases} \qquad (4)$$

Equation (4) states that in case of a layer with zero thickness, its material contains up to 100 % of the additional grain class. Vice versa in case of erodible layers the additional grain class does not occur. This is formulated in (5), which claims that in this case the sum of residual grain classes must be 100 %.

$$\text{if } ES_k > 0 \text{ then } \begin{cases} AVAIL_{k,NSICLA} = 0 \\ \sum_{i=1}^{NSICLA-1} AVAIL_{k,i} = 1 \end{cases} \qquad (5)$$

From physical point of view this additional grain class can be compared to a large boulder which cannot be moved by the flow, which is quite close to reality. The implementation of this treatment requires modification in some relevant subroutines showed in the following list:

- *bedload_formula.f*
- *bedload_hunz_meyer.f*
- *bedload_main.f*
- *init_avai.f*
- *init_compo.f*
- *init_sediment.f*
- *init_transport.f*
- *layer.f*
- *mean_grain_size.f*
- *qsform.f*
- *tob_sisyphe.f*

In fact, the subroutine *noerod.f* to define the rigid bed is not needed anymore, as this function is now fully integrated into *init_compo.f*. In case of using the bed roughness predictor, suitable values for Nikuradse grain roughness k_s must be specified, since SISYHPEs bed roughness predictor options might not work proper on nonerodible nodes.

D. River bed decomposition

In the SISYPHE system, the river bed is decomposed into vertical layers, initially in the *init-compo.f* and *init_avai.f* subroutines and during the simulation in the *layer.f* subroutine. It is important to note that the initially defined number of layers at each node NOMBLAY remains the same during the calculation. Furthermore, for each layer a maximum possible thickness has to be defined. In case of the first layer, the active layer, this is named ELAY0, which can be either constant or depending on the diameter of the material in the active layer. The second layer, the active stratum thickness is named ESTRAT0 and must be also defined. The last layer has no thickness limit. Otherwise, it could happen that in case of high deposition the defined number of layers are not capable to represent the total sediment thickness. Vice versa it is not possible that a layer can get a negative value. It is determined as follows:

$$ZF - ZR = \sum_{k=1}^{NOMBLAY} ES_k \qquad (6)$$

The river bed elevation ZF is determined in a geometry file, which includes the information BOTTOM. The rigid bed level can be defined either constant or varying for each node depending on the river structures. Here an algorithm is implemented to read the information ZR from the same file. This function works the same as for BOTTOM or BOTTOM FRICTION and is therefore not explained here further.

The new layer treatment considers the following three different options, depending on the defined number of layers:

- One layer case

- Two layer case

- Multilayer case

In case of only one layer (NOMBLAY = 1) the total available thickness is equal to the thickness of the active layer after:

$$ES_{NOMBLAY} = ZF - ZR \qquad (7)$$

A two layer case (NOMBLAY = 2) includes an active layer with a maximum defined thickness and one residual layer below, as shown in (8).

$$ES_1 = \min(ELAY0; ZF - ZR) \qquad (8)$$

$$ES_{NOMBLAY} = ZF - ZR - ES_1$$

The following lines describe the code sequence for decomposition of a multilayer case (NOMBLAY ≥ 3):

$$ES_1 = \min(ELAY0; ZF - ZR) \qquad (9)$$

$$ES_2 = \min(ESTRAT0; ZF - ZR - ES_1)$$

$$....$$

$$ES_k = \min\left(ESTRAT0; ZF - ZR - \sum_{k=1}^{k-1} ES_k\right)$$

$$ES_{NOMBLAY} = ZF - ZR - \sum_{k=1}^{NOMBLAY-1} ES_k$$

After that, the available percentages of each class i in each layer k has to be defined ($AVAIL_{k,i}$). This can be done explicitly for each layer in *init_compo.f*. Via mass balance the volumetric amount of sediment VOL in the domain is calculated using (10).

$$VOL = \sum_{k=1}^{NOMBLAY} ES_k * \sum_{i=1}^{NSICLA} AVAIL_{k,i} \qquad (10)$$

In fig. 1 the discretization of the river bed surface and the nonerodible level is schematized for an exemplary case with maximum five layers at three nodes. Node one is initially nonerodible and so the bottom surface is equal to the nonerodible level (ZF=ZR) and all layer thicknesses are zero. At node two the nonerodible level is lower than the surface and the difference is distributed to into layers, starting from the top. Layer one to four attains their maximum defined thickness and the last one reaches to the rigid bed. The third nodes rigid bed is at a medium height and only four layers are necessary to distribute the river bed. The thickness of layer 5 is zero.
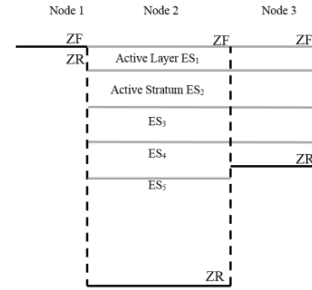

Figure 1.   Scheme of vertical river bed discretization at three different nodes.

E. Vertical layer interaction

Based on the initial discretised bed, the model calculates the interaction of layers to each other and to the flow. The key concept is the existence of an active layer, where the flow picks up the transportable sediment and receives the grains that the flow is unable to transport [1].

For erosion of the river bed the temporal change of the volumetric percentage of a fraction i in the active layer is calculated considering the taken material from the flow and the available material in the stratum below. This is done via a mass balance, given in (11).

$$\frac{\partial AVAIL_{1,i}}{\partial t} * ES_1 = \frac{\partial Z_{b,i}}{\partial t} - \frac{\partial Z_b}{\partial t} * AVAIL_{2,i} \qquad (11)$$

using $\frac{\partial AVAIL_{1,i}}{\partial t}$ = change of fraction i in the active layer, ES_1 = active layer thickness; $\frac{\partial Z_{b,i}}{\partial t}$ = bed level change of fraction i; $\frac{\partial Z_b}{\partial t}$ = total bed level change; $AVAIL_{2,i}$ = available percentage of fraction i in the active stratum layer. The active stratum is capable of an exchange with the stratum below, balanced in (12). If the layer below is nonerodible or the maximum number of layer is reached, no interaction will take place.

$$\frac{\partial AVAIL_{k,i}}{\partial t} * ES_k = \frac{\partial Z_b}{\partial t} * (AVAIL_{k,i} - AVAIL_{\min(NOMBLAY,k+1),i}) \quad (12)$$

For deposition case, the material enters the top element, so no relation with lower layers has to be considered here, see (13).

$$\frac{\partial AVAIL_{1,i}}{\partial t} * ES_1 = \frac{\partial Z_{b,i}}{\partial t} - \frac{\partial Z_b}{\partial t} * AVAIL_{1,i} \qquad (13)$$

Due to the deposition the active stratum gets some upward directed movement and material is in exchange with the layer above, the same for other substrate layers:

$$\frac{\partial AVAIL_{k,i}}{\partial t} * ES_k = \frac{\partial Z_b}{\partial t} * (AVAIL_{k-1,i} - AVAIL_{k,i}) \qquad (14)$$

After updating the available percentages of each fraction in each layer, the thickness of each layer is new distributed according to the procedure shown in part *D* (see (7) – (9)). Finally via a counter check mass balance is ensured and the total amount of sediment within this time step is reached.

F. Empirical transport functions

The transport function after Hunziker has been developed in 1995 using the data conducted by Günter. This equation is already implemented in SISYPHE. However, the hiding function has to be adapted for the additional grain class treatment and the code is rewritten to solve the equations within one loop over all grid nodes. The basic of this transport function is the concept of equal incipient motion for all sediments. Sediment transport starts only if the dimensionless shear stress of the flow is higher than the dimensionless threshold. The determining parameters are here the critical shields parameter θ_c and a relation between the mean grain diameter of the surface layer d_m and subsurface layer d_{mo}. The critical shear stress is then modified according to the following equation.

$$\theta_{cm} = \theta_c * \left(\frac{d_{mo}}{d_m} \right)^{0.33} \qquad (15)$$

According to the Günter experiments a hiding/exposure function is evaluated and parametrized in order to describe which sediments are more or less exposed to the flow. The sediment discharge after Hunziker is given in (16).

$$Q_{b,i} = \sqrt{(s-1)*g*d_m^3} * AVAIL_{1,i} * 5 * (\varphi_i(\mu*\theta_{dm} - \theta_{cm}))^{3/2} \qquad (16)$$

using s = relative density, g = gravity, d_m = mean diameter of the surface layer, φ_i = hiding factor, μ = parameter for skin friction correction, θ_{dm} = dimensionless shear stress parameter depending on the mean diameter and flow condition, θ_{cm} = modified critical shields parameter considering mean diameters of surface and subsurface layers [4].

The empirical transport function after Wu assumes that the probability of a grain to be exposed to the flow is depending on the diameter of the grain and the surrounding grains as well as the availability. Including a correlation parameter m = 0.6, which can be used in the calibration, the hiding and exposure function is formulated in (17) with

$$\theta_{cm} = \theta_c * \left(\frac{p_{e,i}}{p_{h,i}} \right)^m \qquad (17)$$

using the critical shields parameter θ_c and the probability of exposure $p_{e,i}$ and hiding $p_{h,i}$ of a grain i at the surface layer. The transported bedload discharge is given as

$$Q_{b,i} = \sqrt{(s-1)*g*d_i^3} * AVAIL_{1,i} * 0.0053 * \left(\mu*\theta_{d_i}/\theta_{cm} - 1 \right)^{2.2} \qquad (18)$$

using θ_{d_i} = dimensionless shear stress parameter depending on the diameter of each grain and flow condition, θ_{cm} = modified critical shields parameter including the hiding factor. For more details and full description of the formulas after Wu see [3].

IV.   CALCULATION RESULTS

G. Günter experiment – grain sorting

The new developed subroutines are validated by modelling the laboratory experiments conducted by Günter in 1971 at the ETH Zürich. The experiments were performed in a 40 metres long and 1 meter wide rectangular channel. Sediment mixtures of a certain defined composition were installed in this channel according to a defined slope. Running the experiment with constant flow conditions after around 40 days, erosion leads to a development of new slopes and armoured layers by wash out of fine materials [2].

It was decided to recalculate the laboratory experiments with the bed load transport formula after Hunziker and Wu. For the validation two experiments were numerically modelled, experiment #3 and #9. The initial river bed composition in case #3 according to Günter is close to a typical river bed composition in an alpine river bed. The second case #9 is rather unnatural, with high amount of fine and coarse grains and less intermediate ones [3]. For each test case are the determining parameters given, in table I hydrodynamic quantities and in table II the morphodynamic ones.

The numerical mesh consist of around 900 elements with an average edge length of 33 centimetres. This mesh allows with an average time step of 0.5 seconds the simulation of 40 days in an acceptable duration. The boundary conditions for the hydrodynamic part are constant discharge at the inlet and fixed water level at the outlet, 1 centimetre lower than estimated water depth at the end of the experiment h_G. River bed roughness is defined after Nikuradse with a temporal bed roughness predictor, depending linearly on the ratio between skin friction and mean dimeter of the active layer, with $k_s = \alpha d_m$ [4]. The ratio coefficient α is used for calibration.

Morphological boundary conditions are defined as free, so that no material enters the domain and the river bed can evolve without constraints. The river bed is discretised into three layers, with a constant active layer thickness of three times the initial d_{90}. Active stratum is defined to be three times the active layer. Shields parameter θ_c and the hiding-factor of Wu transport function are assumed to be most influencing the result and are used in the calibration, too.

TABLE I. BOUNDARY AND FINAL FLOW CONDITIONS

Case	Q_{in}	I_0	h_G	I_G
[/]	[l/s]	[‰]	[cm]	[‰]
#3	56.0	2.50	9.91	2.327
#9	39.4	4.00	6.87	4.176

TABLE II. INITIAL SEDIMENT COMPOSITION

size class i	1	2	3	4	5	6
$d_{m,i}$ [cm]	0.051	0.151	0.255	0.360	0.465	0.560
#3-Initial	0.359	0.208	0.119	0.175	0.067	0.072
#9-Initial	0.336	0.117	0.099	0.139	0.129	0.180

The simulations were performed using the existing codes, named "old", insofar as it was possible, and the new developed codes, named "new". The calibration parameters are adjusted in order to get good results in all versions with the same parameter set for each test case. The simulations are analysed regarding to grainsize distribution in the surface layer, water depth and river bed inclination. All values of the domain are considered and averaged. Table III shows the defined parameters and results together with the corresponding bed load functions and different versions of the program. The development of the grainsize distribution in the surface layer is shown in fig. 2 to fig. 5 separately for each experiment and bed load function. Important is, that with the "old" codes of SISYPHE no simulation could be performed using version v7p1, as in all cases the simulation stops after a few time steps with "Error in layer". Using the new code structures the crashes does not occur, but the gained results are unrealistic, which points to a deeper error in the source code of the program. However, this error seems to be corrected in the newest unreleased version of TELEMAC, the trunk-version, and more realistic results are gained for old and new layer treatment. This topic was also discussed in the TELEMAC-MASCARET user forum.

TABLE III. RESULTS OF THE SIMULATIONS

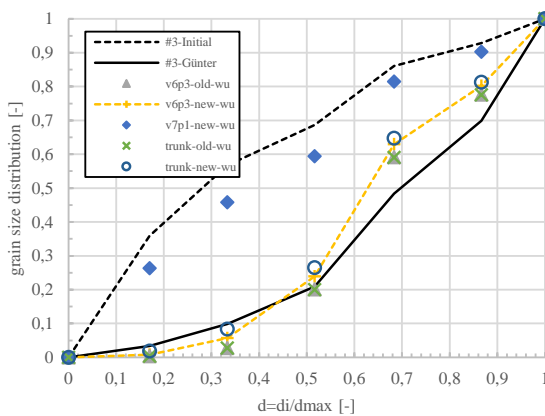|		#3				#9			
		Hunziker		Wu		Hunziker		Wu	
α		2.5		2.5		2.0		2.0	
θc		0.044		0.044		0.047		0.047	
m		/		0.7		/		0.7	
		h_G [cm]	I_G [‰]	h_G [cm]	I_G [‰]	h_G [cm]	I_G [‰]	h_G [cm]	I_G [‰]
v6p3	old	10.42	1.8	9.87	2.5	6.75	3.9	6.75	3.9
	new	9.99	2.2	9.97	2.5	6.75	3.9	6.81	4.2
v7p1	old	/	/	/	/	/	/	/	/
	new	10.51	1.6	11.45	1.0	7.01	3.1	7.63	2.3
trunk	old	10.11	1.8	9.87	2.5	6.74	3.9	6.82	4.1
	new	9.98	2.4	10.0	2.4	6.75	3.9	6.82	4.1

Figure 2.   Case #3 - grain size distribution using Wu's function
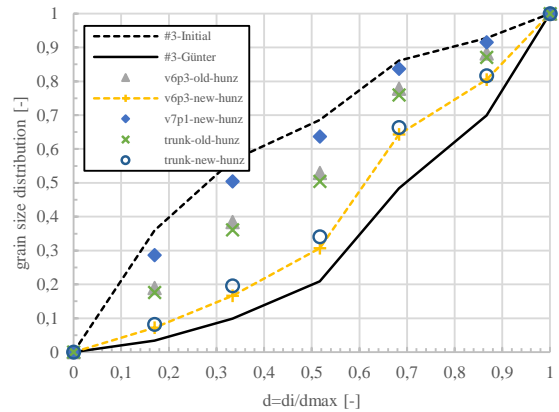
Figure 3.   Case #3 – grainsize distribution using Hunziker's function
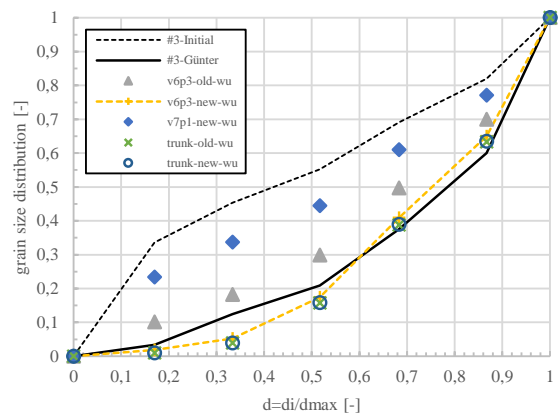
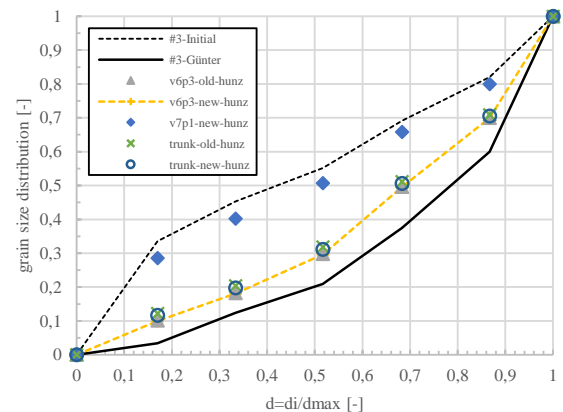Figure 4.   Case#9 – grainsize distribution using Wu's function

Figure 5.   Case#9 – grainsize distribution using Hunziker's function

The bed load function after Wu shows very good agreement with the measurements conducted by Günter for test case #3 and #9 (fig. 2 and fig. 4). The water depths are

close to the measurements with an absolute difference lower than 1 millimetre and the inclination has an absolute maximum deviation of 0.2 per mille. However, the discrepancy between old and new layer treatment is rather small and in both cases the armouring of the river bed is well represented. The small differences are a result that the Wu bedload function takes the diameter of the subsurface layer not directly into account. In the Wu's formula only the available percentage of a grain in the surface layer is considered. The Hunziker's function (abbr. hunz) instead uses the diameter of the substrate layer directly to modify the critical shields parameter, see (15). Therefore, the exchange between layers gets more important. In fig. 3 the differences of the grain sorting process are more significantly visible. With the new layer treatment a better sorting is achieved for test case #3 applying version v6p3 and the unpublished trunk version. Also the water depth and bed slope are more accurate simulated with the new codes. For simulation test case #9 only slightly better results are gained with the new layer treatment compared to the existing codes (fig. 5).

The new layer treatment allows to simulate the Günter experiments with a numerical model with high accuracy. But it must be considered that also the existing codes can be used to simulate the experiment, in most cases. However, when the calculation domain contains nonerodible nodes, the existing codes shows their weaknesses. With the new layer treatment this problem can be solved, as it can be seen the following part.

H. River case – nonerodible treatment

The functionality of the new treatment for nonerodible areas is now tested by the application to the real case, where the problems arises first by applying the original SISYPHE codes. The test case is a three kilometres long river stretch with floodplain in the southern part of Germany, which includes an open stone ramp to limit the erosion in this region. Furthermore, in the river stretch exists a ground sill below a bridge to prevent scour. The ramp, the ground sill and the floodplain with embankment dams are initially classified as nonerodible. The domain consist of around 130'000 nodes and 250'000 elements, which does not allow a manual identification of nonerodible nodes via node number.

Applying the new subroutines for nonerodible areas and layer treatment, this river stretch is finally analysed by a quite accurate and stable hydromorphological model. The simulations are also performed successfully on a server in parallel mode. In fig. 6, a longitudinal section along the river channel is given, with flow from left to right. From the initial river bed (black line) with the fixed parts at the ramp rkm 4.6 and the ground sill at rkm 2.975 the simulation of a flood event over six days leads to significant bed level change. The model is able to simulate the observed water levels along the domain in a very good manner and the shape of the flooded area is close to the expected one. The initial nonerodible ramp is after the flood event covered with sediments, which is a problem for the maintenance. The ground sill keeps the river bed upstream of it on a similar level, but downstream of the ground sill large erosion is observed due to the weir operating during the flood event at the outflow boundary.
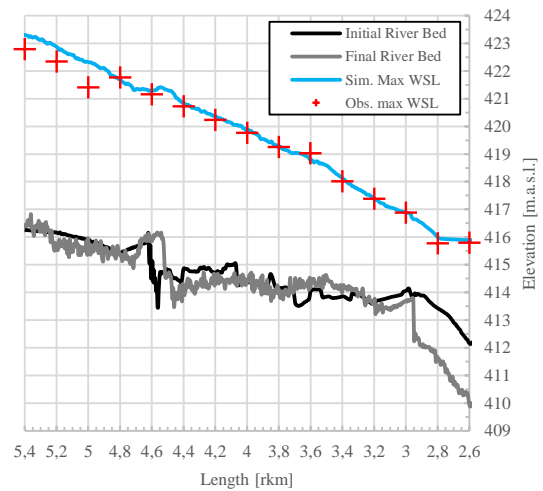

Figure 6.   Longitudinal section of the river case for initial (back line) and final (grey line) river bed and for simulated (blue line) and observed (red crosses) water surface levels.

With the developed model several scenarios and modifications were analysed to increase the flood safety for the surrounding cities. By a modification at the ramp and the ground sill the water levels of a 100-year flood could be halved to a maximum height of 1 m at the floodplains, which offers in combination with a flood protection dam a feasible protections system.

V. CONCLUSION

The modelling environment TELEMAC-MASCARET is a powerful tool to analyse river engineering issues. The problem of numerical errors regarding fractional sediment transport leads to the implementation of an alternate treatment of grain sorting processes and nonerodible structures on the river bed. The newly developed code increases the stability and flexibility of the TELEMAC-SISYPHE system. The code was validated by the numerical modelling of laboratory test cases. The measurements of the bed armouring, flow depth and final river bed slope were accurately represented. The final adaption to a real case study shows the model capacity for long river stretches with complex bed structures. This model provides a promising tool to analyse the impact of sediment transport during a flood event in fluvial rivers.

REFERENCES

[1] M. D. Bui, P. Rutschmann, "Numerical modelling of non-equilibrium graded sediment transport in a curved open channel", Computers & Geosciences 36: pp. 792-800, 2010

[2] A. Günter, "Die kritische mittlere Sohlenschubspannung bei Geschiebemischungen unter Berücksichtigung der Deckschichtbildung und der turbulenzbedingten Sohlenschubspannungsschwankungen", VAW Reports 3, ETH Zürich, 1971

[3] R. Hunziker, "Fraktionsweiser Geschiebetransport", VAW Reports 138, ETH Zürich, 1995

[4] P. Tassi, C. Villaret, "Sisyphe v6.3 User's Manual", EDF R&D, 2014

[5] W. Wu, "Computational river dynamics", Taylor & Francis Group, London, 2007

Chapter 3

An integrated approach for investigating the correlation between floods and river morphology

An integrated approach for investigating the correlation between floods and river morphology: A case study of the Saalach River, Germany

Markus Reisenbüchler [a],*, Minh Duc Bui [a], Daniel Skublics [b], Peter Rutschmann [a]

[a] Technical University of Munich, Arcisstrasse 21, 80333 Munich, Germany
[b] Wasserwirtschaftamt Rosenheim, Königstrasse 19, 83022 Rosenheim, Germany

HIGHLIGHTS

- Morphological developments and activities influence inundation.
- River engineering structures and straightening alter the morphology of the river.
- Stationary hydrodynamic models underestimate the flood risk.
- The developed integrative model represents flood events more accurate and realistic.

GRAPHICAL ABSTRACT
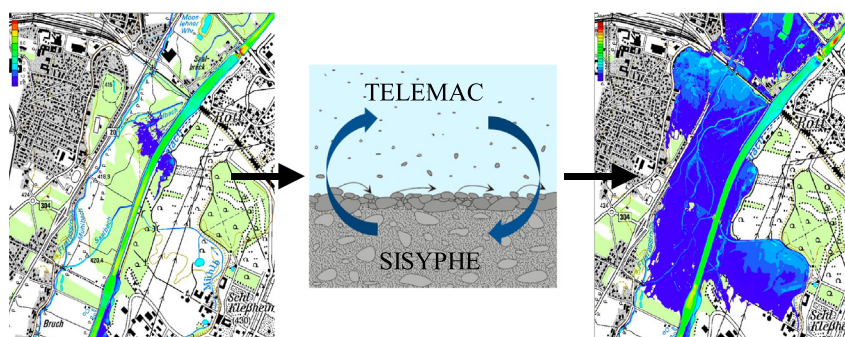
ABSTRACT

Man-made structures in the Saalach River have changed the hydromorphological characteristics of the river regime. In some river reaches, the Saalach has lost the high morphological versatility and high variation in sediment transport characteristic of a mountain river. Among the negative effects, an extreme flow discharge in combination with riverbed variation could be one of the possible causes of flood disasters along the river. For example, the heavy and long lasting rainfall in June 2013 led to a peak discharge of 1100 m^3/s, which was slightly above the 100-year flood return period, inundating a nearby city. However, the influence of the man-made structures on this flood event in this reach is unclear. In this study an integrative hydromorphological model is applied to evaluate this impact by a comparison with a standard clear water model with fixed bed. Moreover, a comparative analysis of a three-and two-dimensional flow model is performed to assess the models suitability representing the flow in this river stretch. The integrative model concept is based on the software TELEMAC-MASCARET, in an enhanced version for better representing graded sediment transport in rivers. In contrast to our integrative model, the standard clear water model with fixed bed overestimates the water elevations as it cannot take the significant changes in morphology into account. Results demonstrate that our proposed model more accurately represents the inundation in the floodplain and could thus be used to provide more reliable predictions to decision-makers for improved flood protection strategy.

© 2018 Elsevier B.V. All rights reserved.

1. Introduction

Flood events are frequent and often disastrous events worldwide. They are not usually directly linked to specific spatial conditions but can occur almost everywhere, triggered by long lasting or heavy rainfall

or the combination of both (Bronstert, 2003). In 2013, middle Europe was affected once again by an extreme flood event. This caused losses of over €8 billion nationwide in Germany and can be classified as the most severe flood event in Germany for the last 60 years (Thieken et al., 2016). In order to mitigate the impact of future events, a lot of research and post-processing on this event has been done to understand the causes leading to the flooding (Blöschl et al., 2013; DKKV, 2015; LfU, 2014; Thieken et al., 2016). In the past, flood inundation maps were used to ascertain whether certain areas are likely to be affected by floods or not. In flood management, this is now extended by including a risk assessment based on the following considerations: overall hazard (e.g. flood magnitude, effect of climate change, etc.), spatial exposure (number of people affected and impact on infrastructure) and vulnerability (i.e. the sensitivity to a hazard). Röthlisberger et al. (2017) employed a spatial clustering approach identifying highly endangered regions. The Free State of Bavaria, Germany, implemented a similar approach, which was improved, adapted and extended after each flood event (StMUV, 2015). Many of these measures and suggested methodologies are based on the representation of flood events from numerical models. These models simulate the extension of 'design floods' and assess whether the floodplain and cities are at risk. In Germany, the design flood for river defense systems refers to a flood discharge with a return period of 100 years (LAWA, 2010a). Such models are commonly used to determine countermeasures, risk-maps and insurance premiums, and are therefore an important factor in the total flood risk management context (LAWA, 2010b; Thieken et al., 2016).

However, floods are not of course confined to clear water phenomena, and rivers are not stable over time. Different fields of research focus on the broader morphodynamic influence on flooding. Rickenmann et al. (2016) highlight the significant influence of sediment motion during flood events in alpine catchments and their damage potential. The profound influence of riverbed dynamics on flood events becomes even clearer when comparing the historic states of rivers with their present state, as Skublics et al. (2016) shows for the Danube River. Morphological activities can lead to an increase in the flood peak and to more severe situations. Guan et al. (2015) and Guan et al. (2016) confirmed this in experimental and real-world conditions using numerical hydromorphological modeling. Similarly, Carr et al. (2015) and Tu et al. (2017), analyzed the magnitude of flood inundation under changing morphological conditions using numerical models. In the framework of hydromorphological modeling, a morphological model is connected to a hydrodynamic one, using different coupling approaches (Duc et al., 2005; Nelson et al., 2016; Wu, 2004). In this procedure, the hydrodynamic model provides information on the flow, turbulence and shear stress, from which the morphological model calculates sediment transport rates, which in turn lead to erosion or deposition. However, the calculation of sediment transport rates commonly applies to several empirical formulae derived from regression or dimensional analyses of laboratory experiments as no formula sufficiently describes all processes (Meyer-Peter and Müller, 1948; van Rijn, 1984; Wilcock and Crowe, 2003; Wu, 2007). The variability of available formulas includes several adjustable parameters, representing the site-specific conditions and characteristics of sediments (e.g. a threshold of motion after Shields (1936)), which means they cannot be simply extrapolated from one river to another. In short, the complexity and heterogeneity of fluvial sediments and the difficulty of measuring them - for instance, bedload transport rates over time - makes the modeling process and defining reliable boundary conditions challenging (Habersack et al., 2017).

This brief survey of the literature makes clear that the representation of the effects of hydrodynamics and morphodynamics cannot be considered in isolation. However, the application of hydromorphodynamic models is not yet the standard for representing a flood event. It is evident that excluding morphological changes can lead to a false impression of the real situation when we examine the event in June 2013, which led to the 100-year flood in the Saalach River, located in southern

Bavaria, Germany. In this river reach, several man-made structures might influence the flood wave propagation and produce feedback on the inundation. However, taking measurements during events is difficult and information is often only available after the event. In order to understand and represent the processes during the event, especially at man-made river structures, we developed a numerical hydromorphological model for a section of the Saalach. Such numerical models can extend the knowledge about the effects of man-made structures on flood events and morphology and contribute to sustainable river management. To demonstrate that a two-dimensional hydrodynamic model is able to accurately represent the flow situation even close to structures in the absence of detailed measurements, we performed a comparison with a three-dimensional flow model. Our model was then compared with a standard clear water model with a fixed bed for the same flood event to test the hypothesis that an integrative approach would provide more accurate and realistic results. For the simulations, we applied TELEMAC-MASCARET software, extended with a newly-developed morphological module, which provides stable and reliable results (Reisenbüchler et al., 2016). The present work serves to illustrate: (1) applicability of a two-dimensional flow model to this river stretch, (2) accurate representation and analysis of the processes during the 2013 flood event, and (3) remarks on possible measures for flood impact reduction taking morphological changes into account.

2. Study area

We studied the Saalach River, which is located in the southeastern part of Germany close to the Austrian border. All elevations in this study are therefore referenced to the German vertical elevation system in meters above sea level. The Saalach River has its source in the Austrian Alps at 1940 m, and after 103 km flows into the Salzach River at a level of 404 m, close to Salzburg in Austria. The river length is defined according to the German system, starting at x = 0.0 km at the confluence to the Salzach River, and increases towards to the river source in the Alps. The data used in this study was provided by the regional water agency, the Wasserwirtschaftsamt Traunstein (abbr.: WWA-TS) (WWA-TS, 2013). The study area is confined to the lower part of the Saalach River from x = 20.6 km to x = 2.4 km, Fig. 1. This section of the river forms the border between Bavaria (Germany) on the orographic left and the county of Salzburg (Austria) on the right bank. At the Siezenheim gauge at x = 5.5 km, the river still has the typical characteristics of an Alpine river with a high variation in discharge (statistical mean discharge MQ = 39.1 m^3/s; statistical mean flood discharge MHQ = 440.0 m^3/s and a statistical 100 year return period flood discharge HQ_{100} = 1093 m^3/s; from the time series 1976–2013) (BMLFUW, 2013) and rapid morphological activity (WWA-TS, 2016). However, the shape of the river has changed greatly over the last 200 years, (BVV, 2017). Based on the comparison of the estuary of the rivers Saalach and Salzach in their historical and current state, this change is shown in Fig. 2, which is representative of the entire river. The historical river had a winding and meandering shape, changing morphologically after every flood event. In 1820, in order to create a clear border and facilitate river management, regulation and straightening were performed along the national border (Schramm, 2012). Further benefits of this measure were the gain in land for agricultural use and the increase of flood protection due to higher flow velocities in a trapezoidal, straight channel. These higher velocities not only affect the flood wave propagation but also increase the shear stress acting on the bed and therefore the sediment transport capacity of the river. However, river training is not the only influencing factor. At the beginning of the 19th century, energy demand increased, particularly for the railway which connected the rural area around the city of Freilassing with the then urban center of Berchtesgaden. To this end, the hydropower plant (HPP) Saalach was constructed in Bad Reichenhall (x = 20.6 km), including the Kibling dam, in 1913 (Zitka, 1959), (Fig. 1). To counteract sedimentation of this reservoir, the accumulated gravel has
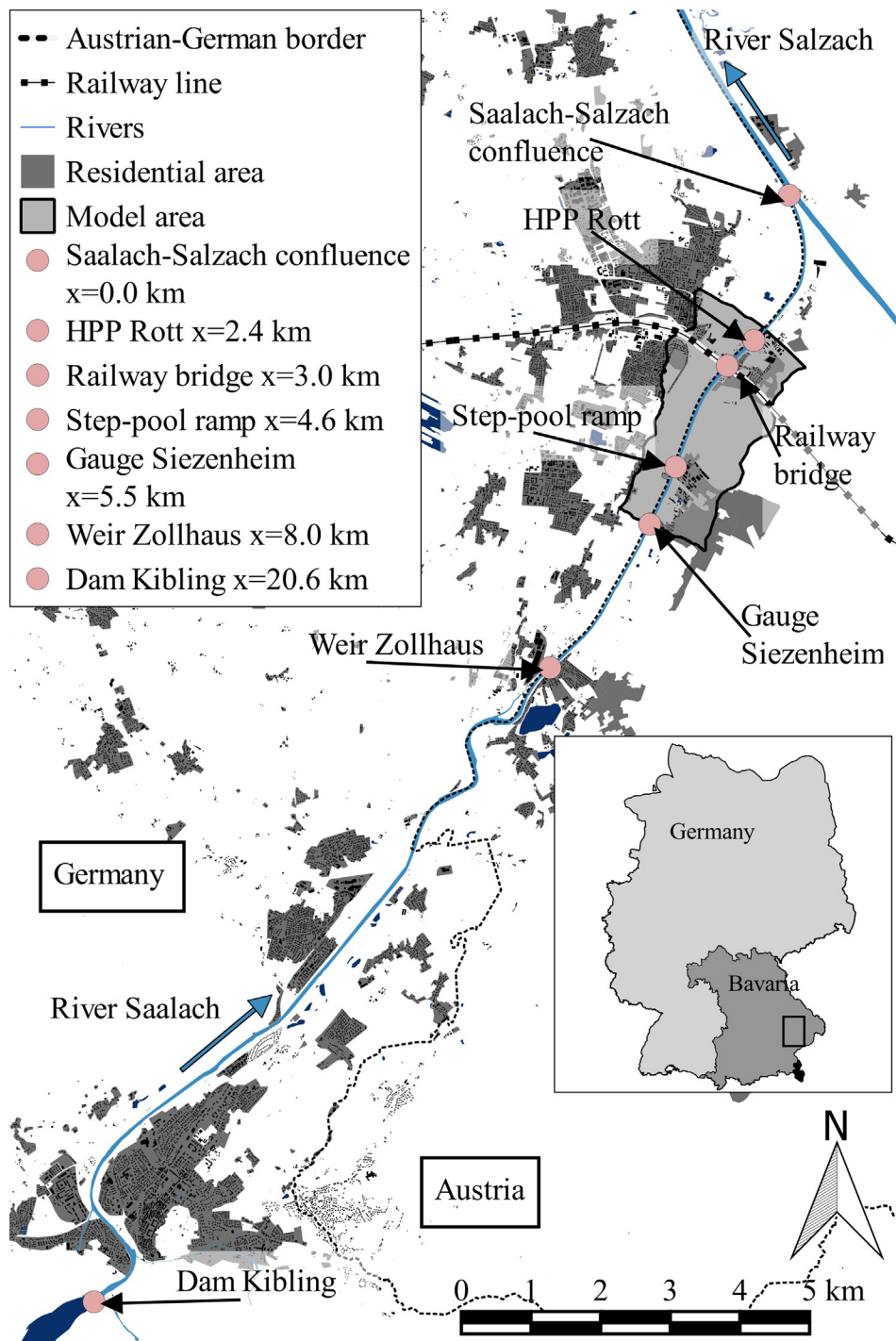
Fig. 1. Overview of the study area, highlighting relevant sites. Map after (OpenStreetMap contributors, 2018).

been excavated since 1940 and used for industrial purposes. Over time, further barriers have been constructed in the river for energy production and to improve timber rafting in the river, which has had a further negative impact on its morphology due to retention of sediment. Also important in the context of this study is the HPP Rott (x = 2.4 km, Fig. 1), constructed in 1940–1951 and rebuilt 100 m downstream in 2005 after exceeding its lifespan (WWA-TS, 2016; Zitka, 1959). One additional purpose of this HPP is to protect the foundations of the railway bridge (x = 3.0 km) located upstream at 413.8 m elevation. Sediment management by flushing and dredging is performed at the HPP Rott when aggregation of the riverbed elevation in the reservoir becomes

too high. The combination of increased sediment transport capacity due to higher velocities resulting from the straightening of the river and the loss of supplied sediment from the source in the Saalach reservoir has led to a sediment deficit downstream, which has caused erosion and deepening of the riverbed. Analysis of cross-sections close to the confluence shows that 80 years after training the riverbed is around 4.50 m deeper than before (1920–1999). Fig. 3 shows cross-sectional profiles of the river close to the confluence at x = 0.6 km over several years. In order to prevent further deepening, sediment in the order of 50,000 m^3/a has been dredged from the reservoir head of the Kibling dam, transported by road and fed into the river downstream of the
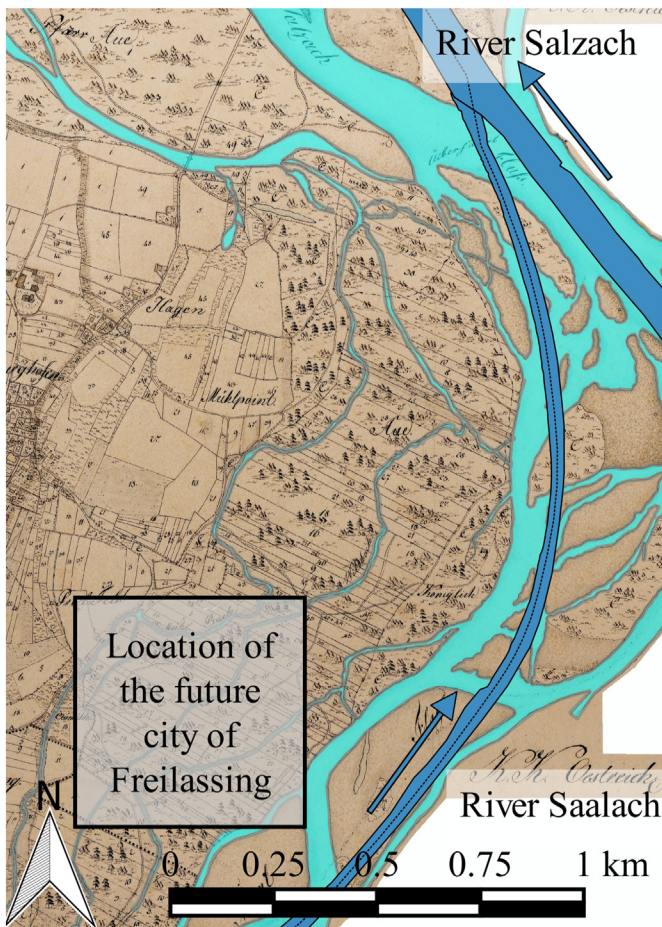
Fig. 2. Historical, meandering (cyan) and present, straight (blue) shape of the Saalach River at the confluence with the Salzach River, after (BVV, 2017). (For interpretation of the references to colour in this figure legend, the reader is referred to the web version of this article.)

dam since 1999 (WWA-TS, 2016). If there is a flood event, the supplied material is transported downstream along the river.

In addition, an open, step-pool ramp has been constructed in the river, situated at x = 4.6 km upstream of the HPP Rott reservoir in order to increase the stability of the river between the unregulated
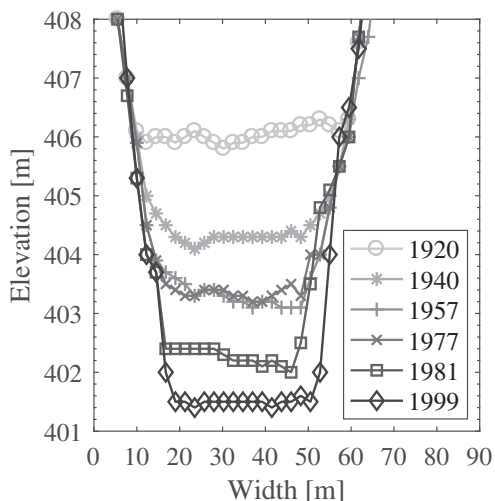

Fig. 3. Cross-sectional profiles of the Saalach riverbed for several years at x = 0.6 km.

Zollhaus weir, x = 8.0 km, and the HPP Rott, x = 2.4 km, in 2005–06. Hengl (2014) and Stephan and Hengl (2010) showed that such embedded structures can provide morphological riverbed stability as they prevent erosion, but are at the same time ecologically friendly in the context of fish migration and sediment transport. A physical scale model of the step pool ramp was developed at the TU Wien, Austria, to test the stability of the construction, flood security, and sediment transport consistency. The structure consists of independent modular pools delimited by stone settings (Fig. 4). The final ramp design consists of eight stone barriers, with a crest at 416.10 m and the lowest point at 414.05 m. The inclination is 1:32, which results in a length of 65 m in total. Furthermore, the ramp is situated in an artificial lateral extension (original 35 m, now 52 m), which delivers ecological benefits (Gostner, 2005; Hengl et al., 2007). The purpose of this measure is to increase the riverbed upstream of the ramp by around one meter and to keep it stable at 415.50 m. This is necessary to protect the fine sediment layers below the riverbed surface from erosion. The aggregation and the flow over the fixed, stepped structure lower the energy potential of the river and therefore decrease the erosion potential. This ramp structure dissipates energy and thereby results in a mild slope in the upstream channel reach. Downstream, the ramp should have no effect on the river, as this section is already in the HPP Rott reservoir. However, some recently performed studies e.g. Beckers et al. (2015a) show that unexpected depositions occur in several sections of the Saalach River, which are counterproductive for flood protection.

3. Review of the 2013 flood event

Seasonal flood events induced by snow melting or short intense summer storms are typical for this region, (Ertl, 1940). However, in May and June 2013, almost continuous rainfall saturated the catchment area of the Saalach so that the subsequent heavier rain could not drain away, leading to extreme discharge into the river (Blöschl et al., 2013). This combination resulted in a flood event observed at the gauge Siezenheim (x = 5.3 km), named HQ_{2013}, which had a peak discharge of around Q = 1100 m^3/s, slightly higher than the statistical 100-year event. This caused extreme flooding on the Bavarian side of the floodplain, including the city of Freilassing, but did not affect the Austrian side of the river, where the city of Salzburg lies, thanks to the flood protection dam (Fig. 5). Analysis of the time series at the Siezenheim gauging station (1976–2014) shows that an event of this magnitude had never previously been observed (Eybl et al., 2013).

In addition to the unexpectedly high discharge, the extent of the inundation was not anticipated. It was assumed that the capacity of the channel would be approximately HQ_{100} and that a flood of this size would have a minimal impact on the region. However, the WWA-TS applied the measured discharges of the 2013 flood to a 2D-hydrodynamic model, HYDRO_AS-2D (Nujic, 2002), to a river bathymetry measured in March 2013. This reconstruction showed a severe inundation, close to the approximate extension of the actual flood (Fig. 5). Local residents' observations and photographs confirmed this scenario (WWA-TS, 2013). In a comparative study, WWA-TS applied the same hydrograph to their older model of river bathymetry measured in February 2002; this showed the flood passing through the region with only minor impact (Fig. 6).

The reason for the difference in the modeled inundations is due to spatial-temporal differences in the elevation of the riverbed. Fig. 7 shows average riverbed elevations along the channel over several years. While in the upper part from x = 8.0 km to x = 5.5 km only minor changes can be detected, in 2002 the lower part of the riverbed (grey line), from x = 5.5 km to x = 2.4 km, was significantly lower than in 2013 (black crossed line).

This comparison shows how sediment transport and morphological change over several years could affect the damage potential of flood events and ignoring these processes may lead to an underestimation of its magnitude.
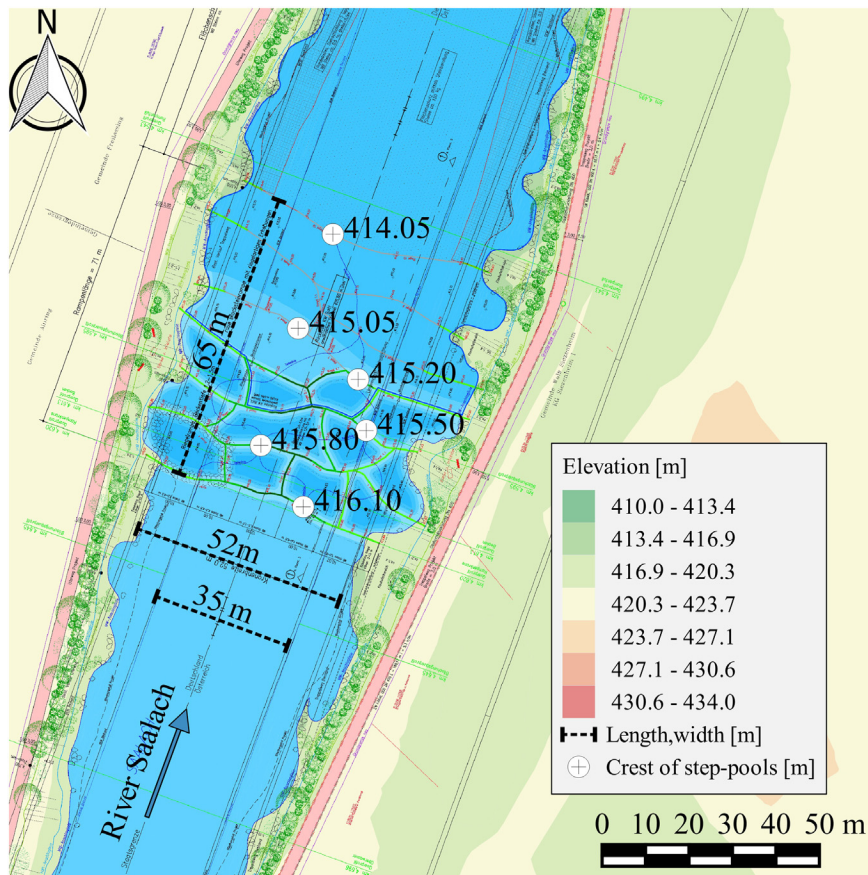
Fig. 4. Construction plan of the step-pool ramp at x = 4.6 km with scales and elevations, after (Gostner, 2005).
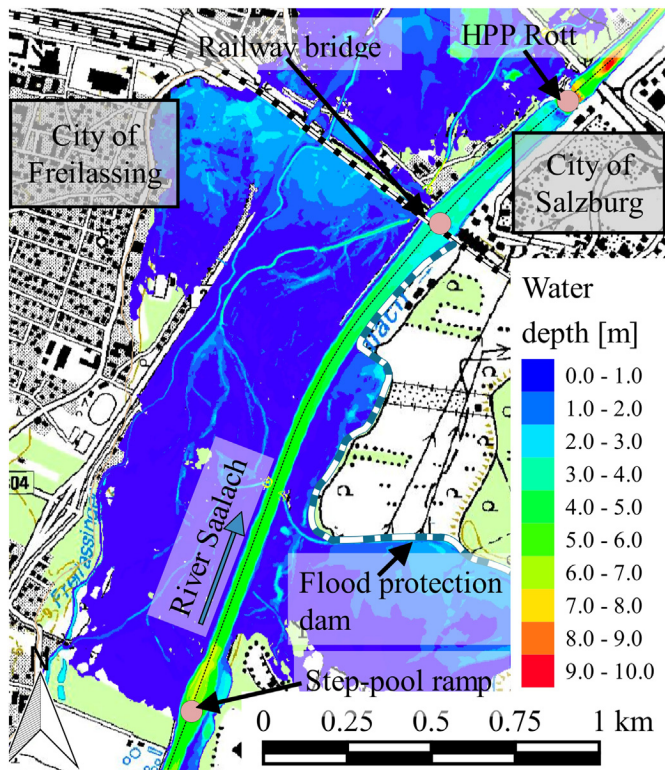

Fig. 5. Maximum simulated inundation, resulting from the 2013 flood hydrograph on a river bathymetry, which was measured in March 2013, after (WWA-TS, 2013).
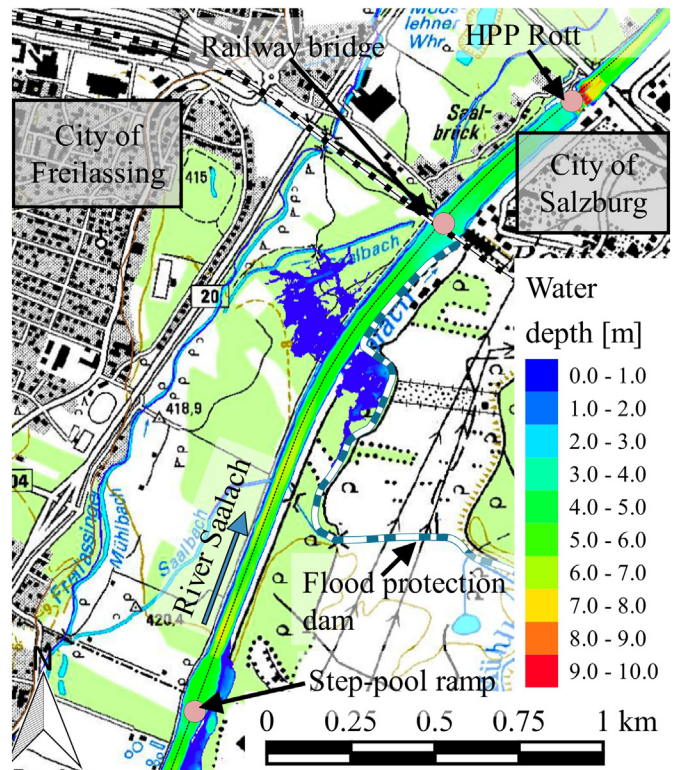
Fig. 6. Maximum simulated inundation, resulting from the 2013 flood hydrograph on an older river bathymetry, which was measured in February 2002, after (WWA-TS, 2013).
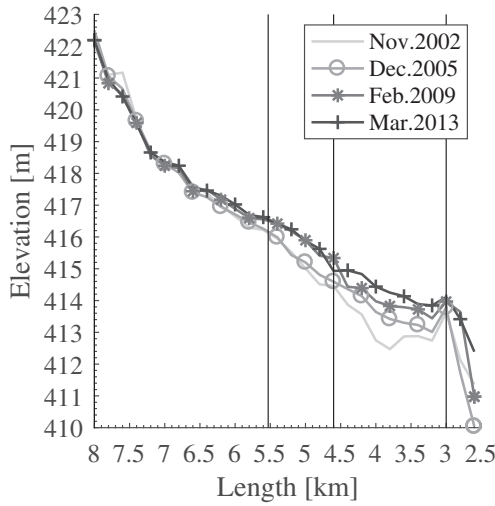
Fig. 7. Longitudinal section of mean riverbed elevations along the Saalach River for several years.

4. Methodology

In order to analyze the processes during this flood event in more detail, and to evaluate the influence of man-made structures, a numerical hydromorphological model was developed. In addition, a comparative analysis shows that a clear water model misrepresents this flood event. The model system TELEMAC-MASCARET is applied for the numerical modeling, including new code fragments to increase its numerical stability, accuracy, and the flexibility of the morphological module. The basics of the extensions and improvements are described in Reisenbüchler et al. (2016). The new model structure is here applied to our real-world scenario under heterogeneous and complex conditions. The applied methodology described below begins with the model generation, after which a clear water calibration with a fixed bed to determine the riverbed roughness is performed, followed by the selection of a suitable hydrodynamic model, and, finally, the application of the newly developed morphological codes to represent the flood event in 2013, which we treat as validation. This is followed by a further simulation, where the potential to mitigate the flood impact is discussed.

4.1. Hydrodynamic module

TELEMAC-MASCARET is an open source software package, capable of representing free surface flows with sediment transport. The suite consists of different modules, which can be coupled depending on the purpose.

TELEMAC3D (T3D) is the module for representing the Reynolds-Averaged-Navier-Stokes-Equations (RANS). The governing equations, in the non-hydrostatic version, are the following (Hervouet, 2007; Janin et al., 1992):

$$\frac{\partial U}{\partial x} + \frac{\partial V}{\partial y} + \frac{\partial W}{\partial z} = 0 \tag{1}$$

$$\frac{\partial U}{\partial t} + U\frac{\partial U}{\partial x} + V\frac{\partial U}{\partial y} + W\frac{\partial U}{\partial z} = -\frac{1}{\rho}\frac{\partial p}{\partial x} + \nu\Delta U + F_x \tag{2}$$

$$\frac{\partial V}{\partial t} + U\frac{\partial V}{\partial x} + V\frac{\partial V}{\partial y} + W\frac{\partial V}{\partial z} = -\frac{1}{\rho}\frac{\partial p}{\partial y} + \nu\Delta V + F_y \tag{3}$$

$$\frac{\partial W}{\partial t} + U\frac{\partial W}{\partial x} + V\frac{\partial W}{\partial y} + W\frac{\partial W}{\partial z} = -\frac{1}{\rho}\frac{\partial p}{\partial z} + \nu\Delta W + F_z - g \tag{4}$$

where U, V, W = components of a three dimensional velocity vector $\overrightarrow{U}$ (m/s) in x, y (horizontal) and z (vertical) direction; t = time (s); ρ = density of fluid (kg/m³); p = pressure (kg/ms²); ν = coefficient of kinematic viscosity (m²/s), F_x, F_y and F_z = source or sink terms in dynamic equations (m/s²) representing forces such as Coriolis force or bottom friction, and g = gravitational acceleration (m/s²). The three-dimensional model is applied worldwide though often in combination with high-performance-computing (HPC) due to the high computational effort (Hajivalie and Arabzadeh, 2017; Mattic, 2017; Moulinec et al., 2011; Ricci et al., 2015).

The module TELEMAC2D (T2D) consists of depth-averaged, two-dimensional Shallow-Water-Equations (SWEs). These equations normally fit well to free-surface river engineering problems, when the river width is significantly larger than the water depth. However, this approach is not suitable for modeling the flow over or around obstacles (e.g. bridge piers) (Hervouet, 2007). The 2D SWEs are used in the model in their conservative form as follows (Ata, 2017):

$$\frac{\partial h}{\partial t} + div\left(\overrightarrow{q}\right) = 0 \tag{5}$$

$$\frac{\partial q_x}{\partial t} + div\left(q_x\overrightarrow{u}\right) = -gh\frac{\partial Z_S}{\partial x} + div\left(h\nu_e\overrightarrow{\nabla}u\right) + hF_x \tag{6}$$

$$\frac{\partial q_y}{\partial t} + div\left(q_y\overrightarrow{u}\right) = -gh\frac{\partial Z_S}{\partial y} + div\left(h\nu_e\overrightarrow{\nabla}v\right) + hF_y \tag{7}$$

where h = depth of water (m); $\overrightarrow{q}$ = vector of the scalar discharges q_x and q_y per unit length (m²/s); u, v = depth averaged components of a two-dimensional velocity vector $\overrightarrow{u}$ (m/s) in x and y (horizontal) direction; g = gravitational acceleration (m/s²); ν_e = diffusion coefficient, including dispersion and turbulence (m²/s) and Z_S = free surface elevation (m). The software has been applied to many different fields of numerical modeling and research (e.g. (Capra et al., 2017; Chen et al., 2015; Sanyal, 2017; Stark et al., 2016; Vittecoq et al., 2017)).

4.2. Sediment transport and morphological module

The modeling package consists of an extra module for morphological issues, namely SISYPHE (SIS), which can be coupled to one of the above-mentioned hydrodynamic modules using a quasi-steady-state approach. Sediment transport is divided into suspended load and bed load. Furthermore, the module can represent multi-grain approaches such as hiding/exposure effects and riverbed armoring. The module is based on a mass-conservation equation - the Exner-Equation - to calculate the updating of the riverbed (Villaret et al., 2013). As only bedload is considered in this study, the Exner-Equation can be stated as follows:

$$(1-n)\frac{\partial Z_b}{\partial t} + div\sum_i \overrightarrow{q}_{b,i} = S_b \tag{8}$$

where n = non cohesive bed porosity (−); Z_b = river bottom elevation (m); $\overrightarrow{q}_{b,i}$ = vector of bedload transport rate of fraction i per unit width (m²/s) and S_b = local source for bottom elevation (m/s). Further information on the module can be found in Tassi and Villaret (2014).

The empirical, fractional bedload transport equation after Hunziker (1995) is applied in this study with the following structure:

$$|q_{b,i}| / \sqrt{(s-1)gd_{m,a}^3} = 5f_i[\phi_i(\Theta_i - \Theta_{hunz})]^{1.5} \tag{9}$$

$$\Theta_{hunz} = \Theta_{crit}\left(\frac{d_{m,s}}{d_{m,a}}\right)^{0.33} \tag{10}$$

$$\phi_i = \left(\frac{d_i}{d_{m,a}}\right)^{-\alpha} \tag{11}$$

where $|q_{b,i}|$ = magnitude of bedload transport rate of fraction i per unit width (m²/s); s = specific density; g = gravitational acceleration (m/s²); $d_{m,a}$ = mean diameter of surface bottom layer (m); f_i = availability of fraction i in the surface layer; ϕ_i = hiding/exposure factor of fraction i; Θ_i = dimensionless shear stress of fraction i; Θ_{hunz} = modification of the critical shear stress threshold Θ_{crit}; $d_{m,s}$ = mean diameter of subsurface bottom layer (m); d_i = diameter of grain class i (m) and α = correlation factor.

In applying the original morphological module for graded sediment transport, two main types of numerical instabilities and errors were observed. Firstly, for the numerical representation of sediment erosion to very thin layers, the sum of all sediment fractions was incomplete (i.e. <100%), which caused the simulation to abort. Secondly, cumulative errors occurred where simulations covered several days as the rounding error of the individual fractions was added up, which also led to termination. These errors are due to the implemented sediment layer concept, which updates the thickness and composition of the riverbed resulting from erosion and sedimentation. Similar errors are described by Dorfman et al. (2012). Reisenbüchler et al. (2016) developed an updated version of this module, which is applied in this study. These modifications are based on a vertical sediment layer concept, but in an implementation that follows Bui and Rutschmann (2010). Furthermore, this concept is extended by treating non-erodible regions in the domain differently, which are now represented by an additional, artificial grain class. This distinction provides a clear separation between movable and non-movable regions.
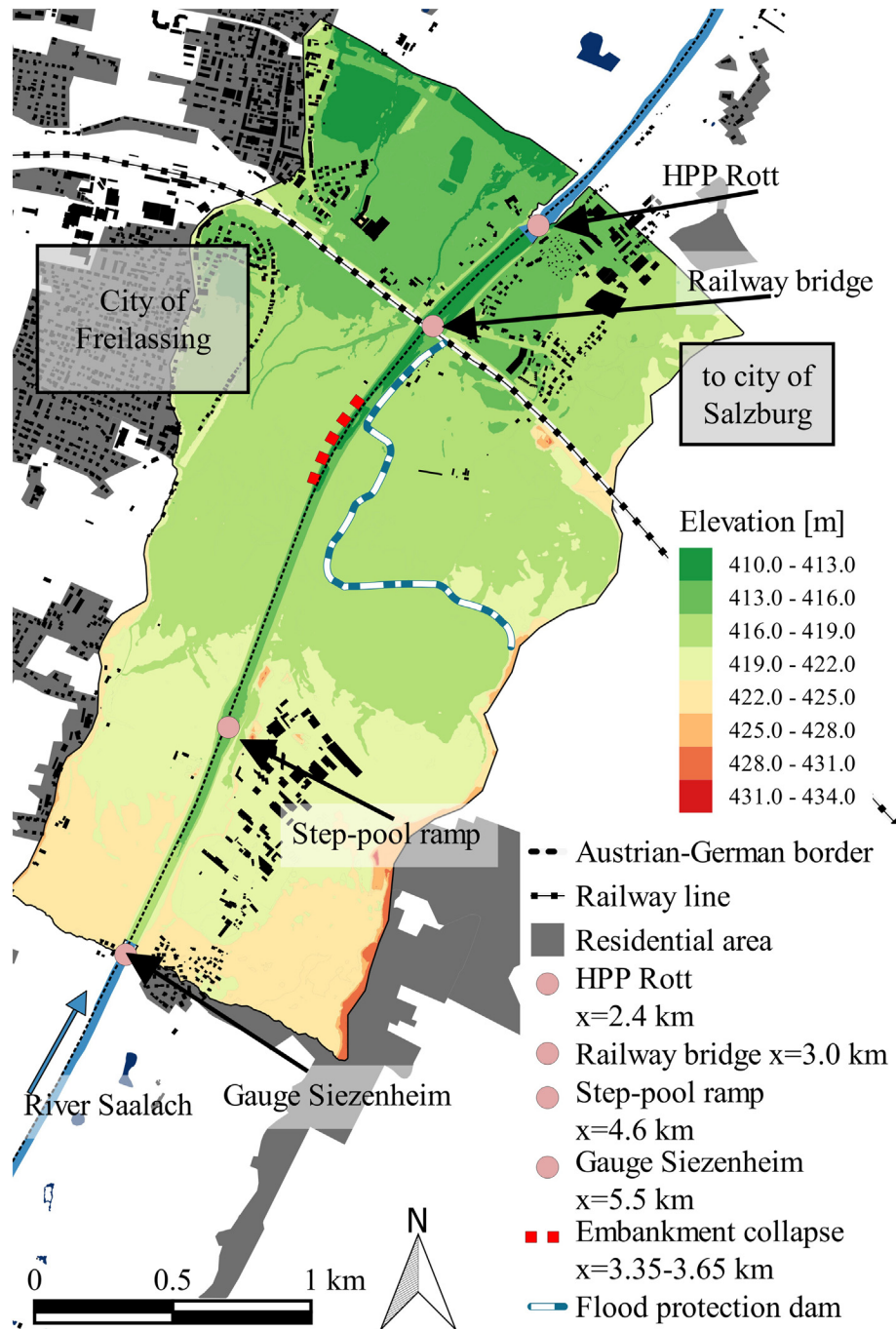

Fig. 8. Overview of the model area, including relevant sites. Map after (OpenStreetMap contributors, 2018).

Table 1
Definition of the developed geometrical and the applied numerical models.

Application	Date of the river bathymetry	Model designation	Applied numerical model
Calibration	Dec. 2005–Feb. 2006	M2006	T2D, T3D
Validation	Mar. 2013	M2013	T2D, T2DSIS
Scenario application	Mar. 2013 and maximum acceptable riverbed elevation at the HPP Rott	MSC	T2DSIS

4.3. Model setup

The modeled river reach is defined as a three-kilometer long section from the Siezenheim gauging station (x = 5.5 km) to the HPP Rott (x = 2.4 km) passing the step-pool ramp (x = 4.6 km) and a railway bridge, with an existing groundsill over the cross-section (x = 3.0 km), as shown in Fig. 8. At the Siezenheim gauging station, reliable measurements of the discharge in fifteen-minute time intervals have been available since 1985 (LfU, 2017). At the HPP Rott, information is available for the weir-operating-regulation, which defines the water elevation according to the discharge, as well as measurements during the latest flood events. The domain is discretized using a triangular unstructured grid with an average mesh size equal to 6.0 m along the river channel and a coarser mesh, with an average edge length of 10 m, to represent the floodplain. The heights of the geometry used for the floodplain are a digital elevation model, and interpolated cross-sectional measurements for the river, which were recorded every 200 m in distinct years (WWA-TS, 2013). In this study, several models are developed, whose specifications and applications are listed in Table 1.

The step-pool ramp, built in 2005–2006 was manually integrated in each model to represent its shape according to the construction plans (see Fig. 4). In total, the geometry consists of around 250,000 triangular elements and covers an area of 4.8 km². Data on the riverbed's granulometry are available from a previously performed drill-program in 1999, as well as from Beckers et al. (2015a); Beckers et al. (2016b); Beckers et al. (2015b). Based on this information, it can be assumed that the riverbed consists mostly of coarse gravel, which is discretized in eight different grain classes for modeling purposes. Furthermore, a vertical layering of the riverbed with a constant active layer thickness of $l_a = 0.14$ m thickness ($=d_{max}$ of the sediment) and an active stratum with several additional substrate layers is defined, each up to three times the active layer. The characteristic mean diameter of the active layer is initially $d_{m,a} = 68$ mm and $d_{m,s} = 19$ mm for the substrate layers.

One pivotal issue in this framework is the correct representation of man-made structures in and along the river. Within the model area, there are several points to consider: the fixed embankments, the step-pool ramp with large stone settings (x = 4.6 km), the groundsill below the bridge (x = 3.0 km), and the intake structure in front of the hydropower plant (x = 2.4 km). These areas are considered as non-erodible in the context of sediment transport.

During the flood event of 2013, some parts of the fixed embankment structure collapsed. This not only lowered the elevation of the embankment, but supplied additional sediment material to the river. According to the WWA-TS, along x = 3.65 km to x = 3.35 km a volume of 21,000 m³ bank materials was eroded (WWA-TS, 2013). The representation of such a sliding process cannot be captured by the applied morphological model directly. However, to include this aspect in the integrative modeling of the flood event in 2013, the following method is applied: the additional material is supplied in the river along this section via a temporal source during the high flood beginning at $t = 47.75$ h to $t = 80.25$ h. The collapsed embankments along the Bavarian side are lowered in our geometry of M2013 by up to 1 m to 416.7 m, according to the measurements after the event. By comparison, in a clear water model, it would not be possible to represent this additional material input.

5. Results and discussion

The TELEMAC-MASCARET system is capable of running in parallel mode using domain decomposition and MPI based codes, allowing us to decrease the computational time. The calibration, validation and scenario simulations have been carried out on a Linux-server with 64-cores at the Chair of Hydraulic and Water Resources Engineering, TUM.

5.1. Model calibration

During calibration, we determine if a 2D flow model represents the flow structures in the section of river analyzed or if a 3D model is necessary. Furthermore, we investigate whether available information on the riverbed roughness can be applied to our model, as this is the most important parameter for hydraulic simulations (Lane, 2014). Because the river has been straightened, the flow processes in the Saalach River are very regular; however, obstacles at the ramp, the groundsill, and the piers of the bridge may introduce some complex flow structures. Therefore, we simulated clear water first with T2D and T3D and then compared (fixed bed and no sediment transport). We selected a high flow event, as the desired model will be applied under these conditions. This comparison reveals the most accurate model taking into consideration computational effort. Models accuracy is evaluated using statistical goodness of fit (GOF) criteria. The GOF of the simulations is assessed by means of the coefficient of determination R^2, Nash-Sutcliffe-efficiency (NSE), the root mean square error (RMSE), and mean absolute error (MAE) (Moriasi et al., 2007). From an existing 2D model at the WWA-TS, roughness parameters are input in the models. The bed of the Saalach is a uniform Strickler roughness of $k_{st} = 35$ m$^{1/3}$ s^{-1}, representing coarse gravel material, and $k_{st} = 25$ m$^{1/3}$ s^{-1} at the fixed embankment. In the floodplain, Strickler values have been selected in line with the WWA-TS model, based on land use maps (meadows $k_{st} = 20$ m$^{1/3}$ s^{-1}; forest $k_{st} = 11$ m$^{1/3}$ s^{-1}; farmland $k_{st} = 24$ m$^{1/3}$ s^{-1}; residential area $k_{st} = 17$ m$^{1/3}$ s^{-1} and streets $k_{st} = 40$ m$^{1/3}$ s^{-1}) (WWA-TS, 2013). Furthermore, at modeled ramp, the roughness is adjusted according to the results of the technical report with $k_{st} = 20$ m$^{1/3}$ s^{-1} (Gostner, 2005). For T3D, nine vertical levels are defined to properly quantify the influence of vertical velocities.
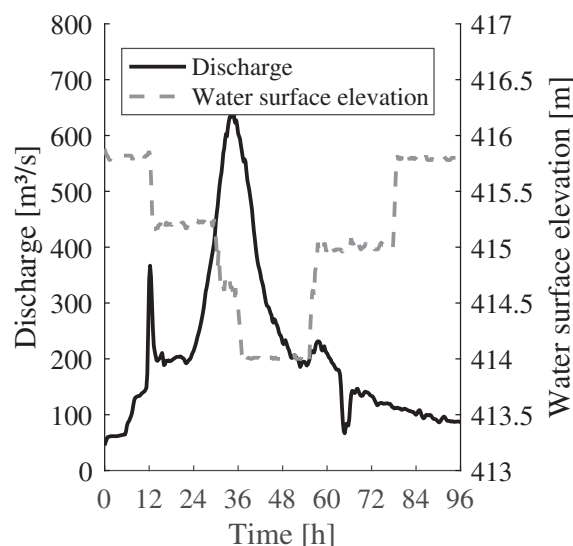
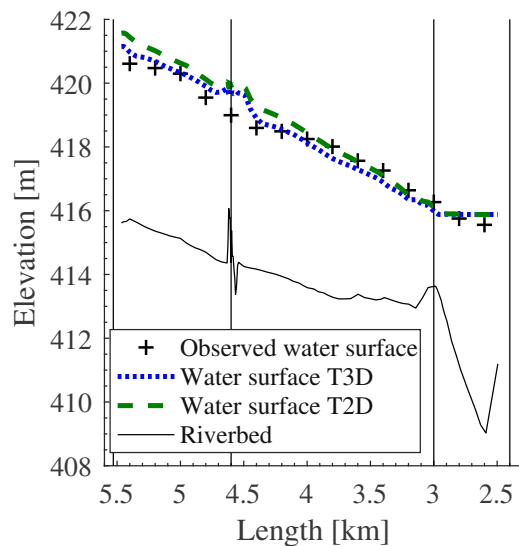**Fig. 9.** Hydrodynamic boundary conditions for the calibration.

Fig. 10. Longitudinal section of observed and simulated water surfaces (T3D and T2D) and the riverbed elevation for the calibration.

Fig. 11. Longitudinal section of mean velocity differences ($dv = \bar{v}_{T3D} - \bar{v}_{T2D}$) at different times t.

The number of vertical layers should be sufficiently high to represent 3D flow phenomena.

Water surface measurements along the river are used to quantify the accuracy of the simulations. In contrast to low or mean discharge situations, the information for flood events is often based on indirect measurements, performed after the event, e.g. derived from flood pathways or sediment lines at the embankment, and may include uncertainty.

Based on the available measurement data, an unsteady calibration scenario is run over a longer time frame, starting from a steady initial state with mean discharge conditions (Fig. 9). During calibration, we simulate the flood event in August 2006 using the geometry M2006. The discharge increases from the mean flow and reaches the first peak ($Q = 350 \text{ m}^3$/s) at $t = 12$ h. At this point, the weirs at the HPP Rott are opened, leading to a drop in the water elevation. At $t = 24$ h, the flood wave increases to its final peak and at the hydropower plant the water elevation is lowered to 414.00 m (corresponding to the weir operating regulative). When the flood recedes, the reservoir is filled again by progressively closing the gates. During the flood event, no inundation of the floodplain occurs. We consider the morphological evolution during this flood event to be very low because the river is still dominated by the damming of the HPP Rott during the flood peak. Therefore, though some local sediment relocations may occur, the riverbed remains largely unchanged and thus allows a clear water model estimate of the roughness of the riverbed.

Fig. 10 provides the calculated distributions of water surface elevation using T2D and T3D and the observations, and Table 2 contains the corresponding statistical performance. The analysis demonstrates for this case that both models precisely predict the water surface elevation. The performance of the 2D model is only slightly lower than the 3D. In a visual comparison, the largest differences occur close to the location of the ramp, possibly because the flood event occurred half a year after the river bottom measurements were taken. In the intervening period,
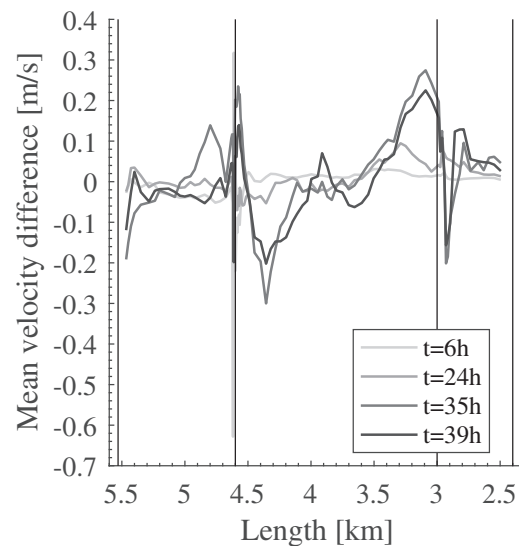
the area upstream of the ramp likely aggregates, so the transition from river to ramp is probably smoother than simulated. Errors in the observation are also possible, but cannot be quantified.

The differences between T2D and T3D, regarding the mean velocity, is evaluated in cross-sections at multiple, selected time steps. The flow velocities and the shear stresses derived from them are the driving force for sediment transport. If there are large velocity differences between the models, a different morphological development will occur. The selection of the time frames was made to capture all flow situations: the first time, $t = 6$ h, is selected at $Q = 80.02 \text{ m}^3$/s; the second right before the flood wave at $t = 24$ h; the third at the peak $t = 35$ h; and the last when the discharge is already decreasing at $t = 39$ h. Since velocity measurements were not conducted in this section of river, a comparison with the actual water velocity cannot be provided. Instead, the simulated mean velocities from T3D are set as reference values and compared with T2D. Fig. 11 provides absolute differences ($dv = \bar{v}_{T3D} - \bar{v}_{T2D}$) in the mean velocities at corresponding times along the river, and Table 3 shows the resulting error parameters, which also quantifies the difference between T2D and T3D.

During the 2006 flood event, velocity differences occur in a range between 0.35 and − 0.65 m/s. We found that the magnitude of the differences is roughly proportional to the discharge. At time $t = 6$ h, the discharge and the error display their minimum values representing identical velocities. The largest error appears at the peak discharge of around $Q = 650 \text{ m}^3$/s,; however, coefficients R^2 and NSE are still in the optimum range, and the RMSE and the MAE are very small, taking into account the high discharge and the absence of velocity measurements. The largest differences occur at the stone ramp ($x = 4.6$ km) since the structure introduces vertical velocities, whose influence can only be detected to a limited extent in a 2D model. A similar situation obtains at the groundsill of the railway bridge ($x = 3.0$ km), where the opening of the weirs causes something similar to a hydraulic jump.

Table 2
Performance criteria of the calibration for each applied numerical model.

Model	R^2	NSE	RMSE	MAE
	[−]	[−]	[m]	[m]
T2D	0.978	0.916	0.464	−0.293
T3D	0.976	0.961	0.317	−0.050

Table 3
Comparison of the simulated mean velocities using GOF criteria.

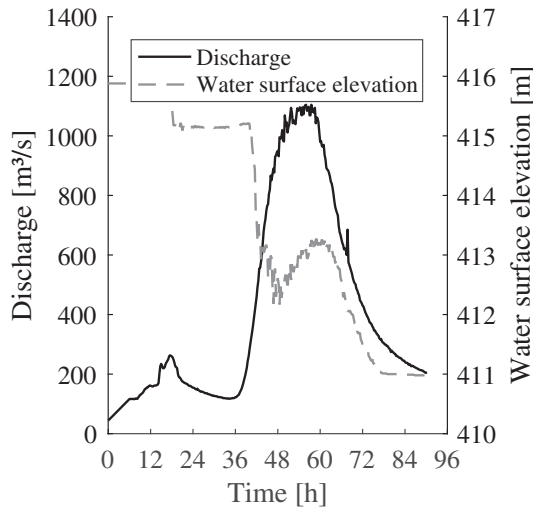| Time t	Discharge Q	R^2	NSE	RMSE	MAE
[h]	[m³/s]	[−]	[−]	[m/s]	[m/s]
06:00	80.02	0.972	0.957	0.089	0.040
24:00	214.32	0.994	0.994	0.039	0.031
35:00	649.85	0.964	0.952	0.132	0.096
39:00	502.29	0.976	0.972	0.094	0.074

Fig. 12. Hydrodynamic boundary condition for the validation.

In summary, the comparison of the average velocity profiles of both flow models shows that, in the modeled river section, the T2D model is quite accurate, almost as precise as T3D. The good agreement between both models justify using T2D, as its computing time is about 12 times lower than that of T3D. As a result, the following hydromorphological simulations are performed with T2D.

5.2. Model validation

The representation of the processes during the 2013 flood event using the integrative model, T2D coupled with SIS, on the M2013 geometry, is carried out in this paper as the next step of model validation for accurate hydraulic calculation and as model calibration for hydromorphological calculation. The same bedload transport function is applied as Beckers et al. (2015a) use in their study, with the fractional bedload transport equation of Hunziker (1995), with a lowered critical Shields parameter of $\Theta_{crit} = 0.04$ for the beginning of sediment motion. With this adaptation, higher transport rates are modeled, which more realistically represents the characteristics of the Saalach River (Beckers et al., 2016a). A grain dependent roughness correction is applied to take into account granular changes in the riverbed. Here the quadratic grain dependent Nikuradse roughness is set in relation to the constant
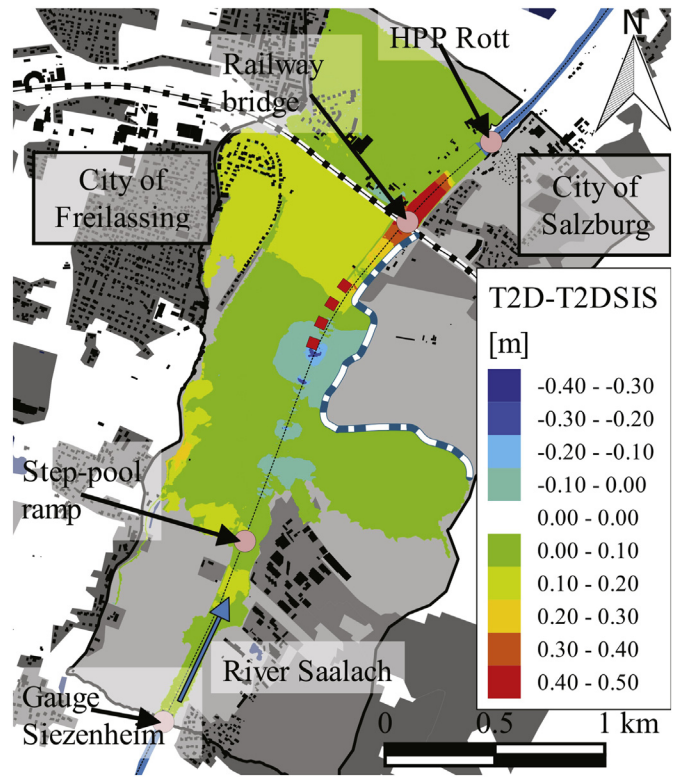

Fig. 14. Spatial differences of simulated maximum water surface elevation from clear water T2D and from integrative T2DSIS, on the geometry M2013. Map after (OpenStreetMap contributors, 2018).

quadratic bottom friction coefficient derived from the clear water simulation (Tassi and Villaret, 2014). This treatment directly affects the calculated bottom shear stress and therefore the sediment transport. In addition to the integrative approach including the morphology, a clear water simulation with T2D, excluding the morphology, is conducted for the flood event to highlight the importance of the integrative approach and identify any differences between both models.

The hydrodynamic boundary conditions are provided in Fig. 12, which shows the discharge at the inlet and water surface elevation at the outlet. Where an extraordinary discharge is indicated at $t = 12$ h, the weir is opened at the arrival of the first flood peak to decrease the
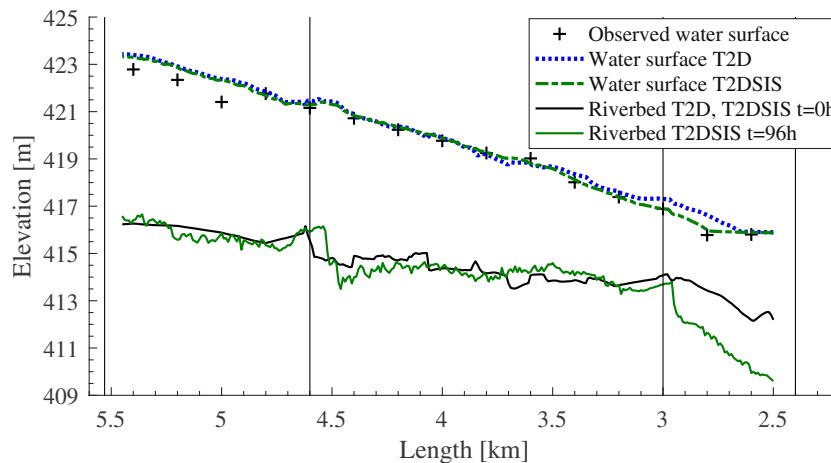

Fig. 13. Longitudinal section of the riverbed at $t = 0$ h (black) and at $t = 96$ h (green) and the maximum water surface from T2DSIS (green dashed) using the M2013 geometry; for comparison the maximum water surface from T2D (blue dashed) using the M2013 geometry at t = 0 h. (For interpretation of the references to colour in this figure legend, the reader is referred to the web version of this article.)
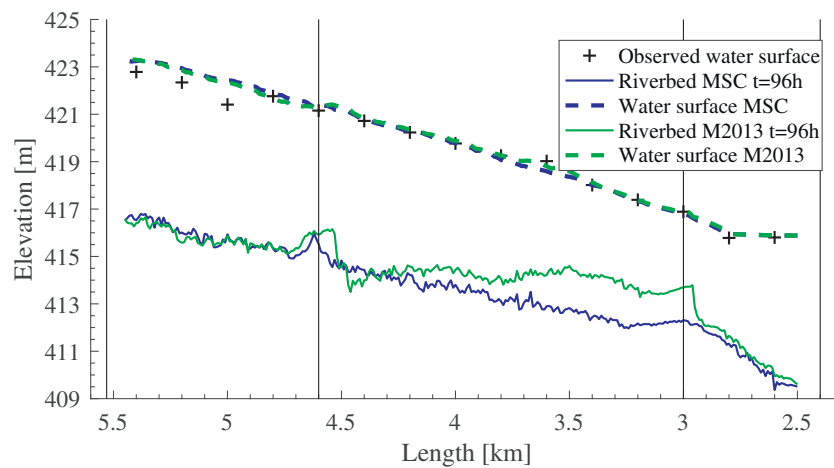
Fig. 15. Longitudinal section of the riverbed at t = 96 h (blue) and the maximum water surface (blue dashed) using the geometry MSC; for comparison the riverbed at t = 96 h (green) and the maximum water surface (green dashed) using the geometry M2013. (For interpretation of the references to colour in this figure legend, the reader is referred to the web version of this article.)

water elevation. At time $t = 36$ h, the weir is opened completely to provide the maximum discharge capacity in free-flow conditions. In this river, no bedload measurements are available, which would be necessary to define the sediment boundary condition. To overcome this limitation, a morphological equilibrium condition is defined at the inlet (Tassi and Villaret, 2014; Villaret et al., 2009). This boundary condition automatically delivers the bedload at the model inlet, defined by grain proportions and quantity, to keep the riverbed elevation at the inlet cross-section constant in time. An analysis of riverbed measurements from 2002 to 2013 validates this approach (Fig. 6). From 2002 to 2005 only very small changes can be identified in the upper reach x = 8 km
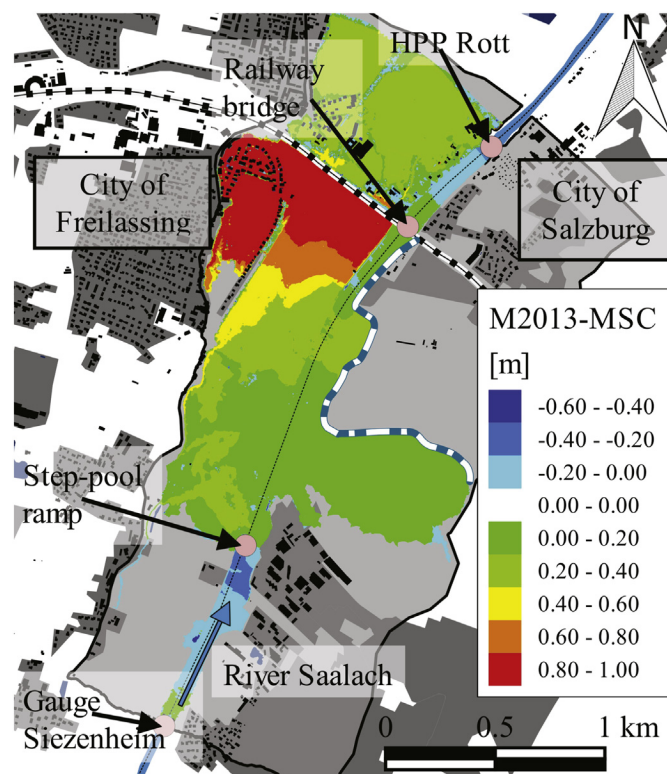
to x = 6.0 km, but high variations are apparent in the reservoir in front of the HPP. As expected, the riverbed has risen in the section upstream of the ramp to x = 6.0 km since its construction in 2005–06. However, from 2009 to 2013, no further rising of the riverbed is apparent, and this sections seems to be in an equilibrium state. High morphological dynamics are visible only in the downstream section between the stone ramp x = 4.6 km and the groundsill x = 3.0 km.

Because no riverbed measurements were taken immediately after the 2013 event, the accuracy of the integrative model can only be assessed from the observed water surface elevation along the river. In Fig. 13, the longitudinal section of the modeled river is provided including the initial and final riverbed after the flood event and the maximum simulated water surface of the integrative model T2DSIS. The integrative model closely conforms to the measurements from the visual comparison as well as to the evaluation criteria ($R^2 = 0.989$, NSE = 0.979, RMSE = 0.325 m, MAE = 0.215 m). The morphological change during the flood event can be divided into three parts: one upstream of the ramp at x = 4.6 km, a second between the ramp and the groundsill at x = 3.0 km, and a third downstream of the groundsill. In the most upstream part x = 5.5 km to x = 4.6 km, only small bed changes occur, influenced by the equilibrium inlet boundary condition and the non-movable ramp structure. The step-pool ramp itself was filled with coarse sediment, a process that was also observed by the WWA-TS (WWA-TS, 2013). The second section between the ramp at x = 4.6 km and bridge x = 3.0 km, which is already part of the hydropower plant reservoir, was not significantly affected by flushing processes from the Rott HPP. The reason for this is the fixed ground structure at the bridge (x = 3.0 km) at 413.8 m, where a hydraulic jump breaks the flow. Only the third section, directly before the hydropower plant, shows greater morphological changes due to flushing. The WWA-TS and the operator of the HPP confirmed the simulated effects, which include partial flushing of the reservoir and aggregation at the ramp (WWA-TS, 2013).

Additionally, in Fig. 13 the maximum water surface elevations of the clear water model T2D are visible. The clear water model shows less agreement with the measurement according to the statistics ($R^2 = 0.980$, NSE = 0.961, RMSE = 0.439 m, MAE = 0.342 m), which is due to the differences in the region around the railway bridge at x = 3.0 km. Here the clear water model overestimates the water surface by up to 0.7 m because the reservoir flushing and the resulting higher channel capacity cannot be represented. The absence of sediment representation not only influences the modeling of water surface in the river but also the floodplain. Fig. 14 shows the absolute differences in the inundation between T2D and the coupled T2DSIS. T2D consequently

Fig. 16. Spatial differences of maximum water surface elevations using the T2DSIS model on the geometry M2013 and MSC. Map after (OpenStreetMap contributors, 2018).

shows higher water surface elevations in the floodplain in a range of up to 0.20 m.

The results demonstrates that our integrative hydromorphological model is able to reproduce the measured water surface elevations more accurately than a clear water model, and at the same time provides a better understanding of the processes during the flood event.

5.3. Model application

We used the developed integrative model to analyze several technical measures designed to improve flood management in this region. The groundsill below the railway bridge was identified as a limiting factor for sediment transport during the 2013 flood event. Furthermore, the artificial extension at the step-pool ramp could have led to an accumulation of sediment close to the ramp and likely to a higher water surface elevation. We developed to study the impact of these structures, an additional geometry, called MSC. In this geometry, the non-erodible elevation below the bridge is defined 2 m lower at 411.85 m and the extension at the ramp is reduced by 17 m back to the original 35 m channel width. In addition, the riverbed elevation in the reservoir was adapted to represent the defined maximum allowed bed elevation. This adaptation is necessary to provide a statement that conforms to the legal regulations. For this scenario, the same hydro- and morphodynamic boundary conditions as for the validation scenario are applied (Fig. 12).

Fig. 15 shows that there is a difference in morphological development compared to the river section in original bed condition (M2013) and the modified one, MSC. The sedimentation of the ramp can be decreased even if this only has a very limited impact on the water surface at x = 4.6 km. Due to the reduction of the groundsill at x = 3.0 km, the riverbed in the whole reservoir is flushed out during the flood event and lower water elevations are reached. This has a further effect on the flood extension and the magnitude in the floodplain as can be seen in Fig. 16, which shows the differences in water surface between MSC and M2013. The depth of the simulated inundation in the city region of Freilassing is thereby decreased by up to 0.80 m, with an overall decrease of around 50% of the real flood event. The evaluated measures would help to design an efficient and suitable flood protection system for the city. For instance, future flood levees around the city could be lower if our proposed modifications were made to the river. This would reduce the construction costs of the planned measures drastically. On the other hand, if the levees are built at the planned height, our measures would ensure a higher level of security.

6. Conclusion

The TELEMAC-MASCARET modeling system incorporating our own developments for graded sediment transport was applied to simulate hydromorphodynamic processes in the lower Saalach River. The model reproduces the behavior of river flows for a high water condition using a 2D and a 3D model. Both models yield very accurate performance parameters. Applying a comparative analysis, we show that for this river section a computationally demanding 3D calculation does not provide more accurate results.

The 2D hydromorphodynamic model was successfully applied to the flood event of 2013 with the aim of improving process representation during the event and achieving accurate simulated high water surface elevations. As no real-time measurements of the riverbed or the transported material during the flood event were available, the morphological model is calibrated qualitatively based on process observations but not on real measurements. Furthermore, simulations were carried out for different scenarios to evaluate the effects of the step-pool ramp and potential improvements to the river for flood events. In addition, we demonstrated that lowering the groundsill below the railway bridge would significantly reduce water surface due to improved reservoir flush during flood events.

Moreover, this study shows that hydrodynamic flood inundation maps based on fixed riverbeds can lead to inaccurate estimates of the flood risk potential of a river. Only an integrative approach which includes the morphology and takes into account changes in the river structure is likely to ensure reliable inundation mapping for risk analysis. Water authorities should consider a bandwidth of possible riverbed elevations as benchmarks for inundation maps. We have also demonstrated the flood mitigation potential of riverbed flushing in a reservoir, which we recommend be analyzed further.

References

Ata, R., 2017. Telemac2d User Manual. 7.2, EDF, online published. http://www.opentelemac.org/.

Beckers, F., Noack, M., Wieprecht, S., 2015a. Ergebnisse der Geschiebetransportmodellierung (GTM) im Unterlauf der Saalach. Publications of the Dept. of Hydraulic Engineering and Water Resources Management, Universität Stuttgart, online. http://www.iws.uni-stuttgart.de/publikationen/docs/Kurzfassung-Teilmodell%202.pdf.

Beckers, F., Sadid, N., Haun, S., Noack, M., Wieprecht, S., 2015b. Contribution of Numerical Modelling of Sediment Transport Processes in River Engineering: An Example of the River Saalach. IAHR World Congress 36, pp. 1–5. https://www.researchgate.net/publication/283666981_Contribution_of_numerical_modelling_of_sediment_transport_processes_in_river_engineering_an_example_of_the_river_Saalach.

Beckers, F., Noack, M., Wieprecht, S., 2016a. Geschiebetransportmodellierung (GTM) Salzach und Saalach - Teilmodel 2: Untere Saalach. Technical Report, Dept. of Hydraulic Engineering and Water Resources Management, Universität Stuttgart (unpublished).

Beckers, F., Noack, M., Wieprecht, S., 2016b. Reliability Analysis of a 2D Sediment Transport Model: An Example of the Lower River Salzach. Proceedings of the 13th International Symposium on River Sedimentation, pp. 147–152. https://www.researchgate.net/publication/308920158_Reliability_analysis_of_a_2D_sediment_transport_model_An_example_of_the_lower_river_Salzach.

Blöschl, G., Nester, T., Komma, J., Parajka, J., Perdigão, R.A.P., 2013. The June 2013 flood in the Upper Danube Basin, and comparisons with the 2002, 1954 and 1899 floods. Hydrol. Earth Syst. Sci. 17 (12), 5197–5212. https://doi.org/10.5194/hess-17-5197-2013.

BMLFUW, 2013. Hydrografisches Jahrbuch von Österreich 2013. 121. The Austrian Federal Ministry of Agriculture, Forestry, Environment and Water Management, Vienna, Austria. https://www.bmlfuw.gv.at/dam/jcr:bb100102-eac3-4b51-8d8d-f40b94e5d546/Jahrbuch_2013_Datenteil.pdf.

Bronstert, A., 2003. Floods and climate change: interactions and impacts. Risk Anal. 23 (3), 545–557. https://doi.org/10.1111/1539-6924.00335.

Bui, M.D., Rutschmann, P., 2010. Numerical modelling of non-equilibrium graded sediment transport in a curved open channel. Comput. Geosci. 36 (6), 792–800. https://doi.org/10.1016/j.cageo.2009.12.003.

BVV, 2017. Historical map of the River Saalach. Geoportal Bayern - BayernAtlas, Bayerische Vermessungs Verwaltung, online. https://v.bayern.de/bw8Gs, Accessed date: 12 November 2017.

Capra, H., Plichard, L., Bergé, J., Pella, H., Ovidio, M., McNeil, E., Lamouroux, N., 2017. Fish habitat selection in a large hydropeaking river: strong individual and temporal variations revealed by telemetry. Sci. Total Environ. 578, 109–120. https://doi.org/10.1016/j.scitotenv.2016.10.155.

Carr, K., Tu, T., Ercan, A., Kavvas, M., Nosacka, J., 2015. Two-dimensional Unsteady Flow Modeling of Flood Inundation in a Leveed Basin. World Environmental and Water Resources Congress 2015, pp. 1597–1606 https://doi.org/10.1061/9780784479162.156.

Chen, T., Joly, A., Pan, R., Ji, P., He, M., Chen, G., 2015. A methodology to analize the safety of a coastal nuclear power plant against the typhoon external flooding risks. J. Nucl. Radiochem. Sci. 3 (1), 7. https://doi.org/10.1115/1.4034974.

DKKV, 2015. Das Hochwasser im Juni 2013: Bewährungsprobe für das Hochwasserrisikomanagement in Deutschland. DKKV-Schriftenreihe 53, Deutsches Komitee Katastrophenvorsorge, Bonn, Germany. http://www.dkkv.org/fileadmin/user_upload/Veroeffentlichungen/Publikationen/DKKV_53_Hochwasser_Juni_2013.pdf

Dorfman, C., Harb, G., Zenz, G., 2012. Simulation of Hydrodynamic and Sediment Transport Processes – Two Austrian Case Studies. XIXth TELEMAC-MASCARET User Conference 2012, pp. 53–58. https://hdl.handle.net/20.500.11970/104215.

Duc, B.M., Bernhart, H.H., Kleemeier, H., 2005. Morphological numerical simulation of flood situations in the Danube River. Int. J. River Basin 3 (4), 283–293. https://doi.org/10.1080/15715124.2005.9635268.

Ertl, O., 1940. Der mittlere jährliche Gang des Wasserhaushalts der Saalach. Archiv für Wasserwirtschaft. 54. Reichsverband der Deutschen Wasserwirtschaft, Berlin.

Eybl, J., Godina, R., Lalk, P., Lorenz, P., Müller, G., Pavlik, H., Weilguni, V., Heilig, M., 2013. Hochwasser im Juni 2013–Die hydrographische Analyse. The Austrian Federal Ministry of Agriculture, Forestry, Environment and Water Management, Vienna, Austria. https://www.bmlfuw.gv.at/dam/jcr:c9a7d559-390a-4733-9888-acf8dc77a917/Hochwasser-VII3_Juni%202013-Hydrografie_1A_HP.pdf.

Gostner, R., 2005. Sohlrampe Saalach km 4,600 Bauentwurf/Einreichdetailprojekt. Technischer Bericht Ingenieurbüro Gostner und Aigner, Wals, Austria. http://geowasser.at/wp-content/referenzen/referenzdatenblaetter/WW_Seite3_Zeile7_Saalach-Sohlrampe_km_4-6.pdf.

Guan, M., Wright, N., Sleigh, P.A., 2015. Multiple effects of sediment transport and geomorphic processes within flood events: Modelling and understanding. Int. J. Sediment Res. 30 (4), 371–381. https://doi.org/10.1016/j.ijsrc.2014.12.001.

Guan, M., Carrivick, J.L., Wright, N.G., Sleigh, P.A., Staines, K.E.H., 2016. Quantifying the combined effects of multiple extreme floods on river channel geometry and on flood hazards. J. Hydrol. 538 (Supplement C), 256–268. https://doi.org/10.1016/j.jhydrol.2016.04.004.

Habersack, H., Kreisler, A., Rindler, R., Aigner, J., Seitz, H., Liedermann, M., Laronne, J.B., 2017. Integrated automatic and continuous bedload monitoring in gravel bed rivers. Geomorphology 291, 80–93. https://doi.org/10.1016/j.geomorph.2016.10.020.

Hajivalie, F., Arabzadeh, A., 2017. JAWRA Journal of the American Water Resources Association Science of the Total Environment. Int. J. Coast. Offshore Eng. 1 (1), 33–41. https://doi.org/10.18869/acadpub.ijcoe.1.1.33.

Hengl, M., 2014. Dimensionierung aufgelöster Rampen und praktische Erfahrungen. Forschung und Entwicklung zur Qualitätssicherung von Maßnahmen an Bundeswasserstraßen. Bundesanstalt für Gewässerkunde, Koblenz, Germany, pp. 119–123 https://doi.org/10.5675/BfG_Veranst_2015.1.

Hengl, M., Krouzecky, N., Baumer, A., Ulmer, B., 2007. Aufgelöste Rampe in der Saalach. Sohlrampe Saalach Fluss-km 4.6, Bundeswasserbauverwaltung, Salzburg, Austria. https://landversand.salzburg.gv.at/WebRoot/Store/Shops/Landversand/5252/A40F/7ED4/A3EA/16E9/4DEB/AE3E/2475/2043-20007-2007saalachrampe.pdf.

Hervouet, J.M., 2007. Hydrodynamics of Free Surface Flows: Modelling With the Finite Element Method. John Wiley and Sons, Chichester, England https://doi.org/10.1002/9780470319628.

Hunziker, R.P., 1995. Fraktionsweiser Geschiebetransport. 11037. Laboratory of Hydraulics, Hydrology and Glaciology (VAW), ETH Zürich, Zürich, Switzerland. https://doi.org/10.3929/ethz-a-001503776.

Janin, J.M., Lepeintre, F., Péchon, P., 1992. TELEMAC-3D: a finite element code to solve 3D free surface flow problems. In: Partridge, P.W. (Ed.), Computer Modelling of Seas and Coastal Regions. Springer Netherlands, Dordrecht, Netherlands, pp. 489–506 https://doi.org/10.1007/978-94-011-2878-0_36.

Lane, S.N., 2014. Acting, predicting and intervening in a socio-hydrological world. Hydrol. Earth Syst. Sci. 18 (3), 927–952. https://doi.org/10.5194/hess-18-927-2014.

LAWA, 2010a. Recommendation for the Establishment of Flood Risk Management Plans. 139. German Working Group on Water Issues of the Federal States and the Federal Government (LAWA), Dresden, Germany. http://www.lawa.de/documents/LAWA_HWRM-Plaene26032010_Text_Germany_ENG_337.pdf.

LAWA, 2010b. Recommendations for the Establishment of Flood Hazard Maps and Flood Risk Maps. 139. German Working Group on Water Issues of the Federal States and the Federal Government, Dresden, Germany. http://www.lawa.de/documents/LAWA_HWGK15062010_Text_Germany_ENG_f72_4d8.pdf.

LfU, 2014. Junihochwasser 2013. Wasserwirtschaftlicher Bericht, Bavarian Environment Agency Augsburg, Germany. https://media.hnd.bayern.de/berichte/Junihochwasser2013_2014-02-26_2.pdf.

LfU, 2017. Hochwassernachrichtendienst. http://www.hnd.bayern.de/pegel/inn/siezenheim-18643505/statistik.

Mattic, O., 2017. Telemac3d user manual. 7.2, EDF. online published. http://www.opentelemac.org/.

Meyer-Peter, E., Müller, R., 1948. Formulas for Bed-load Transport. Proc., Proceedings of the International Association for Hydraulic Research, IAHR pp. 39–64.

Moriasi, D.N., Arnold, J.G., Van Liew, M.W., Bingner, R.L., Harmel, R.D., Veith, T.L., 2007. Model evaluation guidelines for systematic quantification of accuracy in watershed simulations. Trans. Am. Soc. Agric. Eng. 50 (3), 885–900. https://doi.org/10.13031/2013.23153.

Moulinec, C., Denis, C., Pham, C.T., Rougé, D., Hervouet, J.M., Razafindrakoto, E., Barber, R.W., Emerson, D.R., Gu, X.J., 2011. TELEMAC: an efficient hydrodynamics suite for massively parallel architectures. Comput. Fluids 51 (1), 30–34. https://doi.org/10.1016/j.compfluid.2011.07.003.

Nelson, J.M., McDonald, R.R., Shimizu, Y., Kimura, I., Nabi, M., Asahi, K., 2016. Modelling flow, sediment transport and morphodynamics in rivers. In: Kondolf, G.M., Piegay, H. (Eds.), Tools in Fluvial Geomorphology. John Wiley & Sons, Ltd., pp. 412–455 https://doi.org/10.1002/9781118648551.ch18.

Nujic, M., 2002. Hydro_As-2d - Ein zweidimensionales Strömungsmodell für die wasserwirtschaftliche Praxis, Benutzerhandbuch (User Manual).

OpenStreetMap contributors, 2018. MapData. online:. https://www.openstreetmap.org.

Reisenbüchler, M., Bui, M.D., Rutschmann, P., 2016. Implementation of a new layer-subroutine for fractional sediment transport in Sisype. In: Bourban, S. (Ed.), Proceedings of the XXIIIrd Telemac-Mascaret User Conference. HR Wallingford Ltd, Wallingford, England , pp. 215–220. http://www.opentelemac.org/images/clubu/2016/XXIII-TELEMAC-MASCARET-user-conference-2017.pdf.

Ricci, S., Piacentini, A., Weaver, A., Ata, R., Goutal, N., Lollino, M.A.G., 2015. Variational data assimilation with telemac. Proof of concept for model state correction on the berre lagoon 3D-model. In: Guzzetti, F., Culshaw, M., Bobrowsky, P., Luino, F. (Eds.), Engineering Geology for Society and Territory. Springer, Cham, Germany, pp. 633–637 https://doi.org/10.1007/978-3-319-09048-1_123.

Rickenmann, D., Badoux, A., Hunzinger, L., 2016. Significance of sediment transport processes during piedmont floods: the 2005 flood events in Switzerland. Earth Surf. Process. Landf. 41 (2), 224–230. https://doi.org/10.1002/esp.3835.

van Rijn, L.C., 1984. Sediment transport, part III: bed forms and alluvial roughness. J. Hydraul. Eng. 110 (12), 1733–1754. https://doi.org/10.1061/(ASCE)0733-9429(1984)110:12(1733).

Röthlisberger, V., Zischg, A.P., Keiler, M., 2017. Identifying spatial clusters of flood exposure to support decision making in risk management. Sci. Total Environ. 598 (Supplement C), 593–603. https://doi.org/10.1016/j.scitotenv.2017.03.216.

Sanyal, J., 2017. Uncertainty in levee heights and its effect on the spatial pattern of flood hazard in a floodplain. Hydrol. Sci. J. 62 (9), 1483–1498. https://doi.org/10.1080/02626667.2017.1334887.

Schramm, J.-M., 2012. Geologische Folgewirkung einer "nassen Grenze" – Zum kausalen Zusammenhang zwischen Napoleons Kriegen und technisch geologischen Problemen im Salzburger Stadtbereich. In: Angetter, D., Hubmann, B., Seidl, J. (Eds.), Berichte der Geologischen Bundesanstalt. Verlag der Geologischen Bundesanstalt (GBA), Vienna, Austria , pp. 344–374. http://www.zobodat.at/pdf/BerichteGeolBundesanstalt_96_0037-0044.pdf.

Shields, A., 1936. Application of Similarity Principles and Turbulence Research to Bed-load Movement. 167. Hydrodynamics Laboratory California Institute of Technology, Pasadena. https://authors.library.caltech.edu/25992/1/Sheilds.pdf.

Skublics, D., Blöschl, G., Rutschmann, P., 2016. Effect of river training on flood retention of the Bavarian Danube. J. Hydrol. Hydromech. 64 (4), 349–356. https://doi.org/10.1515/johh-2016-0035.

Stark, J., Plancke, Y., Ides, S., Meire, P., Temmerman, S., 2016. Coastal flood protection by a combined nature-based and engineering approach: Modeling the effects of marsh geometry and surrounding dikes. Estuar. Coast. Shelf Sci. 175, 34–45. https://doi.org/10.1016/j.ecss.2016.03.027.

Stephan, U., Hengl, M., 2010. Physical and numerical modelling of sediment transport in river Salzach. In: Dittrich, A., Koll, K., Aberle, J., Geisenhainer, P. (Eds.), River Flow 2010. Federal Waterways Engineering and Resarch Institute, Karlsruhe, Germany , pp. 1259–1265. https://hdl.handle.net/20.500.11970/99777.

StMUV, 2015. Hochwasserrisikomanagement-Plan für den bayerischen Anteil der Flussgebietseinheit Donau. Bavarian State Ministry of the Environment and Consumer Protection, Munich, Germany https://www.lfu.bayern.de/wasser/hopla_donau/doc/hwrmp_donau_endversion.pdf.

Tassi, P., Villaret, C., 2014. Sisyphe user's manual. 6.3, EDF, online published. http://www.opentelemac.org/.

Thieken, A.H., Kienzler, S., Kreibich, H., Kuhlicke, C., Kunz, M., Mühr, B., Müller, M., Otto, A., Petrow, T., Pisi, S., Schröter, K., 2016. Review of the flood risk management system in Germany after the major flood in 2013. Ecol. Soc. 21 (2), 12. https://doi.org/10.5751/ES-08547-210251.

Tu, T.B., Carr, K.J., Ercan, A., Trinh, T., Kavvas, M.L., Nosacka, J., 2017. Assessment of the effects of multiple extreme floods on flow and transport processes under competing flood protection and environmental management strategies. Sci. Total Environ. 607-608, 613–622. https://doi.org/10.1016/j.scitotenv.2017.06.271.

Villaret, C., Hervouet, J., Huybrechts, N., Van, L., Davies, A., 2009. In: Villaret, C., et al. (Eds.), Effect of bed friction on morphodynamic modelling: application to the central part of the Gironde estuary. CRC Press, Proceedings of the River, Coastal and Estuarine Morphodynamics Conference, pp. 890–899.

Villaret, C., Hervouet, J.-M., Kopmann, R., Merkel, U., Davies, A.G., 2013. Morphodynamic modeling using the Telemac finite-element system. Comput. Geosci. 53, 105–113. https://doi.org/10.1016/j.cageo.2011.10.004.

Vittecoq, M., Gauduin, H., Oudart, T., Bertrand, O., Roche, B., Guillemain, M., Boutron, O., 2017. Modeling the spread of avian influenza viruses in aquatic reservoirs: a novel hydrodynamic approach applied to the Rhône delta (southern France). Sci. Total Environ. 595, 787–800. https://doi.org/10.1016/j.scitotenv.2017.03.165.

Wilcock, P.R., Crowe, J.C., 2003. Surface-based transport model for mixed-size sediment. J. Hydraul. Eng. 129 (2), 120–128. https://doi.org/10.1061/(ASCE)0733-9429(2003)129:2(120).

Wu, W., 2004. Depth-averaged two-dimensional numerical modeling of unsteady flow and nonuniform sediment transport in open channels. J. Hydraul. Eng. 130 (10), 1013–1024. https://doi.org/10.1061/(ASCE)0733-9429(2004)130:10(1013).

Wu, W., 2007. Computational River Dynamics. Taylor & Francis, London.

WWA-TS, 2013. In: Heinz, R., Prokoph, R., Skublics, D. (Eds.), Dataset for the Analysis of the Saalach Flood in 2013.

WWA-TS, 2016. Umsetzungskonzepte für die Flusswasserkörper 1-F652 Saalach mit Saalachstausee bis unterhalb Piding und 1-F653 Saalach von unterhalb Piding bis Mündung in die Salzach. EG-Wasserrahmenrichtlinie, Wasserwirtschaftsamt Traunstein, Traunstein, Germany http://www.wwa-ts.bayern.de/fluesse_seen/massnahmen/wrrl_saalach/doc/wrrl_saalach.pdf.

Zitka, H.-R., 1959. Die wirtschaftlichen Veränderungen im bayerischen Raum zwischen Inn und Salzach. Schriften des Instituts für Kultur-und Solzialfoschung e. 6. Edmund Gans Verlag, Munich, Germany.

Chapter 4

Enhancement of a numerical model system for reliably predicting morphological development in the Saalach River

Enhancement of a numerical model system for reliably predicting morphological development in the Saalach River

Markus Reisenbüchler, Minh Duc Bui, Daniel Skublics & Peter Rutschmann

Accepted author version posted online: 14 Jun 2019.
Published online: 01 Jul 2019.

Submit your article to this journal ☐

Article views: 10

View Crossmark data ☐

Taylor & Francis
Taylor & Francis Group

RESEARCH PAPER

Check for updates

Enhancement of a numerical model system for reliably predicting morphological development in the Saalach River

Markus Reisenbüchler [a], Minh Duc Bui [a], Daniel Skublics [b] and Peter Rutschmann [a]

aChair of Hydraulic and Water Resources Engineering, Technical University of Munich, Munich, Germany; bWasserwirtschaftsamt Rosenheim, Rosenheim, Germany

ABSTRACT

Rivers are dynamic systems, changing over time on their own or due to engineering measures and structures. At rivers which are regularly monitored, information on sediment balance can be used to evaluate the morphological development and to assess the impact of such measures. In this paper, we show that the performance of a numerical model can be improved by quantify boundary conditions, and that the simulation results of such a well-developed model will be more useful for civil engineers. As a case study, we develop a model system based on TELEMAC-SISYPHE to study the morphology of the Saalach River, where erosion and sedimentation impacts local ecology and human safety. Based on the available measurements and a sediment balance concept, we estimate the amount of sediment supplied to the river section downstream of a reservoir as well as the volume of the bed sediment transported along the river channel in different years. Using this information as boundary conditions for calibration and validation cases, the model provides a realistic and accurate representation of the river. Furthermore, our model has been successfully employed on the Saalach River to evaluate an alternative strategy for a more sustainable river management.

1. Introduction

Any changes in a river affect its characteristics. The most challenging factor may be climate change leading to higher variability in precipitation and consequently, flow discharge (IPCC 2013). Since a close relationship exists between water flow and sediment transport, climate change may alter sediment loads (Ateeq-Ur-Rehman et al. 2018) as well as river morphology. Besides climate change, a river is itself a dynamic system driven by morphodynamic processes, whose complexity makes developing management strategies challenging (Frings and Ten Brinke 2017). The shape of a river changes due to the input and system drivers, which are primarily water discharge and available sediment loads (Vriend 2015). In particular, great morphological changes are expected during high water conditions. However, the likelihood and occurrence interval of large flood events are difficult to predict. In addition to natural phenomena, engineering structures may have significant influence. For example, due to dam construction sediments become trapped in reservoirs, which may lead to a deficit of sediment and erosion in downstream sections. Moreover, straightening and hence shortening rivers heightens slopes, and increases flow velocities, thus leading to an increased sediment transport capacity, which can also drive river erosion. Normally, the impact of measures and countermeasures are not immediately visible, which makes evaluating and monitoring a river challenging (Parsons 2012). As sediment transport rates can only be accurately measured over time with great difficulty and is a present topic in research (Guerrero et al. 2015, Guerrero et al. 2016, Habersack et al. 2017), the data of sediment transport with detailed spatial and temporal resolutions in rivers is quite limited.

At locations without measurement of sediment fluxed, the sediment budged or balance concept can be applied to describe the morphological character and river development and provide guidance for sediment management (Frings et al. 2014, Wang et al. 2014, Reid and Dunne 2016, Hahn 2017, Hillebrand and Frings 2017). Reid and Dunne (1996) claimed that, sediment budget integrates sources and sinks from upstream to the downstream section of a channel. Such sediment budgets and their temporal development over several years can be used to estimate the impact of measures or to detect trends in river morphology from the past. However, sediment budgets can only be estimated quantitatively; they are not always sufficient for planning and designing river structures.

Numerical modelling is a more precise tool than sediment budgets to analyse morphological river processes. For a long time, one-dimensional models have been used to continuously simulate long periods. However, due to developments in computational technologies during the past few years, multidimensional hydromorphological simulations can be carried out for high temporal and spatial resolutions (Bui and Rutschmann 2010, Radice et al. 2012, Villaret et al. 2013). In order to predict hydromorphological processes realistically, the numerical model must be correctly set up, calibrated and validated, using available field data. However, continuous measurement for sediment transport is difficult and morphological data in the desired quality and quantity are not always available. Hence, one of the weak points of these numerical models is correctly representing the morphological boundary conditions.

In this paper, we present a reliable and consistent integrative modelling approach, which combines the benefits of

---

sediment budgets with conventional numerical modelling to overcome the above-mentioned limitations. The suitability of the model concept is verified by applying it to the Saalach River to examine morphological developments and to present an alternative sediment management strategy.

2. Study site and data

The Saalach is an alpine river in southeastern Germany. River regulation and hydroengineering measures along the river have led to significant changes in flow, sediment transport, and the morphology. The study site is one lower section of the river, which reaches from the Dam Kibling at $x = 20.6$ km to its confluence into the Salzach River at $x = 0.0$ km. The data used in this study were provided by the regional water agency, the Wasserwirtschaftsamt Traunstein (WWA-TS) (WWA-TS 2013). The data elevations refer to the German height system in metres above sea level.

Figure 1 provides an overview of the study region with several points of interest along the river. Since 1976, the water discharge at the Siezenheim gauging station ($x = 5.5$ km) has been measured every 15-minutes. Analyzing these data from 1976 to 2015 yields a statistical mean discharge MQ = 39m³/s, a statistical mean flood discharge MHQ = 436m³/s, and a statistical 100 year return period flood discharge HQ$_{100}$ = 1,093m³/s (BMLFUW 2015). This section has completely lost its meandering character, as it was forced into a straight trapezoidal shaped channel (Reisenbüchler et al. 2019). Furthermore, the river training leads to high imbalances in the sediment transport in this section. The Kibling

Dam (built in 1913 at $x = 20.6$ km), for example, has the greatest impact on the river morphology, because almost all incoming sediments became trapped in the reservoir. Observations from the years 1969–1984 show that an average rate of 95,000m³ of sediment was transported annually into the reservoir and remains there. To counteract this unintended sedimentation, excavations had been carried out at the headwater (Weiss 1996). Since its construction, no other dam of this size has been constructed on the upstream section; therefore, the amount of incoming sediments remains approximately the same for each year. However, weirs and barrages were constructed in the downstream reach, to regulate the water depth and have altered the sediment regime of the river. As can be seen in Figure 1, at $x = 8.0$ km an unregulated weir, the Zollhauswehr, was built in 1992. Further downstream, at $x = 2.4$ km the HPP Rott was built in 1941 to stabilize the riverbed and protect the upstream railway bridge at $x = 3.0$ km from scour. After reaching its lifespan in 2004, the HPP was rebuilt 100 m downstream of the original location. The HPP Rott operator measures the upstream water surface hourly, following a defined weir operating ordinance, which is for instance a water level of $WSE = 415.80$ m during normal flow. If the discharge exceed the ten-year flood event of $HQ_{10} = 630 \frac{m^3}{s}$ the water surface elevation must be lowered to $WSE = 414.00$ m.

All of these structures have resulted in riverbed degradation and erosion to finer sediment layers in some regions, which affect the stability of embankments and the ecosystem along the river (Reisenbüchler et al. 2019). As a countermeasure, the WWA-TS performs an artificial sediment transfer at the Dam Kibling (at $x = 20.6$ km). The material annually excavated from the reservoir is now partially dumped back into the river downstream of the dam. From 1999 until 2013 an average rate of 50,000m³/yr (including voids) was returned to the river, a volume which is lower than the expected natural transport rate. However, defining this rate is a critical point, as several factors influence it, such as annual flood magnitude and frequency, and the operation of the HPP Rott located downstream at $x = 2.4$ km. The impact of the supplied material is monitored indirectly, by measuring cross-sectional profiles of the riverbed every 200 m along the river channel every few years. For the current study, such cross-sectional profiles are available from three different measurement campaigns, namely 12.2005–04.2006, 02.2009, and 10.-12.2013. No measurements of bedload transport rates are available in this region. However, some data on the riverbed granulometry were obtained from a drill core programme carried out along the river in 1997.

3. Methodology

Like most rivers, defining morphological boundary conditions for our numerical model of the Saalach River includes high uncertainty, especially as data are limited. In this work, we develop a hydromorphological model system, where a sediment balance concept is incorporated to overcome this limitation. First, we estimate the sediment balance for the section from $x = 20.6$–8.0 km to verify the morphological boundary conditions, which will then be used to calibrate and validate our numerical model for the river section from $x = 8.0$–2.4 km. Finally, our model will be applied to develop an alternative sediment management strategy for the river.

Figure 1. Overview of the study site (Adapted from (Reisenbüchler et al. 2019)).

For the model, we apply the free software TELEMAC-MASCARET, where the two dimensional hydrodynamic solver TELEMAC2D (here denoted as T2D) is coupled with the sediment transport module SISYPHE (here denoted as SIS). In this paper, a modified version of SIS extended by (Reisenbüchler et al. 2016a), is used to provide a more stable and accurate numerical solution for fractional sediment transport.

3.1. Sediment balance concept

The sediment balance of a particular river section takes into account the sum of all input $(QS_{in}(t))$ and output sediment fluxes $(QS_{out}(t))$ over a defined time interval $[t_1; t_2]$. In the following, the sum of sediment fluxes over time is denoted as $\overline{QS} = \int_{t_1}^{t_2} QS(t)dt$. The difference in the total fluxes must be equal to the change of the riverbed volume in the domain from the beginning of the interval (V^{t_1}) to the end (V^{t_2}) (Slaymaker 2003, Frings and Ten Brinke 2017). In balancing of volumes, one must consider the bed porosity n, defined as follows:

$$n = \frac{V_{\text{voids}}}{V_{\text{total}}} = 1 - \frac{V_{\text{mass}}}{V_{\text{total}}} \quad [/] \quad (1)$$

Where V_{voids} = the volume of voids and V_{mass} = the volume of the material without porosity and V_{total} = the volume of the material in the section with porosity.

The final sediment balance is Equation 2, where we included a term S to describe local sources like dredging $(S < 0)$ or feeding $(S > 0)$ within the section. In this balance, all volumes are considered without porosity.

$$\overline{QS}_{in} - \overline{QS}_{out} + S = V^{t_2} - V^{t_1} = \Delta V \quad (2)$$

The total input $\overline{QS}_{in}$ and output $\overline{QS}_{out}$ can be derived from measured sediment loads and defined sediment supply rates over time. Bathymetrical information, like riverbed cross-sectional profiles or digital elevation models (DEM), defines the bed sediment volume V^t at time t in the section. Several methods can be applied to approximate this volume (Martin and Church 1995, Fuller et al. 2003, Reid and Dunne 2016). Following the approach of LfU (2008), first, we define two boundary points (on the left and right banks), which are used together with the bed elevation to estimate the cross-section area between these two boundary points. A mean riverbed elevation is defined based on the calculated cross-section area and width. We can now calculate the bed material volume between two cross-sections (see Figure 2).
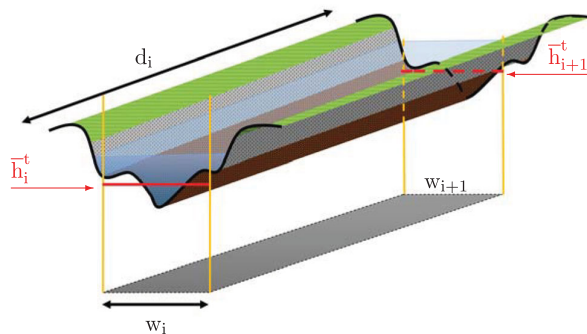
The two boundary points separate the fixed embankment from the movable riverbed and remain unchanged for the whole evaluation period. This approach is useful for regulated rivers with fixed embankments.

Using the Obelisk formula and the bed elevation, the bed material volume V^t between two cross sections can be calculated as follows (Harris and Stöcker 1998):

$$V^t = \frac{1}{6} d_i (2\bar{h}_{i+1}^t w_{i+1} + \bar{h}_i^t w_{i+1} + \bar{h}_{i+1}^t w_i + 2\bar{h}_i^t w_i) \quad (3)$$

where i and $i + 1$ = numbering of two cross sections; d_i = distance between these two profiles [m]; $\bar{h}_i^t$ = mean riverbed elevation at time t and cross section i $[m]$ and w_i = width between two boundary points of cross section i. Similar symbols are used for the cross section $i + 1$.

As can be seen in Equation 2, the total volume $\overline{QS}_{out}$ of output sediment fluxed can be calculated, if the volumetric change ΔV, the total volume $\overline{QS}_{in}$ of input sediment fluxes and the volumetric source S are known. It is similar for calculating $\overline{QS}_{in}$ based on the defined values of $\overline{QS}_{out}$, ΔV and S (Kondolf and Matthews 1991).

Furthermore, we apply the so-called sediment-rating-curve (SRC) approach to estimate the temporal sediment transport rates from the total volume $\overline{QS}$, which provides an explicit relation between the water Q and sediment QS discharges (Ferguson 1986, Gaeuman et al. 2018) as follows:

$$QS(t) = a[Q(t) - Q_c]^b \quad (4)$$

where Q_c = the threshold discharge of bed sediment motion, which provides a more appropriate version of standard two-parameter SRC for coarse gravel bed rivers. According to Gaeuman et al. (2018), the exponent b represents the overall character of the river and is relatively consistent along the channel, but the coefficient a depends on the active channel width and particle size and is subject to temporal changes. One of the two functional coefficients (e.g. b) has to be estimated based on available information or local expertise. The remaining coefficient (e.g. a) is then defined solving the following equation:

$$\overline{QS} = \int_{t_1}^{t_2} a[Q(t) - Q_c]^b dt \quad (5)$$

where the total volume $\overline{QS}$ was previously calculated based on the sediment balance concept mentioned above. After defining the values of a, b and Q_c, Equation 4 can be applied as a boundary condition for morphological calculation.

3.2. Hydrodynamics

In this study, we use the flow module T2D, which is based on the depth-averaged, 2D Shallow-Water-Equations (SWEs), including turbulence models. Ata (2017) and Hervouet (2007) provide a detailed description of the module. The SWEs are normally suitable for free-surface river engineering problems, when the river width is significantly larger than the water depth and vertical velocities are negligible. The module T2D has already been successfully applied to a shorter section of the Saalach River, where a comparative analysis of the two and three-dimensional models showed no clear difference (Reisenbüchler et al. 2019). Therefore, we assume that the 2D approach is similarly valid for this longer part of the Saalach River, where the river channel consists of the same

Figure 2. Evaluation of riverbed volume at a certain time t between the cross section i and the upstream located one $i + 1$ using the width w between the evaluation boundaries, the distance d, and the mean riverbed elevation $\bar{h}$.

regular and trapezoidal shape as in the previously investigated section.

3.3. Morphodynamics

In the TELEMAC-MASCARET system, the morphological module SIS is coupled to the hydrodynamic module using a quasi-steady-state approach. In SIS, sediment transport is divided into suspended load and bedload. The module is capable of representing multi-grain approaches like hiding/exposure effects and riverbed armoring. The SIS module is based on a mass-conservation equation – the ExnerEquation – to update the riverbed (Tassi and Villaret 2014). The driving force and most important parameter for sediment transport is the bottom shear stress, the flow induced force acting on the sediment particle. In SIS the bottom shear stress τ_B [kg/ms^2] is calculated as follows:

$$\tau_B = \frac{1}{2}\rho_{\text{water}}C_d|U| \tag{6}$$

$$C_d = \frac{2g}{k_{st}^2}\frac{1}{h^{1/3}} \tag{7}$$

where $|U|$ [(m/s)^2] denotes the quadratic norm of the two dimensional flow vector, ρ_{water}[kg/m^3] the density of water and C_d [/] the quadratic friction coefficient, taking into account the gravity g [m/s^2], the prescribed Strickler coefficient k_{st} [m$^{\frac{1}{3}}$/s] of the riverbed, and the water depth h [m] (Tassi and Villaret 2014). In this study, we apply the modified SIS module from the Chair of Hydraulic and Water Resources Engineering, TUM, where the fractional sediment transport module has been improved for accurate and more stable simulations (Reisenbüchler et al. 2016a, Reisenbüchler et al. 2019). In this paper, the fractional bedload transport equation from Hunziker (1995) is applied. This formula is an extension of the Meyer-Peter and Müller (MPM) formula, which is widely applied in gravel bed rivers (Meyer-Peter and Müller 1948). A feature of the Hunziker transport formula is its ability to reproduce processes like riverbed armouring, and grain sorting for multi-grain simulations. In the following the components of this equation are provided:

$$q_B = \sum_{i=1}^{N} q_{B,i} \tag{8}$$

$$\Phi_{\text{dms},i} = C*F_i*(\phi_i(\Theta'_{\text{dms}} - \Theta_{\text{cm}}))^{3/2} \tag{9}$$

$$\Phi_{\text{dms},i} = \frac{q_{B,i}}{(s-1)^{1/2}\,g^{1/2}d_{\text{ms}}^{3/2}} \tag{10}$$

$$\phi_i = \left(\frac{d_i}{d_{\text{ms}}}\right)^{-\alpha} \quad \text{with} \quad \alpha = (0{,}11*\Theta'_{\text{ms}})^{-3/2} - 0{,}3 \tag{11}$$

$$\Theta_{\text{cm}} = \Theta_{\text{crit}}*\left(\frac{d_{\text{mo}}}{d_{\text{ms}}}\right)^{0{,}33} \tag{11}$$

$$\Theta'_{\text{dms}} = \mu\frac{\tau_B}{g\rho_{\text{water}}(s-1)d_{\text{ms}}} \tag{13}$$

$$\mu = \left(\frac{k_{st}}{k_{st,r}}\right)^{3/2} \tag{14}$$

The total bedload transport q_B per unit width [m^3/sm] is the sum of the single transportrates $q_{B,i}$ [m^3/sm] for each

fraction i of N (Equation 8). The dimensionless transport rate $\Phi_{\text{dms},i}$ consists of a constant pre-factor, original $C = 5$, the availability of each grain class F_i [/] at the riverbed surface, a hiding/exposure-function ϕ_i and the relation between the dimensionless shear stresses Θ'_{dms} [/] and the modified critical Shields parameter Θ_{cm} [/] (Equation 9). Consequently, bedload occurs if the acting forces are higher than the critical threshold. Further, the dimensionless transport rate $\Phi_{\text{dms},i}$ is transferred into a volumetrically unit $q_{B,i}$, using the dimensionless relative density of the sediment $s = \rho_{\text{sediment}}/\rho_{\text{water}}$ [/], gravitational acceleration g [m/s^2], and the mean diameter of the riverbed surface (active layer) d_{ms} [m] (Equation 10). The hiding/exposure-function uses a relation of the grain diameter d_i to the mean diameter d_{ms} and an empirical coefficient taking into account that larger particles are exposed to the flow while smaller ones can hide (Equation 11). The resisting force is represented by a modified critical Shields parameter with $\Theta_{\text{crit}} = 0.047$ [/] and the relation between the diameter of the active layer d_{ms} [m] to the underlying subsurface layer d_{mo} [m] (Equation 12). The acting force is based on the bed shear stress τ_B [N/m^2](Equation 13). Additional, a relation between the Strickler value of the riverbed k_{st} [m$^{\frac{1}{3}}$/s] and the morphological form roughness $k_{st,r}$ [m$^{\frac{1}{3}}$/s] is incorporated by means of a dimensionless factor μ (Equation 14).

4. Model setup

4.1. Bathymetry

The numerically modelled river section begins at the Zollhaus weir ($x = 8.0$ km), passes a step-pool ramp ($x = 4.6$ km), and a railway bridge with a solid groundsill ($x = 3.0$ km), and ends at the HPP Rott ($x = 2.4$ km) (see Figure 1). The ponding area of the HPP Rott reaches from 2.4 km to 4.6 km. The engineering structures in Figure 1 are represented as non-erodible, as they consist of large stone settings, which can not be moved by the flow. The fine computational grid consists of 334,249 triangular element and has in the river channel an average edge size of 6.0 m, and coarser elements in the floodplain, up to 50 m. Figure 3
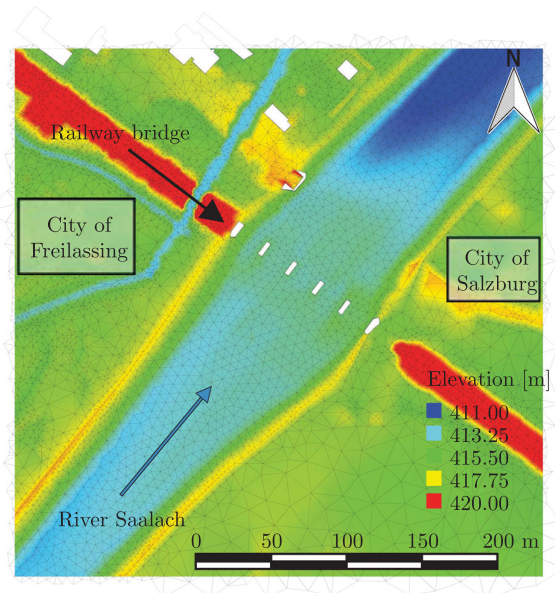

Figure 3. Section of the computational grid for the 2D numerical simulations of the area close to the railway bridge.

shows an exemplary section of the final computational grid. The time step was set to constant 3 sec, which provides numerically stable and fast results.

In total three different models are generated for this study, using the available riverbed information from the measurement campaigns as well as information on the floodplain from a digital elevation model. The first model, named MC, was used in the calibration and represents the Saalach from the end of 2005 to the first quarter of 2006. For validation, a second model (MV) was generated describing the Saalach in February 2009. For the scenario calculation, we created a third model (MS), which is based on the MC-model but with the following modifications:

- The fixed groundsill of the railway bridge at $x = 3.0$ km has been lowered by 2 m (from 413.85 to 411.80 m) – a measure undertaken after the flood event of 2013 to increase the flood capacity of the river in the future.
- Additionally, the authorities are modifying the modular step-pool ramp at $x = 4.6$ km, by reducing the artificial extension and removing the two highest stone bars. A detailed description of the stone ramp can be found in (Gostner 2005, Hengl et al. 2007, Reisenbüchler et al. 2019).

Figure 4 provides longitudinal sections of the mean riverbed along the channel for 2005, 2009, and 2013. From 2005 until 2009, the riverbed elevation aggregated continuously and has remained stable since. In particular, upstream of the ramp at $x = 4.6$ km, which was constructed in 2005/2006, the expected aggregation is clearly visible. Only in the most downstream section, from $x = 3.0$ km to $x = 2.4$ km, was the riverbed lower. This was caused by the flushing of sediments during the 2013 flood event (BMLFUW 2013).

4.2. Boundary and initial conditions

The riverbed consists mainly of coarse gravel, which is discretized into eight fractions $(d_i = 0.5;2;8;16;31.5;60;93;140$ [mm]), with a maximum diameter of $d_{\max} = 140$ mm. Since the bed material in the study is very coarse, only bedload transport is considered in our numerical model. According to the authorities, the grain size distribution as well as the mean diameter of the bed sediment varies along the river

reach and alters over time (WWA-TS 2013). For example, the mean grain size observed in 1997 was $d_m = 121$ mm. However, the mean diameter of the material, which has been supplied since 1999 at $x = 20.6$ km is finer ($d_m = 32$ mm).

In the absence of newer data, we use the grading curves from the 1997-measurement campaign to set up a temporal model, where the initial sediment distributions are assumed to be uniform in three different subdomains delimited by the open stone ramp at $x = 4.6$ km and the railway bridge at $x = 3.0$ km. We ran this temporal model for a constant mean flood discharge $MHQ = 436 \frac{m^3}{s}$ over six days and equilibrium boundary condition for sediment transport with morphological parameters (e.g. bed-load transport formula, shields parameter, hiding factor, etc.) used in (Reisenbüchler et al. 2019) and (Beckers et al. 2015). Figure 5 presents the normalized grain size distribution at the beginning and at the end of this numerical simulation in these three subdomains. In the simulation, the initially very coarse mean diameter became finer. The calculated mean grain size over the whole domain was $d_m = 37.7$ mm, a result also obtained by (Beckers et al. 2016). The results of the grain size distribution at the end of the simulation were then applied as an initial condition for the following calibration and validation. The bed structure in the vertical direction is divided into an active layer, an active stratum and a residual substrate layer.

Numerical simulations require reliable and accurate boundary conditions, namely flow and sediment (bedload) discharge [m³/s] at the inlet and water depth or water surface elevation [m] at the outlet. At the inlet at $x = 8.0$ km, we integrated the discharge values from the Siezenheim gauge. The observed water surface elevations in the reservoir at the HPP Rott ($x = 2.4$ km) were used for the outflow boundary condition. This information allows the model to represent the operation (i.e. the opening and closing of the different weirs) of the HPP correctly, without having to model the weirs directly. The bedload rates at the inlet were specified based on the sediment balance results, which are presented in the next section. At the outlet, the sediment can leave the domain undisturbed, depending on the flow velocity. When the water surface elevation at the HPP is equal to the storage level, the resulting velocities are so small that no sediment transport takes place directly at the outlet. If the water
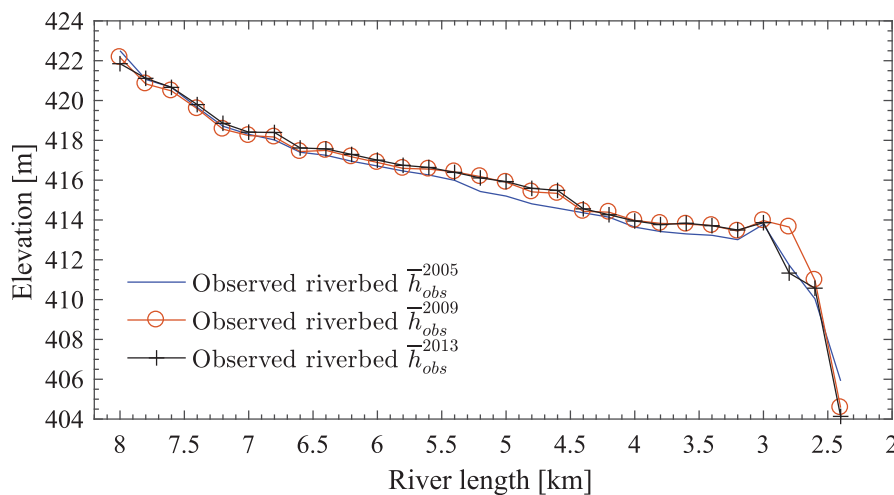
Figure 4. Longitudinal section of the observed mean riverbed elevation $\bar{h}$ at 2005, 2009 and 2013.
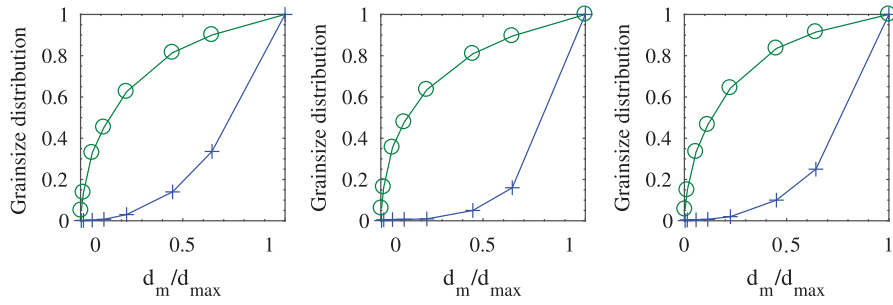
Figure 5. Normalized grain size distribution of d_m/d_{max} for initial riverbed composition in 1999 (blue, crosses) and after the initialization (green, circles) in three regions: left($x = 8.0$–4.6 km), middle ($x = 4.6$–3.0 km) and right ($x = 3.0$–2.4 km).

level is lowered, material can be mobilized and pass through the HPP, a process which happens during flood events caused by opening the weirs for instance.

4.3. Sediment balance

The sediment balance is derived from the Kibling dam at $x = 20.6$ km to $x = 8.0$ km for two periods, which corresponds to the calibration and validation period of the numerical models designed. As almost all sediments are trapped at the Kibling dam, the incoming sediment amount in the studied domain $\overline{QS}_{in} := \overline{QS}_{20.6}$ is defined only by the total sediment volume supplied in the given time frame (see Table 1). The supplied sediments' porosity is $n_{supply} = 0.32$. The additional sediment source S is based on the fact that during the 2013 flood event several embankments collapsed along this river section (WWA-TS 2013). Besides the high flooding period $\left(Q > 500 \frac{m^3}{s}\right)$ of this flood event, no additional sediment source is considered in the numerical models.

Using Equation 3, we evaluated the change of the sediment budget in this river section using the cross-sectional profiles measured every 200 m. A constant porosity for the riverbed as well as for sediment transport $n_{riverbed}$ is used in the models. Applying Equation 2, we calculated the total volume of sediment passing through the Zollhauswehr $\overline{QS}_{out} := \overline{QS}_{8.0}$, which we subsequently applied in the numerical models as the input bedload rates. Table 1 and Figure 6 show the calculated results of the sediment balance along the river reach. Over the calibration period (three years), a total sediment amount of 150,000m³ was supplied at $x = 20.6$ km to the river reach and about 195,000m³ passed through the Zollhauswehr. We consider a section between two neighbouring cross-sectional profiles, firstly when the riverbed is eroded, i.e. when $\overline{QS}_{out} > \overline{QS}_{in} + S$, and secondly when the sediments have accumulated on the riverbed, i.e. when $\overline{QS}_{out} < \overline{QS}_{in} + S$. It can be seen in Figure 6 that erosion and deposition occurred alternatively along this river reach. In total, during both periods more material left the domain.

The obtained volumes $\overline{QS}_{8.0}$ from the sediment balance had to be transferred to sediment fluxed $QS_{8.0}(t)$ for the

corresponding periods, to be applicable as boundary conditions for the numerical model. Therefore, we here applied the SRC-approach explained above, which requires information about the three parameters a, b and Q_c given $\overline{QS}_{8.0}$ (Equation 4 and 5). Additional analysis of the results from (Reisenbüchler et al. 2019) showed a clear threshold of motion at a flow discharge of $Q_c = 50 \frac{m^3}{s}$. Furthermore, Gaeuman et al. (2018) propose that the coefficient b for bed load curves is typically in a range of 2–4, where we defined the value as 2.2 to approximate the data from (Beckers et al. 2015, Beckers et al. 2016, Reisenbüchler et al. 2019). Having defined $\overline{QS}_{8.0}$, b and Q_c, the remaining parameter, here a, is calculated separately after solving Equation 5 for the calibration and validation period taking into account the flow hydrograph $Q(t)$. Finally we obtained the parameter $a_{calib} = 5.631 \times 10^{-7}$ and $a_{calib} = 2.180 \times 10^{-7}$. Furthermore, the volumes of collapsed embankments, which are indicated as a source in the mass balance of the validation period, had to be considered only during the high flows of the 2013 flood $\left(Q > 500 \frac{m^3}{s}\right)$, as we expected this correspond to the time they occurred. Otherwise, this additional volume would be averaged over the whole validation period. Therefore, one additional SRC was developed based on the volume of the embankment collapse S, the exponent $b = 2.2$, $Q_c = 50 \frac{m^3}{s}$, and the hydrograph during the flood peak, resulting in a coefficient $a_{peak} = 0.789 \times 10^{-7}$. In total three curves were developed with this methodology (Figure 7).

As we considered fractional sediment transport in this study, it was necessary to define a discharge dependent distribution of the supplied material. The WWA-TS provided us with information on the average transported grain size distribution over the long term -, gained from a different numerical hydromorphological model – where only discharges over $Q > 150 \frac{m^3}{s}$ were considered, (WWA-TS 2013). Therefore, we assumed this relation was valid for this range, but between $Q_c = 50 \frac{m^3}{s}$ and $150 \frac{m^3}{s}$, no information was available. To address this gap, we used the simulated fractional sediment transport data from (Reisenbüchler et al. 2016b, Reisenbüchler et al. 2019) and approximated a relation between

Table 1. Sediment balance for the Saalach River for calibration and validation period and the total sediment load at the Zollhauswehr $\overline{QS}_{8.0}$. The volumes in brackets are provided without voids.

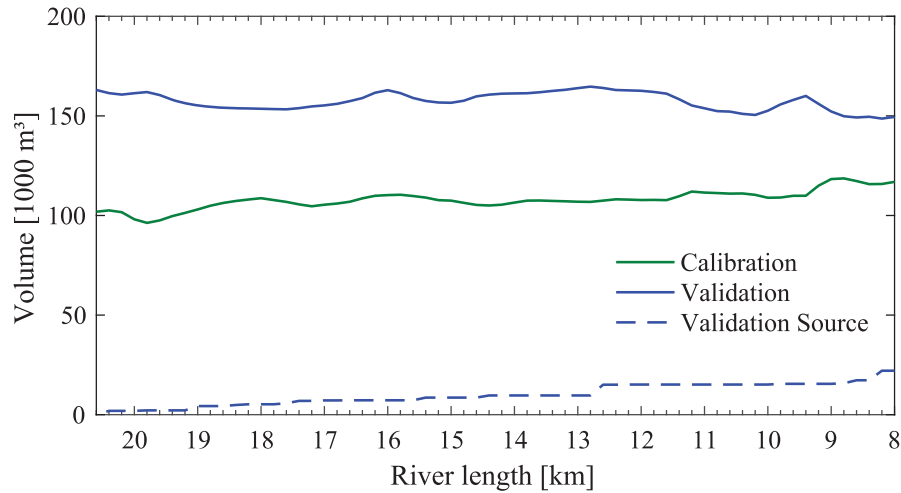|	Period	Input Kibling $\overline{QS}_{20.6}$ (1000 m³)	Source S (1000 m³)	Output $\overline{QS}_{8.0}$ (1000 m³)
Calibration	01.01.2006–01.03.2009	150.0 (101.9)	0	194.8 (116.9)
Validation	01.03.2009–31.12.2013	240.0 (163.0)	36.8 (22.1)	286.0 (171.6)

Figure 6. Sediment balance along the river for the calibration (green) and validation period (blue) and the sediment sources (blue dashed), which occurred during the 2013-flood in the validation period. (Values are without voids)

discharge and transported sediment material at the Saalach (Figure 8). With increasing discharge, the amounts of finer fractions (F1–F4) decrease and the coarser ones (F5–F8) increase correspondingly. For discharges higher than $Q = 150 \frac{m^3}{s}$ the shares remain constant.

5. Results and discussion

5.1. Calibration

We calibrated the model parameters by simulating three years from 01.01.2006 to 01.03.2009 on the geometry MC with the integrative model T2D + SIS, which couples hydrodynamic and morphodynamic. Thus, at the model inlet, measured discharge (Q) from the Siezenheim gauge was used, and the sediment was supplied according to the developed SRC (see Figure 7). At the outlet, the measured water surface elevation (WSE) at the HPP Rott was used. Figure 9 shows the hydrodynamic boundary conditions over the whole simulation period.

We evaluated the accuracy of the model using statistical goodness-of-fit criteria (GOF), such as the Nash-Sutcliffe-Efficiency (NSE), the coefficient of determination (R^2), the
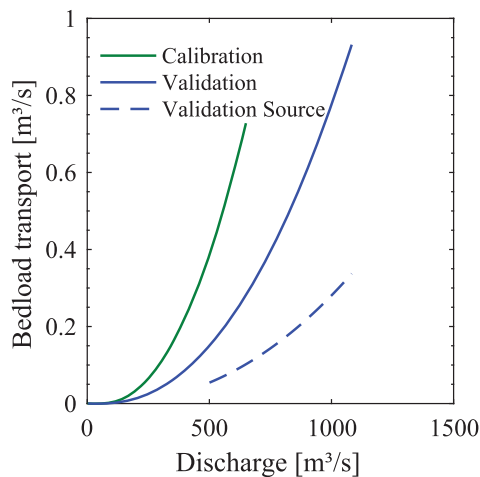
mean absolute error (MAE), and the root-mean-square-error (RMSE) (Moriasi et al. 2007). Available measurements along the channel were the maximum water elevations WSE_{obs}^{2006} during the flood event on 07.08.2006 ($HQ^{2006} = 650 \frac{m^3}{s}$, the peak indicated with a red star in Figure 9) and the cross-sectional riverbed profiles at the end of the period, which are additionally transferred into mean riverbed elevations $\bar{h}_{obs}^{2009}$.

During the calibration process the dominating morphological parameters (e.g. active layer thickness, C, Θ_{crit}, k_{st} and $k_{st,r}$) have to be determined. The thickness of the active layer was set to 0.14 m (= d_{max} of the sediment) (Gessler 1965, Suzuki and Kato 1991, Hunziker 1995). Application of the original bedload transport formula, provided in Section 3.3, led to an unrealistic low transportation of sediment and overly high depositions. We therefore applied a an increased pre-coefficient $C = 8$ (Equation 9), to increase the total sediment transport, following the original bedload equation from
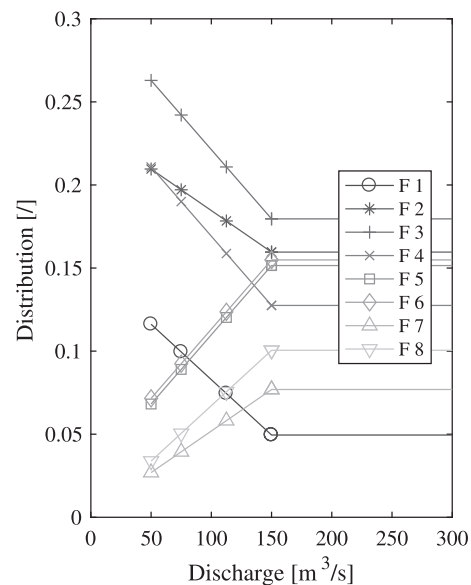

Figure 7. SRCs for calibration and validation.

Figure 8. Discharge depending grain distribution of each supplied fraction F_i at the inlet.
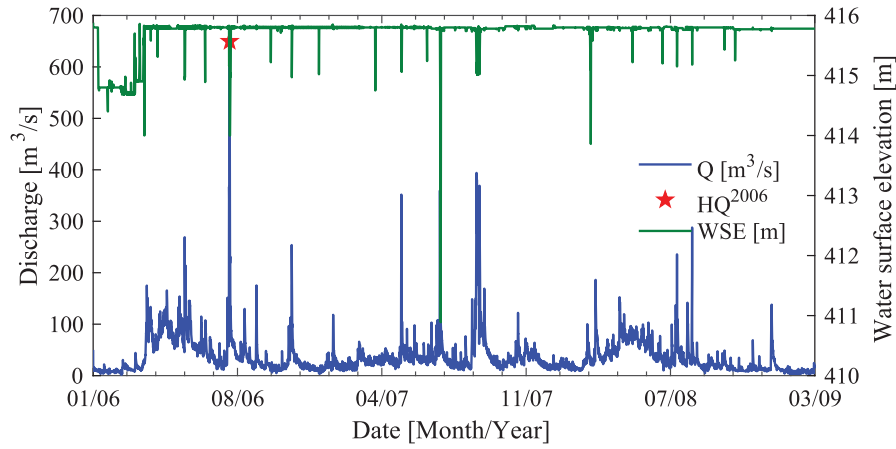
Figure 9. Hydrodynamic boundary conditions for the calibration period.

(Meyer-Peter and Müller 1948). In addition, the critical Shields-parameter for each fraction was lowered to $\Theta_{crit} = 0.04$ for all grain classes, also applied by (Beckers *et al*. 2016, Reisenbüchler *et al*. 2019) for numerical sediment models of the Saalach river. The hydrodynamic riverbed roughness was set as constant using a Strickler value of $k_{st} = 35 \frac{m^{1/3}}{s}$ in the main channel but changed at the steppool ramp at $x = 4.6$ km to $k_{st} = 20 \frac{m^{1/3}}{s}$ after (Gostner 2005), following the results from (Reisenbüchler *et al*. 2019). In the calibration, we identified the skin-friction correction factor μ as a very sensitive morphological parameter (Equation 14). We came to the conclusion that due to the coarse gravel character of the Saalach river, these formulas (Equation 8–14) for sediment transport do not work by default, as they calculate too low a force Θ'_{dms}. This is most likely because these formulas were derived in laboratory conditions for bed slopes 0.0004–0.023 and sediment diameters 0.38–28.65 mm (Meyer-Peter and Müller 1948, Smart and Jäggi 1983), but

not for conditions such as in the Saalach, with slopes of up to 0.047 and sediment diameters up to 140 mm. We therefore used the parameter μ from Equation 14 to modify Θ'_{dms}. This issue is also addressed by Rickenmann *et al*. (2006), whose introduced new semi-empirical formulas describing the ration between total roughness and morphological form roughness for steeper slopes. In addition, van Rijn (1984) propose equations for form resistance, derived on data from low land rivers. However, the characteristics of the Saalach do not fit into the range of these formulas, and are thus not suitable here. Moreover, we tried to keep our model as simple as possible, in the absence of measurements of bed load transport rates, and, therefore, performed a manual assessment of this parameter. We achieved a better agreement in the calibration than previously by tesing the morphological form roughness $k_{st,r}$ piecewise in a range of $15 - 50 \frac{m^{\frac{1}{3}}}{s}$, where changes in the river characteristics were observed (Figure 4). In the upper section $x = 8.0$–7.6 km and $x = 7.6$–
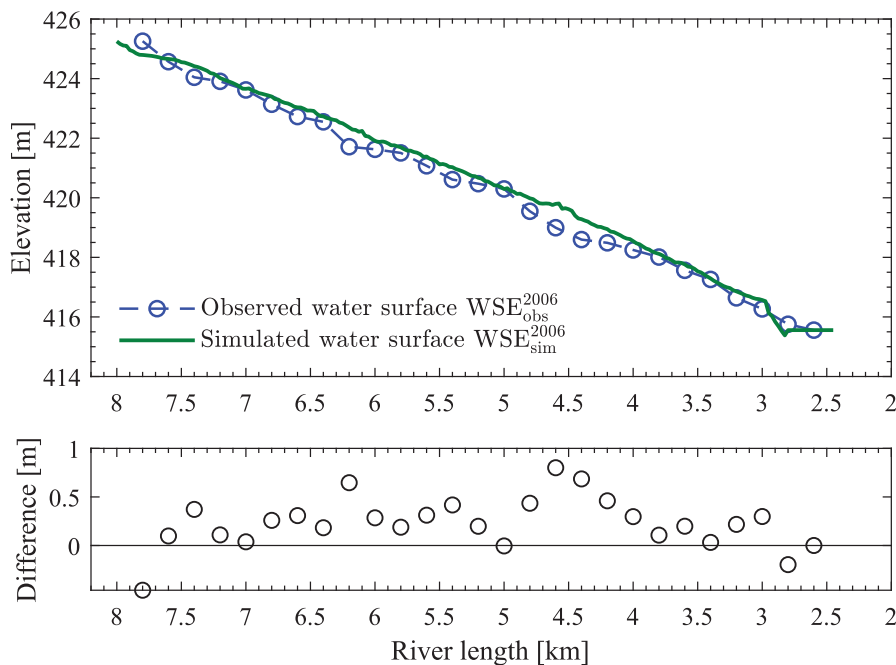

Figure 10. Longitudinal section of the maximum observed WSE_{obs}^{2006} (blue, circles) and simulated WSE_{sim}^{2006} (green) water elevations during the flood event HQ^{2006} at 07.08.2006.

7.0 km a form roughness of $k_{st,r} = 29.4\frac{m^{1/3}}{s}$ respectively $k_{st,r} = 24.6\frac{m^{1/3}}{s}$ yielded the best result. In the following sections, i.e. $x = 7.0$–4.6 km, $x = 4.6$–3.6 km and $x = 3.6$–3.0 km, a higher roughness of $k_{st,r} = 22.0$, 20.1 and 22.0 $\frac{m^{1/3}}{s}$ produces more accurate results. In the last section, which is directly in front of the HPP Rott, the same value as for the hydrodynamic roughness $k_{st,r} = 35\frac{m^{1/3}}{s}$ was applied.

With this setup, we were able accurately to reproduce the maximum water surface elevation during the 2006 flood event (Figure 10). Moreover, the observed riverbed at the end of the period was represented well by the model, visualized as a longitudinal section in Figure 11 and at three selected cross-sectional profiles in Figure 12. In addition to this visual comparison, the statistical GOF are provided in Table 2, which shows that the values were close to the optimum and the difference between observation and simulation was small. The model confirms that the initial riverbed in 2006 remained almost constant over the simulated period in the upper section, i.e. from $x = 8.0$–7.0 km. Downstream, continuous deposition can be seen in the 2009 measurements,

which were accurately reproduced by the simulation. This might have been caused by the construction of the step-pool ramp and the damming at the HPP Rott. According to the sediment balance (Table 1), in total $\overline{QS}_{in} := \overline{QS}_{8.0} = 194,800\,m^3$ material was supplied to the numerical model in this period, but only $\overline{QS}_{out} := \overline{QS}_{2.4} = 49,600\,m^3$ passes the outlet, meaning that the difference was deposited.

5.2. Validation

The morphological parameters, estimated in the calibration period, are validated in a second period from 01.03.2009 to 31.12.2013, whose boundary conditions are provided in Figure 13. In this period, an extraordinary high flood event occurred on 02.06.2013 with $HQ^{2013} = 1,100\,\frac{m^3}{s}$ (peak indicated by the red star in Figure 13).

The observed water surfaces WSE_{obs}^{2013} during this event were compared with the simulated WSE_{sim}^{2013} to validate the models' accuracy (Figure 14). The same was done
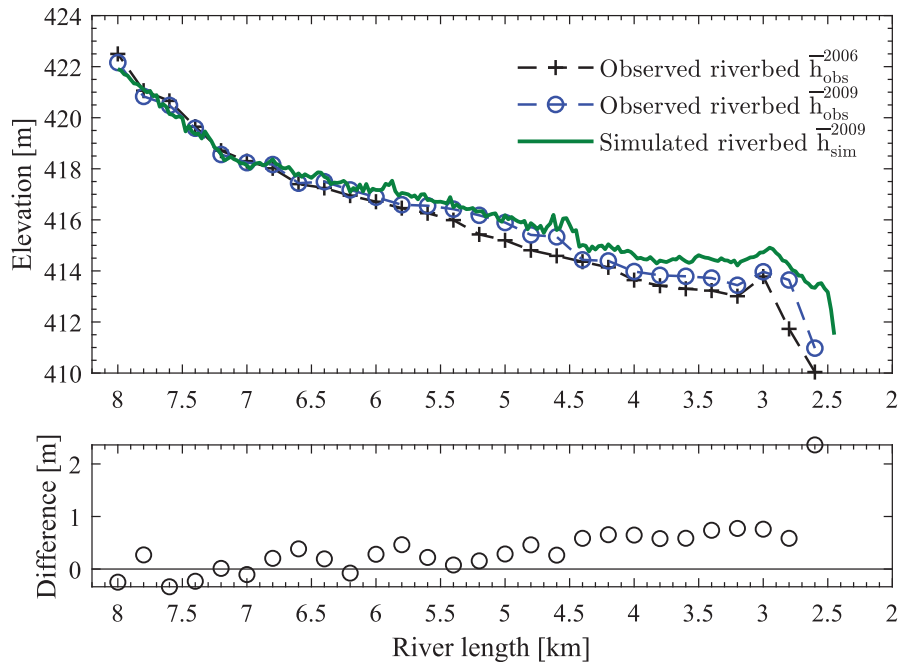

Figure 11. Longitudinal section of the initial $\bar{h}_{obs}^{2006}$ (black, crossed), observed final $\bar{h}_{obs}^{2009}$ (blue, circles) and simulated $\bar{h}_{sim}^{2009}$ (green) mean riverbed elevation for the calibration.
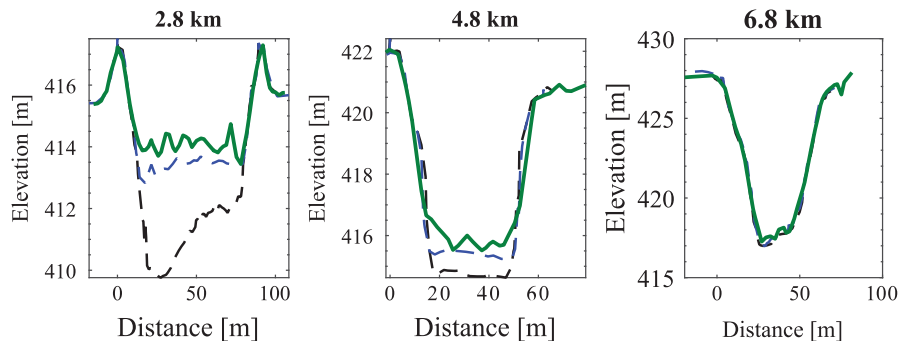

Figure 12. Comparison between observed initial h_{obs}^{2006} (black), observed h_{obs}^{2009} (blue) and simulated h_{sim}^{2009} (green) riverbed profile at three selected cross-sections for the calibration. Measurements starts orographically at left river bank.

Table 2. GOF values for the water elevation during the 2006 flood event WSE^{2006} and the 2009 mean riverbed elevation $\bar{h}^{2009}$ in the calibration.

Model	R^2	RMSE [m]	MAE [m]	NSE
WSE^{2006}	0.99	0.35	0.28	0.99
$\bar{h}^{2009}$	0.98	0.62	0.45	0.94

using the measured mean riverbed elevation along the channel $\bar{h}_{obs}^{2013}$ and the simulated $\bar{h}_{sim}^{2013}$ at the end of the period (Figure 15). In addition, Figure 16 shows three selected cross-sectional profiles. Next to the visual comparison, Table 3 provides the GOF values, indicating the very high accuracy of the simulation. The water levels were simulated accurately, despite the drop around $x =$ 7.0 km. Reasons for this difference might be due to errors in the observed data itself, as they were reconstructed

after the event and not measured directly. Moreover, such variations in slope cannot be really explained, as at this location there is not specific structure that might cause irregularities in the flow. The differences between the initial and final riverbed are fairly small, which means that relocation processes occurred mainly in this period, but there was no clear erosion or deposition. It is only in the section between the railway bridge and the HPP Rott $x =$ 3.0–2.4 km that large erosion can be recognized, which was a result of the opening of the weirs during the flood event. This is also clear from the difference between the total input in the domain $\overline{QS}_{in} := \overline{QS}_{8.0} = 286{,}000 \text{ m}^3$ and the simulated output $\overline{QS}_{out} := \overline{QS}_{2.4} = 332{,}600 \text{ m}^3$ at the HPP Rott. Material was mainly transported during the 2013 flood event, which led finally to the higher output as opposed to input. Our model, with the calibrated parameters, was able to reproduce these processes accurately.
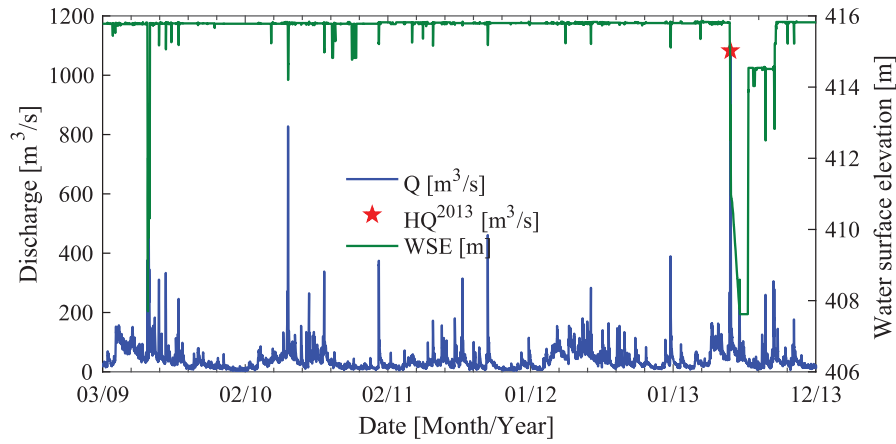

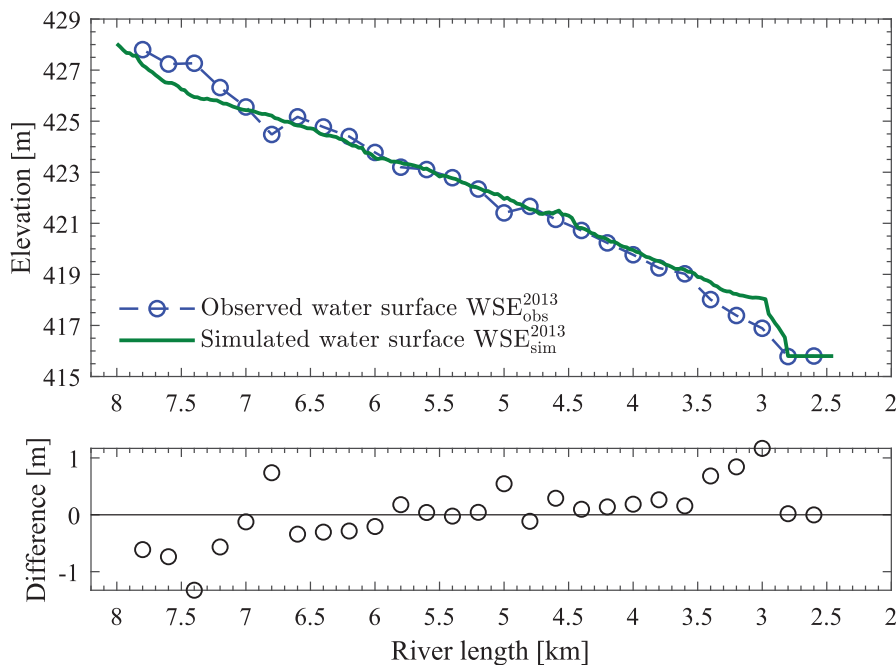**Figure 13.** Hydrodynamic boundary conditions for the validation period.

Figure 14. Longitudinal section of the maximum observed WSE_{obs}^{2013} (blue, circles) and simulated WSE_{sim}^{2013} (green) water elevation during the flood event at 02.06.2013.
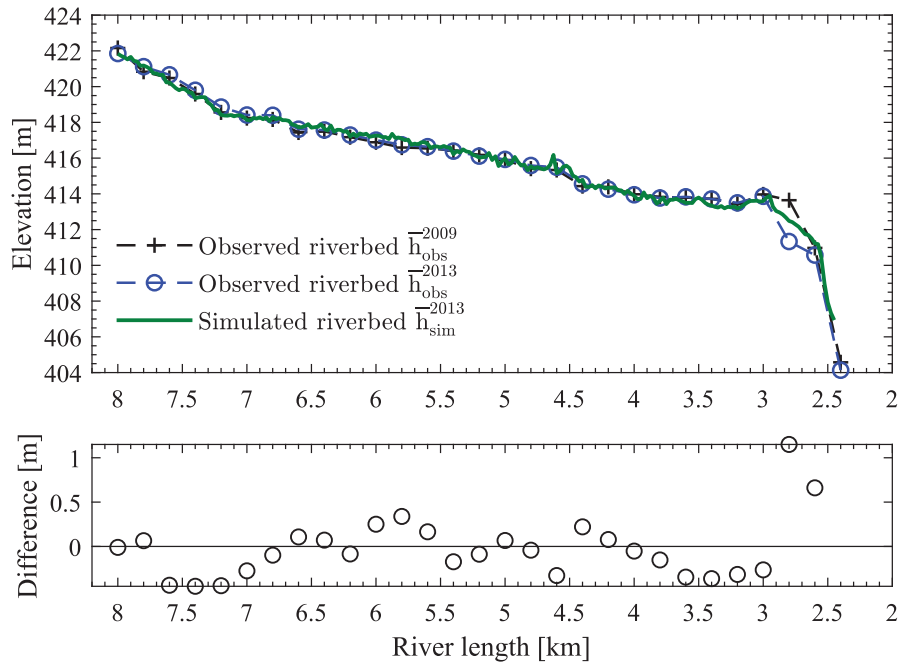
Figure 15. Longitudinal section of the initial $\bar{h}_{obs}^{2009}$ (black, crosses), observed $\bar{h}_{obs}^{2013}$ (blue, circles) and simulated $\bar{h}_{sim}^{2013}$ (green) mean riverbed elevation for the validation.

Table 3. GOF values for the water elevation during the 2013 flood event WSE^{2013} and the 2013 mean riverbed elevation $\bar{h}^{2013}$ in the validation.

Model	R^2	RMSE [m]	MAE [m]	NSE
WSE^{2013}	0.99	0.61	0.45	0.97
$\bar{h}^{2013}$	0.99	0.34	0.25	0.98

5.3. Scenario calculation

The riverbed directly before the HPP Rott had a very high elevation at the end of 2013, taking into account legal regulations and the flood capacity of the river. As Reisenbüchler *et al.* (2019) show, the flood event in 2013 led to a severe flood in this region, also a consequence of the high riverbed. We therefore generated a new geometrical model of this river section, named MS, which is a slight modification of the model MC (details above in Section 4.1). Using this model, we investigate an alternative management strategy for the Saalach River, leading to lower bedlevels in the reservoir. The strategy consisted of two main parts: first, the adaptation of the mean annual sediment supply downstream of the Kibling dam, and second, different operation of the HPP

Rott, which increased the effectiveness of reservoir flushing. The lowered ground sill below the railway bridge at $x = 3.0$ km was also a part of this strategy, as this modification should increase the effectiveness of flushing in the reservoir. We evaluated the strategy by simulating the whole period from 01.01.2006 to 31.12.2013, which was the calibration and validation period. This allowed us to compare the simulated scenario riverbed with the measured ones directly and evaluate the effectiveness.

Figure 17 shows the observed riverbed in 2006 and 2013, and the predicted riverbed at the end of the scenario calculation. Finally, we found that a reduced sediment supply $\overline{QS}_{in} := \overline{QS}_{8.0} = 320{,}000$ m³, which corresponds to an annular rate of $40{,}000\ \frac{m^3}{yr}$ at this section of the Saalach is sufficient enough to keep the free-flowing part of the riverbed stable over the simulated period. The amount can be regulated due to the artificial supply rates at the Kibling dam $x = 20.6$ km. Furthermore, the supplied material was transported more effectively through the HPP, thanks to a different weir operating ordinance, which includes the opening of the weirs for discharges higher than $Q > 250\ \frac{m^3}{s}$. At this
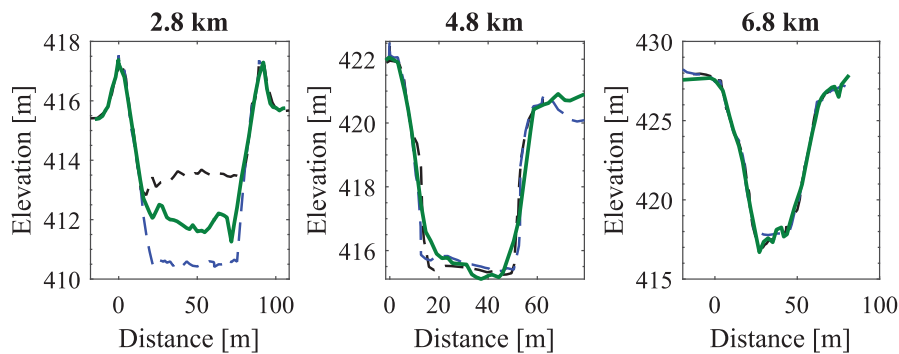

Figure 16. Comparison between observed initial h_{obs}^{2009} (black), observed h_{obs}^{2013} (blue) and simulated h_{sim}^{2013} (green) riverbed profile at three selected cross-sections for the validation. Measurements starts orographically at left river bank.
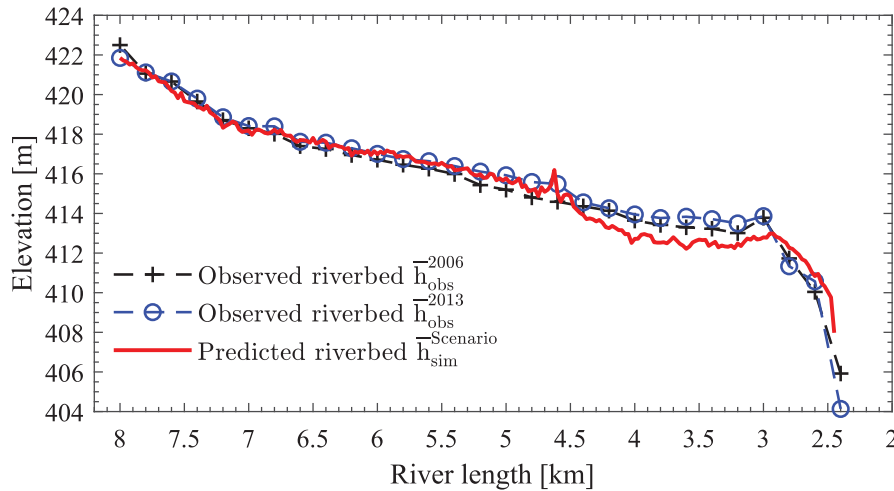
Figure 17. Longitudinal section of the initial $\bar{h}_{obs}^{2006}$ (black, crossed), observed $\bar{h}_{obs}^{2013}$ (blue, circles) and predicted $\bar{h}_{sim}^{2009\ Scenario}$ (red) mean riverbed elevation.

discharge level the HPP has to be shut down, so no loss of produced energy is created. Applying these boundary conditions to the model MS, led to a lower and more stable riverbed in the domain. The overall sediment output from the domain at the HPP Rott was in the simulated period $\overline{QS}_{out} := \overline{QS}_{2.4} = 384{,}000\,m^3$, which is higher than the input $\overline{QS}_{in} := \overline{QS}_{8.0} = 320{,}000\,m^3$. For comparison, in the calibration and validation an amount of $\overline{QS}_{in} := \overline{QS}_{8.0} = 480{,}800\,m^3$, $(194{,}800\,m^3 + 286{,}000\,m^3)$ reaches the domain, but less material $\overline{QS}_{out} := \overline{QS}_{2.4} = 382{,}200\,m^3$, $(49{,}600\,m^3 + 332{,}600\,m^3)$ left. This situation demonstrates that the management strategies we modelled are effective, as the whole reservoir was subsequently lower. Furthermore, the difference between in- and output fluxes in the scenario calculation was smaller, meaning that the river was closer to a state of equilibrium.

6. Conclusion

In this study, we have presented the concept of coupling sediment budget with numerical hydromorphological modelling. The benefit of this framework is that sediment balance can determine the quantity of sediment transport rates even with limited data available. Derived from cross-sectional riverbed measurements and known discrete sediment inputs in the domain, the transported sediment volume at a specific location can be evaluated. This methodology provides a reliable volumetric input for a numerical model. Even if the parameters of the necessary distribution function (here SRC) include some uncertainty, these affect only the distribution over the period, which has less effect than a false total input volume. We successfully applied this methodology to a real-world scenario at the Saalach River, where the morphological budget is heavily influenced by human interactions. Using the sediment balance approach, we were able to estimate reliable and accurate boundary conditions for the numerical model close to the region of interest. The only other alternative would be to numerically model the whole river section (18 km river length instead of 6 km), which would limit the suitability of the numerical model due to drastically increased simulation duration. The evaluated boundary conditions also allowed us to accurately calibrate and validate a hydromorphological model over a period of eight years in total within a short time of only four days on an HPC-system. With this well designed numerical model, we were able to investigate the balance between the minimum amount of sediment preventing further riverbed degradation and the maximum amount allowable to avoid sedimentation at an existing run-off-river HPP. The proposed concept might serve as a reference for other cases with similar problems.

Disclosure statement

No potential conflict of interest was reported by the authors.

ORCID

Markus Reisenbüchler http://orcid.org/0000-0002-3314-3468
Minh Duc Bui http://orcid.org/0000-0002-0756-7136
Daniel Skublics http://orcid.org/0000-0002-3672-7282
Peter Rutschmann http://orcid.org/0000-0002-9903-730X

References

Ata, R., 2017. *Telemac2d user manual*. online published: EDF.

Ateeq-Ur-Rehman, S., Bui, M., and Rutschmann, P., 2018. Variability and trend detection in the sediment load of the Upper Indus River. *Water*, 10 (1), 1–24.

Beckers, F., Noack, M., and Wieprecht, S., 2016. *Geschiebetransportmodellierung (GTM) Salzach und Saalach – Teilmodel 2: Untere Saalach -*. unpublished: Dept. of Hydraulic Engineering and Water Resources Management, Universität Stuttgart.

Beckers, F., *et al.*, 2015. Contribution of numerical modelling of sediment transport processes in river engineering: an example of the river Saalach. *36. IAHR World Congress*, 1–5.

BMLFUW, 2013. *Hydrografisches Jahrbuch von Österreich 2013*. Vienna, Austria: The Austrian Federal Ministry of Agriculture, Forestry, Environment and Water Management.

BMLFUW, 2015. *Hydrographisches Jahrbuch von Österreich 2015*. Vienna, Austria: The Austrian Federal Ministry of Agriculture, Forestry, Environment and Water Management.

Bui, M.D. and Rutschmann, P., 2010. Numerical modelling of non-equilibrium graded sediment transport in a curved open channel. *Computers & Geosciences*, 36 (6), 792–800.

Ferguson, R.I., 1986. River loads underestimated by rating curves. *Water Resources Research*, 22 (1), 74–76.

Frings, R.M. and Ten Brinke, W.B.M., 2017. Ten reasons to set up sediment budgets for river management. *International Journal of River Basin Management*, 16, 1–6.

Fuller, I.C., *et al.*, 2003. Reach-scale sediment transfers: an evaluation of two morphological budgeting approaches. *Earth Surface Processes and Landforms*, 28 (8), 889–903.

Frings, R.M., *et al.*, 2014. Today's sediment budget of the Rhine River channel, focusing on the Upper Rhine Graben and Rhenish Massif. *Geomorphology*, 204, 573–587.

Gaeuman, D., Stewart, R.L., and Pittman, S., 2018. Toward the prediction of bed load rating curve parameter values: the influence of scale, particle size, and entrainment threshold. *Water Resources Research*, 54 (5), 3313–3334.

Gessler, J., 1965. *Der Geschiebetriebbeginn bei Mischungen untersucht an natürlichen Abpflästerungserscheinungen in Kanälen*. Zürich: Eidgenössische Technische Hochschule.

Gostner, R., 2005. *Sohlrampe Saalach km 4,600 Bauentwurf/Einreichdetailprojekt*. Wals, Austria: Ingenieurbüro Gostner und Aigner.

Guerrero, M., *et al.*, 2015. A sediment fluxes investigation for the 2-D modelling of large river morphodynamics. *Advances in Water Resources*, 81, 186–198.

Guerrero, M., *et al.*, 2016. The acoustic properties of suspended sediment in large rivers: consequences on ADCP methods applicability. *Water*, 8 (1), 1–22.

Habersack, H., *et al.*, 2017. Integrated automatic and continuous bedload monitoring in gravel bed rivers. *Geomorphology*, 291, 80–93.

Hahn, C., 2017. Sediment management for the entire Danube. *Aqua Press International*, 2 (2017), 38–40.

Harris, J.W. and Stöcker, H., 1998. *Handbook of mathematics and computational science*. New York: Springer.

Hengl, M., *et al.*, 2007. *Aufgelöste Rampe in der Saalach*. Salzburg, Austria: Bundeswasserbauverwaltung.

Hervouet, J.M., 2007. *Hydrodynamics of free surface flows: modelling with the finite element method*. Chichester, England: John Wiley and Sons.

Hillebrand, G. and Frings, R.M., 2017. *Von der Quelle zur Mündung: Die Sedimentbilanz des Rheins im Zeitraum 1991–2010*. Leystad: CHR/International Comission for the Hydrology of the Rhine Basin.

Hunziker, R.P., 1995. *Fraktionsweiser Geschiebetransport*. Zürich, Switzerland: Laboratory of Hydraulics, Hydrology and Glaciology (VAW), ETH Zürich.

IPCC, 2013. *Climate change 2013: the physical science basis. contribution of working group I to the fifth assessment report of the intergovernmental panel on climate change*. Cambridge, United Kingdom and New York, NY, USA: Cambridge University Press.

Kondolf, G.M. and Matthews, W.V.G., 1991. Unmeasured residuals in sediment budgets: a cautionary note. *Water Resources Research*, 27 (9), 2483–2486.

LfU, 2008. *Merkblatt Nr. 5.4/1 Flussausstattung, Flussaufnahmen und deren Dokumentation*. (online): Bayerisches Landesamt für Umwelt.

Martin, Y. and Church, M., 1995. Bed-material transport estimated from channel surveys: Vedder River, British Columbia. *Earth Surface Processes and Landforms*, 20 (4), 347–361.

Meyer-Peter, E. and Müller, R., 1948. Formulas for bed-load transport. ed. *IAHR Congress, Stockholm, appendix 2*.

Moriasi, D.N., *et al.*, 2007. Model evaluation guidelines for systematic quantification of accuracy in watershed simulations. *Transactions of the American Society of Agricultural and Biological Engineers*, 50 (3), 885–900.

Parsons, A.J., 2012. How useful are catchment sediment budgets? *Progress in Physical Geography: Earth and Environment*, 36 (1), 60–71.

Radice, A., *et al.*, 2012. On integrated sediment transport modelling for flash events in mountain environments. *Acta Geophysica*, 60 (1), 191–213.

Reid, L. and Dunne, T., 1996. *Rapid evaluation of sediment budgets*. Reiskirchen: Catena.

Reid, L. and Dunne, T., 2016. Sediment budgets as an organizing framework in fluvial geomorphology. *In*: G.M. Kondolf and H. Piegay, eds. *Tools in fluvial geomorphology*. England: John Wiley & Sons, Ltd., 357–380.

Reisenbüchler, M., Bui, M.D., and Rutschmann, P., 2016a. Implementation of a new layer-subroutine for fractional sediment transport in Sisype. *In*: S. Bourban, ed. *Proceedings of the XXIIIrd Telemac-Mascaret user conference*. Wallingford, England: HR Wallingford Ltd, 215–220.

Reisenbüchler, M., *et al.*, 2016b. *Geschiebetransportmodellierung Saalachrampe 4.6*. Unpubished: chair of hydraulic and water resources engineering, Technical University of Munich.

Reisenbüchler, M., *et al.*, 2019. An integrated approach for investigating the correlation between floods and river morphology: a case study of the Saalach River, Germany. *Science of the Total Environment*, 647, 814–826.

Rickenmann, D., Chiari, M., and Friedl, K., 2006. *SETRAC, Äì A sediment routing model for steep torrent channels*.

Slaymaker, O., 2003. The sediment budget as conceptual framework and management tool. *Hydrobiologia*, 494 (1), 71–82.

Smart, G.M. and Jäggi, M., 1983. *Sedimenttransport in steilen Gerinnen: sediment transport on steep slopes*.

Suzuki, K. and Kato, K., 1991. *Mobile armouring of bed surface in steep slope river with gravel and sand mixture*. *In*: A. Armanini and G. Di Silvio, eds. Heidelberg, Berlin: Fluvial Hydraulics of Mountain Regions, 393–404.

Tassi, P. and Villaret, C., 2014. *Sisyphe user's manual*. online published: EDF.

van Rijn, L.C., 1984. Sediment transport, part III: Bed forms and Alluvial roughness. *Journal of Hydraulic Engineering*, 110 (12), 1733–1754.

Villaret, C., *et al.*, 2013. Morphodynamic modeling using the Telemac finite-element system. *Computers & Geosciences*, 53, 105–113.

Vriend, H.D., 2015. The long-term response of rivers to engineering works and climate change. *Proceedings of the Institution of Civil Engineers – Civil Engineering*, 168 (3), 139–144.

Wang, Z.-Y., Lee, J.H., and Melching, C.S., 2014. *River dynamics and integrated river management*. Heidelberg, Berlin: Springer Science & Business Media.

Weiss, F.-H., 1996. Sediment monitoring, long-term loads, balances and management strategies in southern Bavaria. *In*: W. D.E., & W. B.W. eds. *Erosion and sediment yield: global and regional perspectives*. Wallingford, England: IAHS Press 575–582.

WWA-TS, 2013. Dataset for the analysis of the Saalach flood in 2013. *In*: R. Heinz, R. Prokoph, and D. Skublics, eds.

Chapter 5

Sediment management at run-of-river reservoirs using numerical modelling

Sediment Management at Run-of-River Reservoirs Using Numerical Modelling

Markus Reisenbüchler [1,*] , **Minh Duc Bui** [1] , **Daniel Skublics** [2] **and Peter Rutschmann** [1]

1   Chair of Hydraulic and Water Resources Engineering, Technical University of Munich, Arcisstrasse 21,
    D-80333 Munich, Germany; bui@tum.de (M.D.B.); peter.rutschmann@tum.de (P.R.)
2   Water Authority Rosenheim, Königstrasse 19, D-83022 Rosenheim, Germany;
    Daniel.Skublics@wwa-ro.bayern.de
*   Correspondence: markus.reisenbuechler@tum.de; Tel.: +49-089-289-23139

Abstract: The worldwide storage volume of reservoirs is estimated to decrease by 0.5–1% per year due to sedimentation, which is higher than the gain in volume by newly built dams. For water supply or flood protection, the preservation of the storage volume is crucial. Operators and authorities, therefore, need sediment management concepts to ensure that the storage volume is sufficient. In this study, we developed a sediment-flushing concept using 2D numerical modelling for a run-of-river hydropower plant located in the Saalach River in southeastern Germany. The calibrated bed elevation was used as the initial bed for a number of simulations with different discharge regimes under varying operational schemes. By comparing the simulated results, we propose an appropriate flushing scheme in terms of intensity and duration to obtain a balance of sediment regime in the river. Furthermore, we demonstrate that such an optimised sediment management can generate synergies for improving measures of flood protection.

Keywords: TELEMAC-SISYPHE; numerical modelling; reservoir management; sedimentation; run-of-river; flushing

1. Introduction

Water is a limited resource, and efficient and sustainable distribution between different sectors is and will be of high importance worldwide [1]. Engineering structures, e.g., dams or weirs, are built to use water more efficiently or to ensure its availability. These structures store water in reservoirs and thus interrupt the hydromorphodynamic continuity of the river; not only water but also sediment transported by the river is accumulated. Globally, this unintended process has led to a decrease of around 0.5–1% of the available storage volume of water and simultaneously to higher riverbed levels [2]. It is predicted that at this decreasing rate around 1/4 of worldwide dams may be lost in the next 25–50 years [3]. Despite a loss in storage volume, the resulting higher riverbed level has additional negative consequences, such as increased flood risk.

In this paper, we focus on the consequences of sedimentation at a run-of-river hydropower plant (HPP) and the corresponding reservoir in a mountainous region. At such structures, water is dammed up to a certain level of operation to increase the difference in height between upstream and downstream water levels, i.e., the head, and thus the energy production potential [4]. In addition, artificial embankments, or storage levees, are commonly built along the upstream river section to further increase the cross-section area of channels, and thus the possible head and the storage capacity of the reservoir. Sedimentation in run-of-river reservoirs lowers the storage volume of water, which might affect the water availability; however, the increase of the riverbed elevation in the reservoir is much more severe in this case. A higher riverbed causes higher water levels, especially during

flood events, and can lead to a breach of the designed embankments [5]. Commonly, during high discharge events, the outlets of the dam or the gates/weirs are opened to stop the water level exceeding a defined threshold, which is lower than the crest of the designed embankments along the river. If the riverbed elevation is too high, this strategy will fail and thus cause harmful inundation. Especially in mountainous regions, where rivers have powerful currents causing high sediment loads of coarse gravel, the correlation between the flow, the morphology and engineering constructions is high. Therefore, measures dealing with sedimentation is a closely studied topic in the literature [4,6].

Developments in achieving a more sustainable sediment management strategy are of high interest for HPP owners, environmental agencies and local residents alike. Depending on the river characteristics (i.e., bed grain size distribution, slope and discharge) and the characteristics of the technical structure (i.e., geometry, length, height and width) different measures and management strategies are appropriate. Annandale et al. [4] classified them into four groups: Reduction of sediment supply from upstream sections, routing of sediment through the dam, removal sediment deposits in the reservoir and adaptive strategies. Numerical and/or physical modelling of reservoirs are important tools for engineers in developing such strategies. Integrative, coupled numerical hydromorphological models are particularly suitable as they can represent reality accurately and are more flexible than physical models. One-dimensional (1D) numerical models are the standard application since they have low computational requirements and deliver solutions quickly, but they include several simplifications and limitations. However, they are applied in several studies [7–9]. More advanced two-dimensional (2D) or three-dimensional (3D) models are more accurate, and thus able to represent reality in more detail, but they require higher computational resources and more data, which are not commonly available. However, several of these numerical models are used to study sedimentation at reservoirs. Gallerano and Cannata [10] proposed a 3D model, which is calibrated on suspended sediment concentration measurements, and assessed the impact of flushing on downstream reaches. Ateeq-Ur-Rehman [11] used a 2D depth-averaged model to predict sedimentation at the Indus River in Pakistan, on a large spatial and temporal scale. Further, Chaudahary et al. [12] showed that numerical 1D in general, and 2D models for detailed analyses are suited to investigating sediment-flushing operations. Bui and Rutschmann [13] demonstrated that a 2D model, which includes treatment for secondary flows, would be suited to simulating sediment processes in complex geometries.

Methods of mechanical excavation or flushing of sediment are commonly applied in run-of-river reservoirs to counter sedimentation. While mechanical excavation is very expensive and time-consuming, flushing can be more effective and efficient, as it uses the power of the river [4,14]. Drawdown flushing is performed by lowering the water levels in the whole reservoir, leading to free-flowing (i.e., riverine flow) conditions at the dam [15]. The accelerated flow causes high shear stresses on the riverbed, and thus high sediment transport rates, resulting finally in a lower riverbed. However, the complexity of the morphological processes and natural variability, which makes each hydrological year unique, requires adaptive solutions and knowledge of flushing schemes.

This paper proposes a concept for developing a sediment management strategy based on drawdown flushing operations using 2D hydromorphological numerical modelling. The framework was applied to an existing HPP in the Saalach River, in southeastern Germany. Two study objectives were considered: (1) evaluate the potential of reservoir flushing to re-establish the sediment continuity in the river by different weir operating regulations; and (2) apply the model with the proposed flushing schemes to a longer and consecutive period.

2. Methods

2.1. Study Area and Data Description

The present study follows the work of Reisenbüchler et al. [5] and Reisenbüchler et al. [16], who developed a numerical hydromorphological model of a section of the Saalach River from upstream at x = 8.0 km, below an unregulated weir, to the HPP at x = 2.4 km downstream, as shown in Figure 1.

The water surface and bed elevation used in this study were therefore referenced to the German vertical elevation system in metres above sea level (masl). This hydromorphological numerical model was successfully calibrated and validated for a period of eight years. More details on the model development can be found in [5,16].
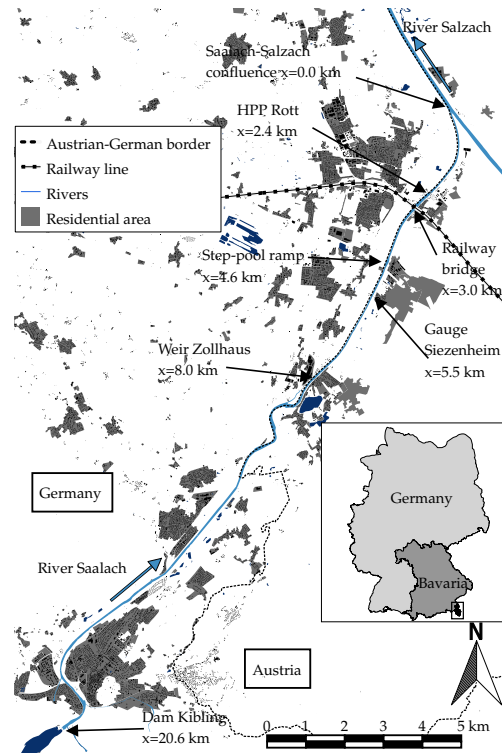

Figure 1. Overview on the study area (Adapted from [5]).

The riverbed consists of coarse gravels with an arithmetic mean diameter of $d_m = 37.7\,\text{mm}$ and a maximum diameter of $d_{max} = 140\,\text{mm}$. The high bed slope (up to 0.047) and high possible discharge generate high hydraulic forces, and thus a high potential of sediment transport. Due to the engineering works at the Kibling HPP-Dam (at $x = 20.6\,\text{km}$) near the city of Bad Reichenhall, the sediment regime is unbalanced in this region, requiring sediment management strategies [16,17]. Weiss [17] reported an average 95,000 m^3/year of sediment deposits in the reservoir. Reducing the amount of sediment available downstream can lead to increased erosion of the bed and banks. This may turn depositional areas into erosional ones or increase the rate of erosion where it already exists. For the dynamic stabilisation of the downstream river reach, an artificial sediment supply station has been established. The dimension of the amount of material and its grain-size composition is mainly aimed at stabilising the transport capacity of the reach and the grain-size of the natural bed load there. Since 1999, on average 50,000 m^3/year of sediment were supplied to the river. In the future, this amount will be reduced to approximately 30,000 m^3/year, since investigations have shown that a lower amount is enough to keep the riverbed stable in free-flowing sections [16]. At the gauging station $x = 5.5\,\text{km}$, discharge and water level are measured, which serves as the inflow boundary condition of the numerical model. Analysing the discharge data for 1976–2015 yields the following statistical flow data [18]: mean discharge MQ = 39 m^3/s, mean flood discharge MHQ = 436 m^3/s and 100-year return period flood discharge HQ_{100} = 1093 m^3/s. Furthermore, Reisenbüchler et al. [16] provided a sediment-rating-curve (SRC) at the model inlet, which describes the amount of transported sediment corresponding to the discharge of water and the annually supplied material at the Kibling dam.

Moreover, at the HPP Rott (x = 2.4 km), which is the model outlet, there is a legally binding operational ordinance for the water level in the reservoir. This document defines how the reservoir is to be operated depending on the discharge in the river. In addition, we obtained the water level measurements in the reservoir from 2005 and 2013, indicating sediment-flushing performed. The HPP has three structurally identical weirs sections, which allows a variable regulation of the water surface elevation. Figure 2 shows the most important facilities of the HPP schematically from the top view (Figure 2a), and as a longitudinal section through one weir (Figure 2b), which are considered in this study.

We modelled the official weir ordinance by applying a stage-discharge relation (see Figure 3). The possible range of discharges is classified into three operational modes: normal, high and extreme flow. For discharges lower than $Q_{normal} = 200 \, m^3/s$, the water level can be up to the maximum storage level of $Z_{f,S} = 415.80 \, m$. When the discharge exceeds Q_{normal}, the water level has to be decreased to $Z_f = 414.65 \, m$ by opening the weirs, considering a maximum speed of $v = 0.5 \, m/h$. This speed must not be exceeded; otherwise, the stability of the embankments is endangered [19]. If the discharge exceeds $HQ_{10} \approx 630 \, m^3/s$, the water level must be further lowered to $Z_f = 414.00 \, m$, taking into account the same lowering speed. In the case of extreme floods and discharges higher than $HQ_{50} \approx 850 \, m^3/s$, the weirs are completely open, allowing free-flowing conditions. A rating-curve for the free-flowing condition at the HPP is approximated with a potential function $Z_f = 403.33 Q^{0.0034}$. The three weirs have a total capacity to allow the design flood discharge $HQ_{100} = 1.093 \, m^3/s$ to pass harmlessly.
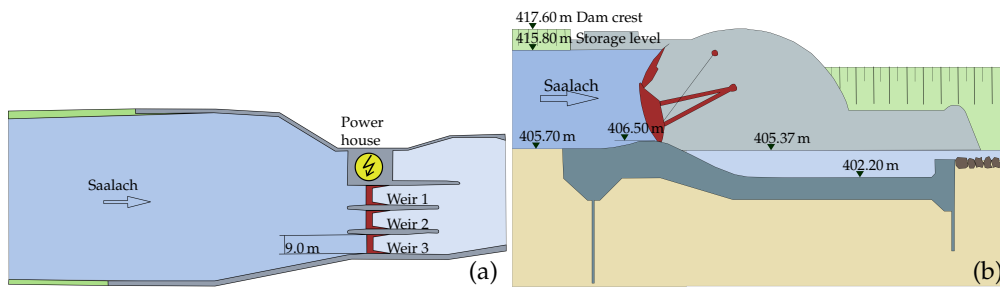

Figure 2. Simplified sketch of the HPP Rott: (**a**) top view, with the upstream reservoir, the weir with gates, and the orographically left located power house with the turbine intake; and (**b**) longitudinal section through one of the weirs.
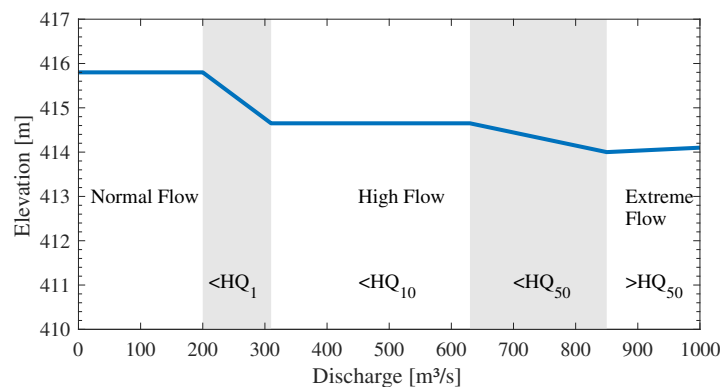

Figure 3. Stage-discharge-relation at the HPP Rott for the different operation modes and the transition zones.

2.2. Numerical Modelling

2.2.1. TELEMAC-SISYPHE

In this study, we applied the numerical modelling software TELEMAC-MASCARET, where the two-dimensional flow solver TELEMAC2D is coupled with the sediment transport module SISYPHE. TELEMAC2D is a depth-averaged flow solver based on the Shallow-Water-Equations (SWEs) including a $k-\varepsilon$-turbulence model. We dis not use the official release of SISYPHE but the modified version after [20], which provides a more stable and accurate numerical solution for fractional sediment transport. A comprehensive description of the numerical background of TELEMAC2D and SISYPHE is given by Ref. [5,21–24]. As mentioned above, the hydromorphological model used in this study was already calibrated and validated by Reisenbüchler et al. [5] and Reisenbüchler et al. [16]. For the sake of completeness, Table 1 provides the most important numerical parameters implemented.

Table 1. Numerical model parameters.

Parameter	Value
Timestep	$3\,\mathrm{s}$
Riverbed roughness (Strickler) k_{st}	$35\,\mathrm{m}^{1/3}/\mathrm{s}$
Form roughness (Strickler) $k_{st,r}$	manually, sectional adapted
Bedload transport formula	Hunziker [25]
Shields-parameter	0.04
Active layer thickness	$0.14\,\mathrm{m} = d_{max}$
Number of grain fractions	8

2.2.2. Grid Mesh and Initial Bathymetry

The existing numerical model for simulating inundation areas during the extreme flooding event cover not only the river channel but also wide areas of the surrounding flood plains. Observations of the water elevation in the Saalach River show that at the flow discharges not larger than that used in this study the water remains in the channel. Hence, to decrease the computation time and lower the computational effort, we created a new grid mesh covering only the river channel. The extracted mesh has 24,831 elements, which is only 7.5% of the initial mesh (Figure 4).

As an initial condition used in this study, bed elevation was updated to the possible maximum based on the designed flood protection levees in this region. Further sedimentation causing a higher bed elevation may increase the flood risk and can led to severe inundations (see [26]). Figure 5 shows a longitudinal section of the mean riverbed $Z_{b,ini}$ and the water surface elevation $Z_{f,MQ}$ during mean discharge conditions, which serve as the initial condition for the following simulations. Furthermore, the river reach was divided into two parts, an upper free-flowing and a lower reservoir section. The reservoir section can be subdivided again into two areas by a ground sill below a railway bridge at x = 3.0 km, with an averaged crest elevation of $Z_{b,GS} = 412.90\,\mathrm{m}$. Upstream of the bridge sedimentation is more critical than usual for flood protection and, at the same time, flushing might not be as effective here as in the lower part because the fixed elevation of the ground sill limits the possible erosion. In addition, at this location the river channel becomes wider, causing a deceleration of the flow (Figure 4).
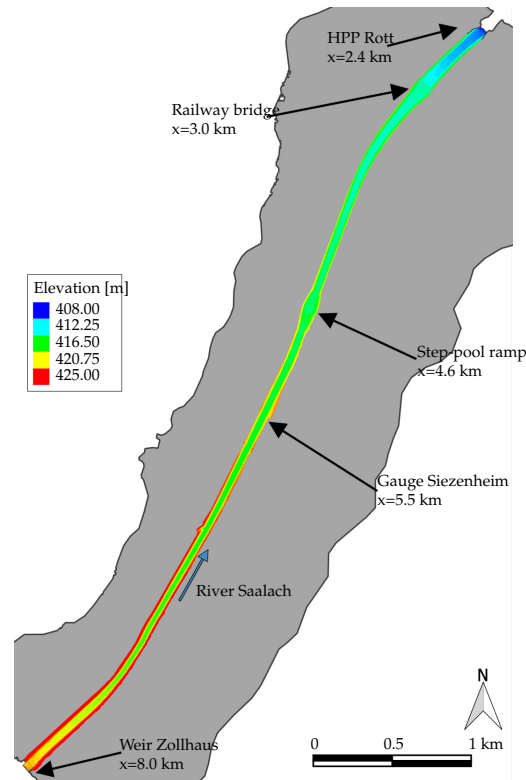
Figure 4. Extension of the original computational grid (**grey**) and the extracted main channel (**colored**).
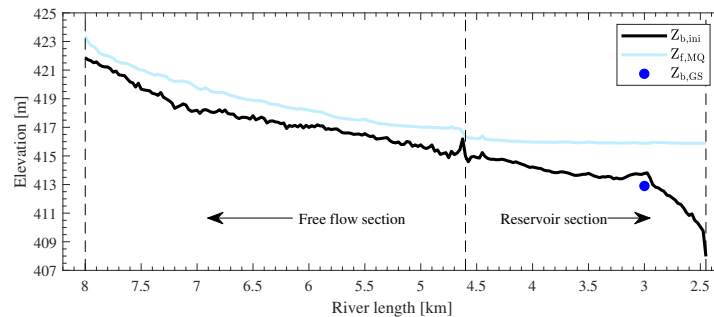

Figure 5. Longitudinal section of the initial bathymetry of the Saalach River, representing the maximum acceptable riverbed in the reservoir $Z_{b,ini}$ (**black**), the water surface level $Z_{f,MQ}$ (**light blue**) during normal mean discharge conditions, and the top edge of the ground sill $Z_{b,GS}$ at x = 3.0 km.

2.2.3. Boundary Conditions

At the inlet boundary, we applied three hydrographs (Figure 6), corresponding to different operation modes. To approximate reality as closely as possible, these hydrographs were selected from the available discharge measurements. The first hydrograph was observed in December 2008, and represents a frequently occurring flow situation, with a peak discharge of HQ_{S1} = 138 m^3/s. We selected this case as such small events occur quite regularly and might provide a reliable and predictable regulation option. Moreover, this flow magnitude is around the size of the incipient of sediment motion [27]. The second hydrograph is a medium sized flood event with a peak discharge of HQ_{S2} = 284 m^3/s, which occurred in January 2015. Such events occur statistically around once a year. The third scenario investigated focuses on the flushing potential during high floods, such as the event in August 2006, with HQ_{S3} = 650 m^3/s. The occurrence of such an event is more uncertain and

unlikely, as events with this magnitude have a recurrence probability of around 1/10 per year [26]. This low probability makes such events less suited for planning; however, we expect them to have the biggest potential for sediment remobilisation.
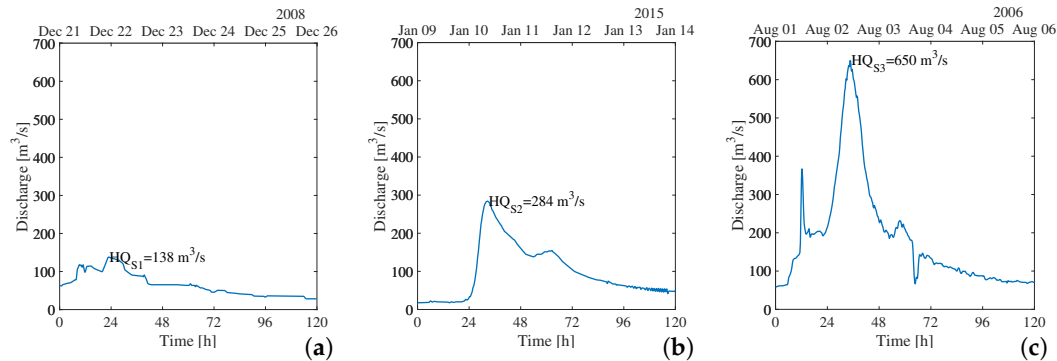

Figure 6. Hydrograph at the inlet boundary: (**a**) normal flow event; (**b**) medium flood event; and (**c**) high flood event.

As an outlet boundary condition, the water surface elevation was defined at the HPP. Hence, reservoir drawdown flushing was simulated directly by lowering this water level. Furthermore, we assumed the same water level for all weirs. Figure 7 shows the computational grid at the model outlet, indicating the boundary segments, where water and sediment can leave the domain.
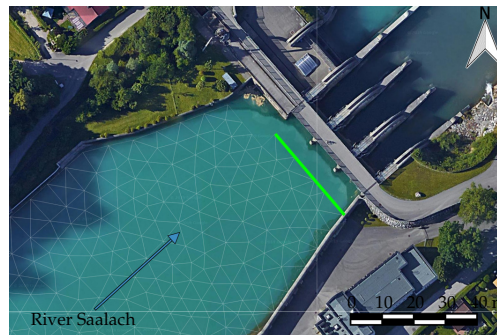

Figure 7. Computational grid close to the model outlet, highlighting the outflow boundary segments (**green**). Satellite image from maps.google.com.

To evaluate sediment-flushing, which is the main objective of this study, we generated four different flushing schemes (denoted as "cases") for each of the three discharge scenarios. The first case follows the standard hydropower plant operation (Figure 3). In the second case, the water level is defined to obtain free-flow conditions with the completely opened weirs during the simulation time. This case serves as reference case for the others, as the highest mobilised volume is expected here. The transition between storage level $Z_{f,S}$ and free-flow conditions follows the maximum lowering speed of the water level until the corresponding value of the water level from the provided stage discharge condition is reached. The last two cases represent intermediate solutions, to achieve a balance of the sediment output and flushing time.

Finally, we applied the model with a new possible flushing scheme for the time period of eight years from January 2006 to 31 December 2013. The predictions were compared with the observed riverbed (i.e., driven by the real operation scheme) to estimate the plausibility and applicability of the findings.

3. Results

3.1. Investigation of Event Based Flushing

3.1.1. Normal Flow Events

The first scenario is a typical and frequently occurring flow situation. Four different operation cases at the HPP were tested (see Figure 8a). In Case 1, the HPP was operated according to the official regulation scheme, defining in these discharge conditions a constant water level equal to the storage level of $Z_{f,S} = 415.80$ m. In Case 2, the weirs were opened completely at the beginning of the simulation, allowing free-flow situations in the reservoir. This lowering will take 12 h until free-flowing conditions are reached. For Case 3, the water level is lowered if the discharge exceeds $100\,\text{m}^3/\text{s}$ and raised again when the discharge falls below $100\,\text{m}^3/\text{s}$. As the peak discharge is only slightly higher than this threshold, and the discharge curve includes some oscillations, the time at lower water level is very short, and thus the water level is only lowered by around 2 m. For Case 4, we simulated a situation with a free-flow condition at the HPP during high discharges. The water level was lowered when the discharge exceeded $100\,\text{m}^3/\text{s}$ (at time t = 20 h). At time t = 31.25 h, the discharge became lower than $100\,\text{m}^3/\text{s}$ again and refilling of the reservoir started.
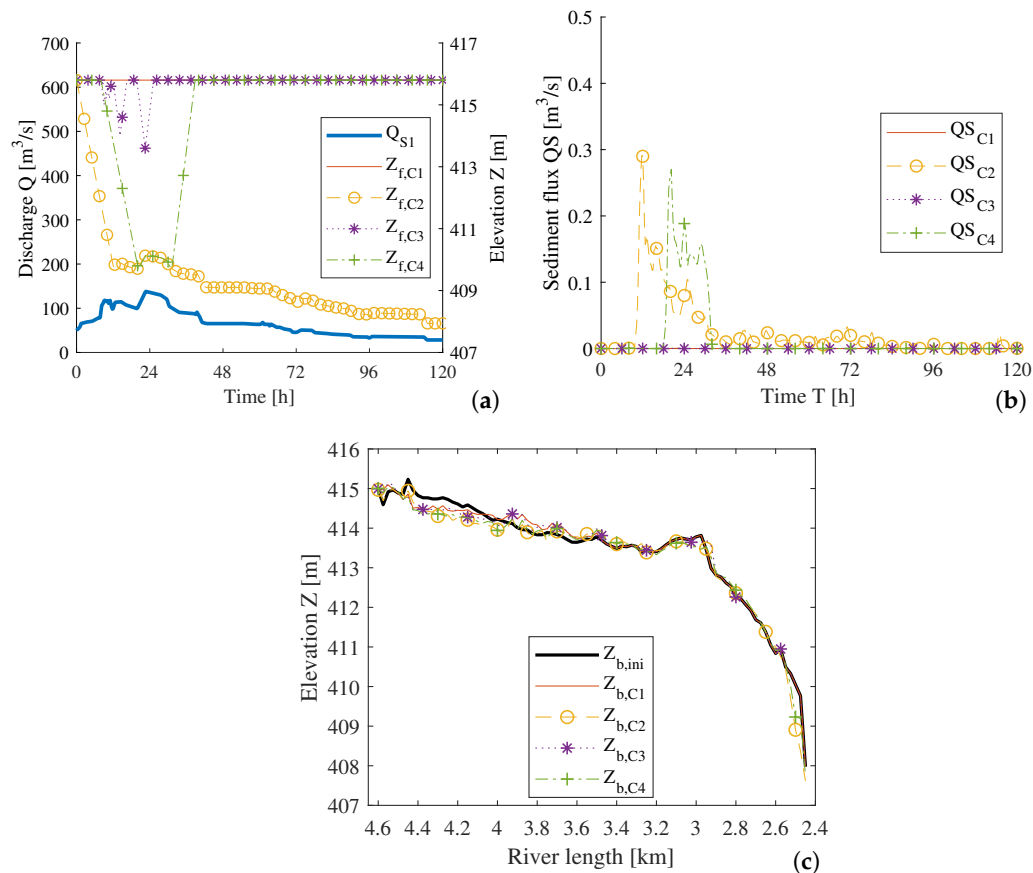
Figure 8. Normal flow scenario: (**a**) boundary conditions for the normal flow discharge and the water surface level of the four cases; (**b**) simulated sediment flux at the outlet boundary for each case; and (**c**) longitudinal section of the mean riverbed in the reservoir for initial conditions (black) and the final situation for each case.

Figure 8b shows the simulated sediment flux leaving from the domain, and Figure 8c the resulting mean riverbed of the reservoir in a longitudinal perspective. The overall effectiveness of the flushing is

given in Table 2, where the total mobilised volumes V_f and the flushing duration t_f are provided. During this flow condition, only a limited amount of bed sediment was mobilised. In Case 1, no sediment leaving from the domain was obtained because the weirs were not open, and, in addition, almost no sediment relocation occurs. In contrast, Case 2, under the free-flow condition, provided the highest volume of sediment leaving from the reservoir ($10{,}240\,\mathrm{m}^3$). For Case 3, the sediment flux at the outlet boundary was zero again. This shows clearly that the resulting forces on the riverbed were low if the water level was not or only slightly lowered. The flushing in Case 4 required 31 h in total, but, during the free-flowing condition (Case 2), a greater amount of sediment was mobilised.

Table 2. Comparison of the total flushed volume during normal flow event.

Case	Flushing Duration t_f (h)	Flushed Volume V_f ($1000\,\mathrm{m}^3$)
1	0	0
2	120	10.24
3	13.5	0
4	31	7.05

3.1.2. Medium Flood Events

The second scenario investigated was based on a flood event with a peak discharge of $Q = 284\,^3/\mathrm{s}$, as mentioned above, a size which occurs frequently. Similar to the normal flow event, we created four possible weir operation schemes, where Case 1 followed the official regulation. In Case 2, a completely opened weir was simulated, and in Case 3 the water level was lowered if the discharge was higher than $100\,\mathrm{m}^3/\mathrm{s}$, leading to free-flow conditions after 11 h at a water level of $Z_f = 410.9\,\mathrm{m}$. In Case 4, the water level was lowered if the discharge was higher than $150\,\mathrm{m}^3/\mathrm{s}$ and thus after 10.25 h free-flow conditions were obtained. However, due to the shape of the hydrograph in this scenario, which consists of a secondary, smaller peak of $Q = 154\,\mathrm{m}^3/\mathrm{s}$ at $t = 62.25\,\mathrm{h}$, an intermediate increase and lowering of the water level occurred in Case 4. The time series of the discharge and the water elevation for the four operation schemes are shown in Figure 9a.

Figure 9b shows the sediment flux at the outlet boundary for each case, and Figure 9c shows the resulting riverbed level after the event. Additionally, in Table 3, the total flushed volumes are listed with the necessary time. Following the official weir regulation scheme (Case 1), only local relocation of sediment occurred in the upper reservoir section from $x = 4.6 - 3.0\,\mathrm{km}$, but no sediment transported through the outlet boundary was observed. In the second case, around $V_{f,2} = 32{,}060\,\mathrm{m}^3$ of sediment were flushed out over a time of $t_{f,2} = 120\,\mathrm{h}$, leading to a clear lowering of the riverbed. Case 3 took only around 50% of the opening time $t_{f,2}$, but during this time around 78% of $V_{f,2}$ were still flushed. Moreover, the simulation showed that in Case 4 the flushing was interrupted due to the refilling process, and eroded material in the upper reservoir section was deposited downstream of the railway bridge again, leading there to a higher riverbed and consequently to a lower amount of sediment transported through the domain.

Table 3. Comparison of the total flushed volume during the medium flood event.

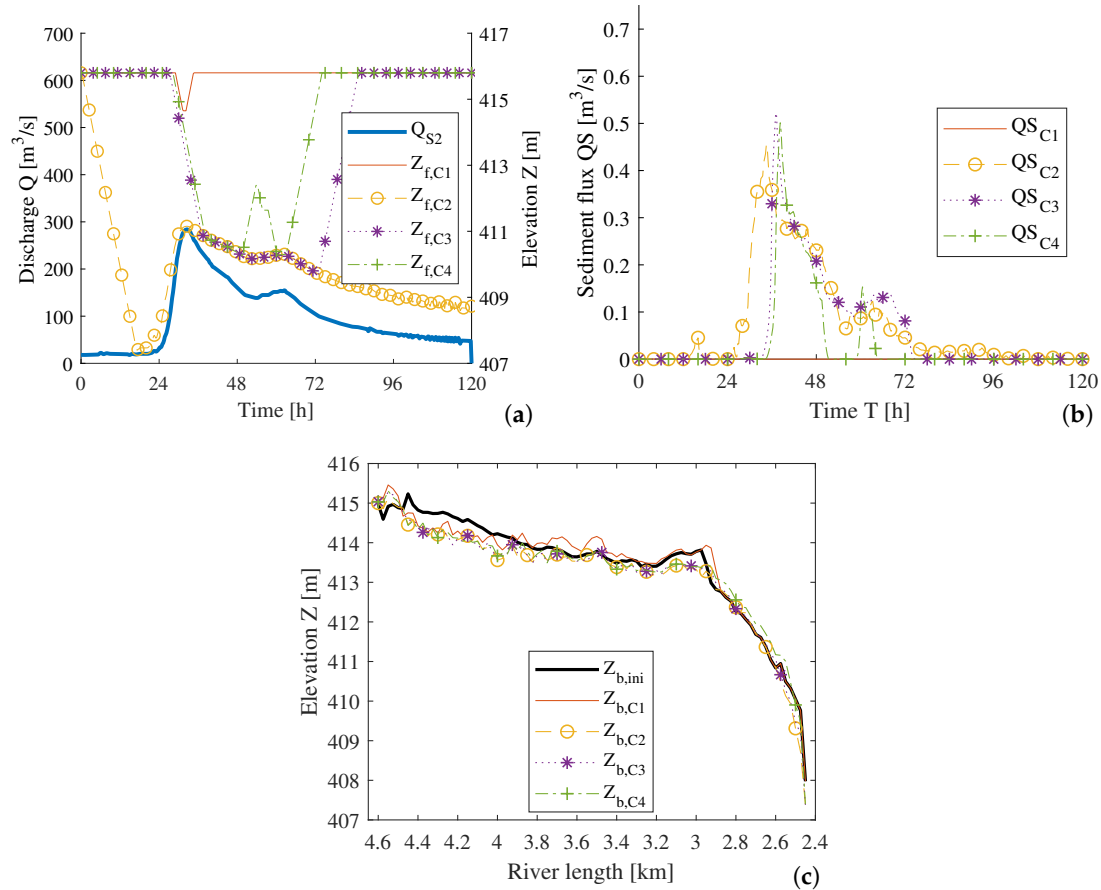| Case	Flushing Duration t_f (h)	Flushed Volume V_f ($1000\,\mathrm{m}^3$)
1	5.75	0
2	120	32.06
3	58	25.11
4	46	14.82

Figure 9. Medium flood scenario: (**a**) boundary conditions for the medium flood scenario and the four investigated regulation schemes; (**b**) simulated sediment flux at the outlet boundary for each case; and (**c**) longitudinal section of the mean riverbed in the reservoir for initial conditions (black) and the final situation for each case.

3.1.3. Extreme Flood Event

During extreme flood events, we expected the greatest hydraulic forces on the riverbed and thus very effective flushing. Again, four cases were investigated and compared, as shown in Figure 10a. The first case followed the official weir regulation, leading to a stepwise lowering of the weirs to a level of 414.65 m. The second case shows the situation for the free-flow condition. In the third case, the weirs were opened completely if the discharge $Q = 100 \, \text{m}^3/\text{s}$, which happened at t = 7 h and lasted until t = 85 h, followed by the refilling of the reservoir. The fourth case used a higher threshold of $Q = 150 \, \text{m}^3/\text{s}$ than in Case 3 in order to see the effect of a shorter flushing.

The simulation results are provided in Figure 10b,c and Table 4. In the first case, only $V_{f,1} = 1180 \, \text{m}^3$ of sediment was flushed, limited by a too short weir opening time and the partial lowering of the water level. Here, only material in the upper section was eroded, but was then deposited downstream before the HPP. Alternatively, a complete opening of the weirs led to an overall erosion of the riverbed and a volume of $V_{f,2} = 81,830 \, \text{m}^3$ of sediment was transported through the HPP. To optimise the opening time, and thus shorten the time without energy production, we investigated two further cases. The simulated flushing considered discharge regimes over 100 and $150 \, \text{m}^3/\text{s}$, leading, as expected, to smaller flushing volumes than in Case 2, but a similar morphological development. The riverbed in the upper section was clearly lower after the flushing and the eroded material   was not deposited in front of the HPP.
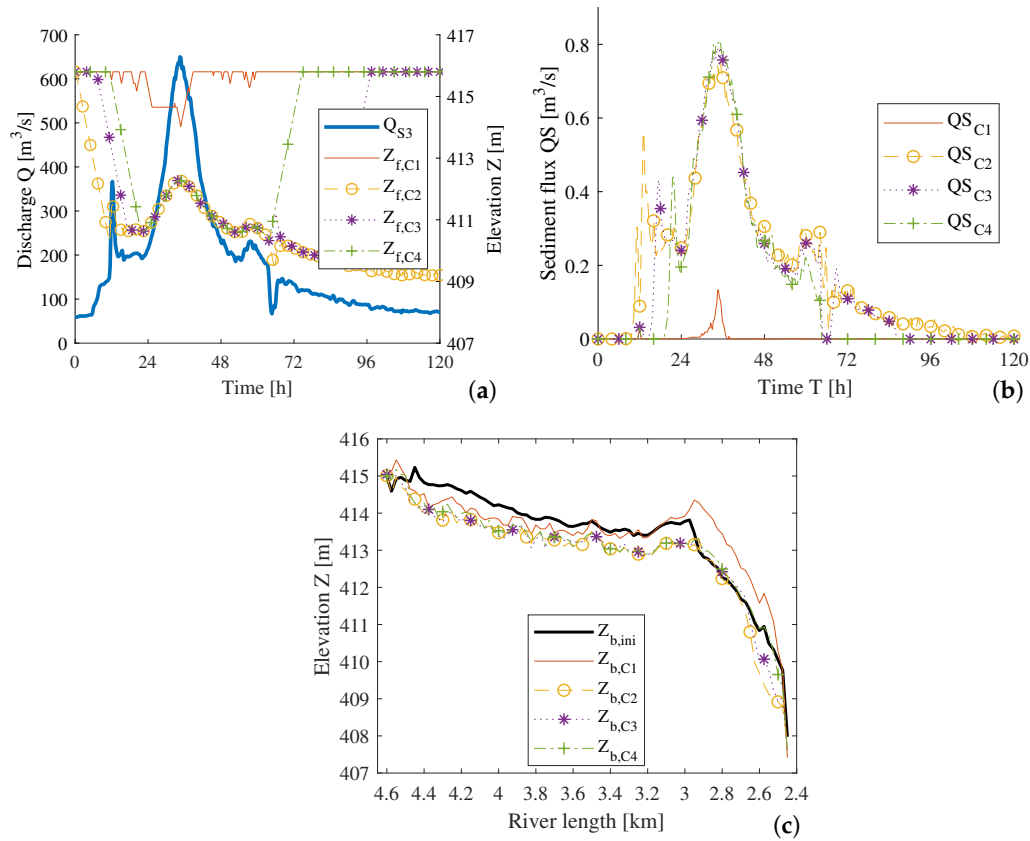
Figure 10. Extreme flood scenario: (**a**) boundary conditions for the extreme flood scenario and the four investigated regulation schemes; (**b**) simulated sediment flux at the outlet boundary for each case; and (**c**) longitudinal section of the mean riverbed in the reservoir for initial conditions (black) and the final situation for each case.

Table 4. Comparison of the total flushed volume during the extreme flood event.

Case	Flushing Duration t_f (h)	Flushed Volume V_f (1000 m^3)
1	16	1.18
2	120	81.83
3	90.5	72.16
4	63.5	59.80

3.2. Scenario Application

Based on the analysis of the simulated results for different scenarios in Section 3.1, we developed a flushing scheme for the study domain. The simulations were conducted for the period from 1 January 2006 to 31 December 2013 on the original calibrated mesh from Ref. [16]. This is necessary as in this period the 2013 flood event occurred and the floodplain must be included (Figure 4). This allowed us a direct comparison with management actually effected, and with the strategy presented in Ref. [16], where a first draft of a modified weir operating regulation was discussed.

In reality (with the real HPP-operation), during this time period, complete drawdown flushing was carried out four times, and partial lowering of the water level eight times. For a time period of 22 days, the water level was lowered on purpose to re-mobilise sediment, which is about 0.8% of the total time (2921 days). Due to the damage caused by the 2013 flood event, the water level after this event was, in contrast to usual practice, kept lower than the storage level for an additional period of 112 days.

Based on the first draft proposed by Reisenbüchler et al. [16], the weirs should be opened, and thus flushing performed, when the discharge is higher than 250 m^3/s. This means for this period of eight years the water surface should have been kept at the designated storage level and the weirs been opened, allowing sediment to pass for a total time period of 30 days (1.1%).

However, based on the results presented in Section 3.1, the total sediment volume transported through the river reach can be increased by an optimised flushing time, starting by lowering the weirs earlier and keeping them open longer than the length of flood wave. We therefore, tested different flushing schemes considering the sediment balance in the reach. The obtained results thus far indicate that flushing is effective when the discharge exceeds 100 m^3/s and the free-flowing condition is obtained. The total flushing time t_f would be increased by an additional 15 days (about 1.6% of the total time).

The effectiveness of three operation schemes (the real HPP-operation, the draft scheme proposed by Reisenbüchler et al. [16] and the new proposed scheme) was evaluated considering the flushing parameters. Figure 11 shows the flow discharge at the inlet and the corresponding water levels Z_f at the reservoir outlet at x = 2.4 km for two selected flood events. From the observed data (for the real HPP-operation), it can be seen that the water level was lowered when the flood peak had already passed through the inlet boundary in the first example (Figure 11a), while, in the second example (Figure 11b), the water level was only slightly lowered during the flood peak and no real flushing performed. Following the draft scheme, the threshold discharge of 250 m^3/s for flushing operations applied only for large floods. However, following the new proposed scheme, the water level would also be lowered for small floods and the weirs kept open longer.
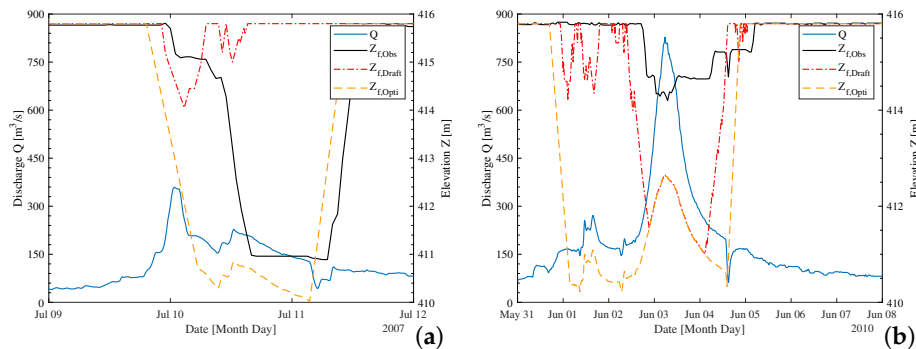

Figure 11. Hydrograph and corresponding water surface levels for sediment-flushing for the observed (black), the draft (red) and the optimised (orange) scheme for two time periods: (**a**) July 2007; and (**b**) June 2010.

Figure 12 provides a stage-discharge relation at the outlet boundary for the three schemes during the study period. In all schemes, the designated storage level of Z_S = 415.80 m can be detected for a wide range of discharges. Moreover, Figure 12a shows the unusual opening after the 2013 flood event, as mentioned above, leading to the low water levels down to an elevation of 408 m. In the proposed and draft schemes is Figure 12b,c, the selected thresholds of 250 m^3/s and 100 m^3/s respectively, are visible as starting points for free-flowing conditions. To define the lowering water level, both the flow discharge and the maximum lowering speed were considered.

Figure 13 presents the calculated mean riverbed levels along the river reach. Starting from an identical bathymetry based on the observed riverbed in 2006 (as mentioned in Section 2.2.2), both proposed flushing schemes led to a clear lower riverbed in the reservoir section, compared with the measured riverbed in 2013. Increasing the flushing time (+0.5%) in the optimised case (the new proposed scheme) led to a lower riverbed elevation than that obtained by the draft case. Analysing the sediment amount transported through the river reach shows a volumetric difference of about 10,000 m^3 at the end of the simulation period between the draft scheme and the optimised one, which is around 1/4 of the annual expected influx of material in the reservoir. In the upper section of the river reach, the free-flowing section, the different operation schemes have no influence and show identical results.
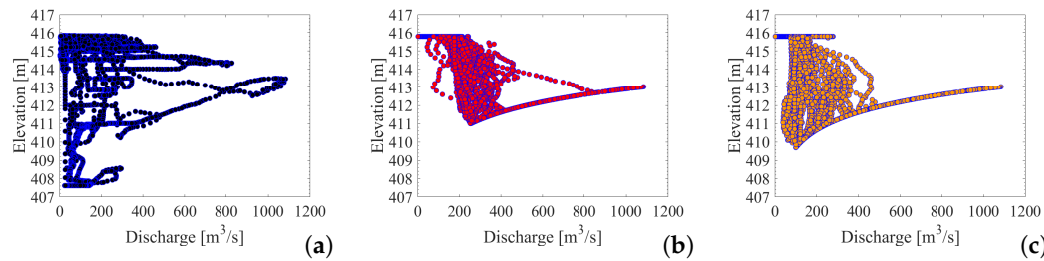
Figure 12. Stage-Discharge-relation for the three weir operating schemes: (**a**) observed; (**b**) draft; and (**c**) optimised.

Moreover, despite the increase of re-mobilised sediment, and thus the re-establishment of the sediment continuity, an additional benefit can be created. During the 2013 flood event, extreme high water surface levels were recorded on 2 June 2013 (see Figure 14), causing large inundation and extensive damage [5]. The simulation showed that, with adaptations in the weir regulation, leading to lower bed levels, the water level during this extreme event could also have been lower. In the case of the draft scenario, the reduced water elevation would be around -0.5 m at the most critical section at x = 3.5 km. For the optimised case proposed here, the decreasing of water elevation would be 1.0 m.
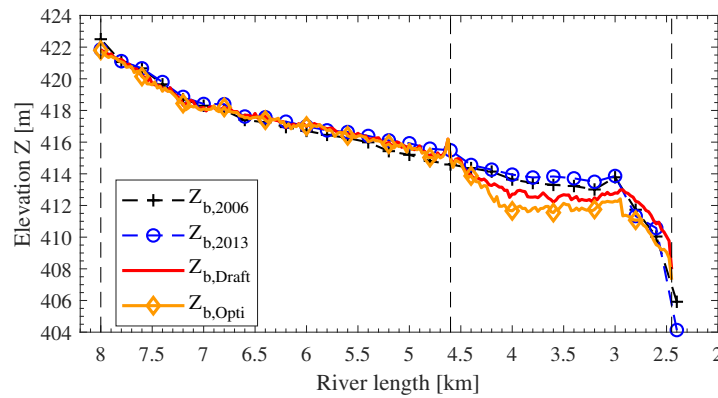

Figure 13. Longitudinal section of the riverbed levels: Observed in 2006 ($Z_{b,2006}$) and 2013 ($Z_{b,2013}$), as well as the result of the draft scenario ($Z_{b,Draft}$) and the simulated optimised case ($Z_{b,Opti}$).
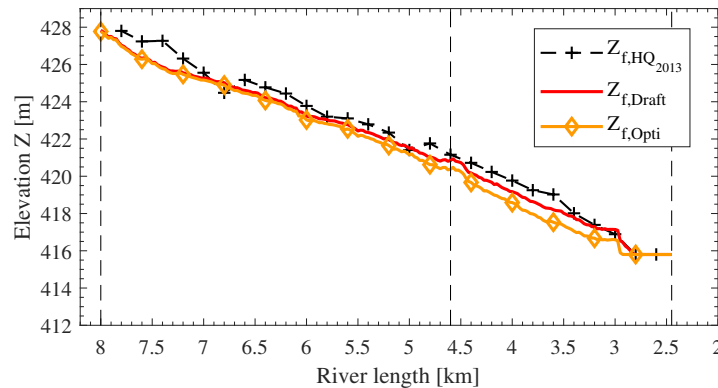

Figure 14. Longitudinal section of the maximum water surface levels: Observed in 2013 ($Z_{f,HQ_{2013}}$), and simulated by the draft scenario ($Z_{f,Draft}$) and the simulated optimised case ($Z_{f,Opti}$).

4. Discussion

The results of this study, obtained by numerical 2D simulations, provide insight into the processes during drawdown flushing at run-of-river HPPs in gravel bed rivers. For this study, a 2D modelling approach is sufficiently accurate, as Reisenbüchler et al. [5] showed that the differences in the flow velocity between 3D and 2D simulations are very low for this reservoir.

Smaller flood events with a peak discharge lower than HQ_1, which were investigated in the first scenario, can mobilise only a low amount of sediment. The results indicate that a complete opening over 120 h, is not an efficient measure as in Case 4 around 70% of the maximum volume $V_{f,2}$ is still transported but needs only 25% (=30 h) of the time $t_{f,2}$. Considering the predicted sediment transported from the river reach with the expected annual average sediment entering the reservoir (approximately 40,000 m³/year) shows that such small events have only a minor impact and do not greatly lower the riverbed. Finally, we classify the simulated processes during this flow scenario more as relocation than real flushing. The reason for this is mobility of the coarse gravel bed of the Saalach, which requires higher hydraulic forces induced by higher shear stresses than during this flow situation.

Sediment-flushing during a medium flood event is a more suitable option for the Saalach River. During such discharges, higher amounts of sediment are mobilised and leave the domain. However, here, the flushing duration plays an important role. If this time is too short, e.g., due to early refilling, re-mobilised sediment from upper reservoir sections is deposited again before it can leave the domain. We estimated that such events could efficiently mobilise up to 25,000 m³ of sediment, which is more than 60% of the annual average sediment input.

As expected, the simulations confirmed that an extreme flood discharge has the greatest potential for sediment-flushing, which mobilised volumes clearly higher than the annual input. Moreover, it is clear that free-flowing conditions during the flushing are much more effective regarding sediment output than only partial lowering of the water level (e.g., down to Z_f = 414.65 m). We also observed that in all cases longer flushing led to higher sediment output given a sufficient discharge intensity.

Based on the simulated results in the river reach for a period of eight years, we found that a morphologically optimised operational scheme can lower bed levels, raise sediment output rates and improve flood security due to lower water level during an extreme event. It is clear that, without an efficient flushing activity at the HPP, sedimentation will cause severe problems such as flooding in the area and probably require more expensive countermeasures such as dredging. This would require an official agreement for energy production and sediment management. Our proposed flushing scheme can be applied as the basis of more sustainable sediment management in the reservoir.

In the future, we would like to continue our research on reservoir flushing with additional tests, such as the comparison of the numerical results with a physical model. Through such hybrid modelling approaches, the combination of numerical and physical model can benefit from the strength of both methodologies, as Stephan and Hengl [28] showed, and thus lead to even more reliable results. Moreover, analysis of the data obtained from the numerical simulation could serve as input data for more advanced data processing tools such as artificial neural networks [29–31]. Furthermore, we plan to continue this study to assess the impact of reservoir flushing on downstream sections of the reservoir, which we expect due to the flushing alterations of the downstream morphology and ecology, as discussed by the authors of Ref. [7,32–35]. A possible methodology for such an investigation is presented in Ref. [36].

5. Conclusions

Our numerical hydromorphological model is suitable for optimisation of reservoir operations and developing a sediment management strategy. By testing different reservoir operation modes, we showed that, under certain conditions, sediment could be more effectively re-mobilised and transported through the HPP. However, not all the cases investigated showed the desired effect. We found that, due to the coarse gravel bed of the Saalach River, low flow forces could not mobilise greater amounts of sediment, but led only to local relocation of sediment along the reach.

One additional finding is that the flushing time, when the water level is lowered and the weirs are open, is an important factor. This time should be sufficiently long for two reasons: first, to obtain free-flowing conditions during the flushing, which are more effective than only partial lowering of the water level; and, second, to ensure that material which is mobilised by the flow in upper reservoir sections has enough time to pass the weirs at the HPP, as otherwise the sediment will remain in the lower section directly in front of the HPP. Application of the developed numerical models can help to determine this necessary time. In addition, we demonstrated that reservoir management can play an important part in integrative flood management strategies. Applying proposed operation scheme, the water levels in the domain could be reduced, thus providing higher flood security for local residents and settlements. This clearly shows that investigations into sediment management strategies can be a valuable solution to develop integrated flood protection system in combination with technical and ecological measures.

Author Contributions: M.R. designed the study, processed and analysed the data, interpreted the results and wrote the paper. M.D.B. and P.R. contributed to the model development stage with theoretical considerations and practical guidance, assisted in the interpretations and integration of the results and helped in preparation of this paper with proofreading and corrections. D.S. provided expertise on the site-specific conditions, organised the data collection and assisted in the interpretations. All authors have read and agreed to the published version of the manuscript.

Abbreviations

The following abbreviations are used in this paper:

HPP	Hydropower plant
GS	Ground sill
masl	metres above sea level
Z_b	Elevation of the riverbed
Z_f	Elevation of the free water surface
$Z_{f,S}$	Storage level
V_f	flushing Volume
t_f	flushing duration
2D	two dimensional
3D	three dimensional
QS	Sediment flux
Q	Discharge of water
HQ	flood peak discharge
MQ	Mean discharge
MHQ	Mean flood discharge

References

1. Assembly, U.G. Transforming Our World: The 2030 Agenda for Sustainable Development. 2015. Available online: https://www.refworld.org/docid/57b6e3e44.html (accessed on 12 December 2019).
2. Schleiss, A.J.; Franca, M.J.; Juez, C.; De Cesare, G. Reservoir sedimentation. *J. Hydraul. Res.* **2016**, *54*, 595–614. [CrossRef]
3. Dams, W.C.O. *Dams and Development: A New Framework for Decision-Making*; Earthscan Publications Ltd.: London, UK, 2000.
4. Annandale, G.W.; Morris, G.L.; Karki, P. *Extending the Life of Reservoirs: Sustainable Sediment Management for Dams and Run-of-River Hydropower*; World Bank Group: Washington, DC, USA, 2016.

5. Reisenbüchler, M.; Bui, M.D.; Skublics, D.; Rutschmann, P. An integrated approach for investigating the correlation between floods and river morphology: A case study of the Saalach River, Germany. *Sci. Total Environ.* **2019**, *647*, 814–826. [CrossRef] [PubMed]

6. Schleiss, A.; de Cesare, G.; Franca, M.; Pfister, M. *Reservoir Sedimentation*; CRC Press: Boca Raton, FL, USA, 2014.

7. Dépret, T.; Piégay, H.; Dugué, V.; Vaudor, L.; Faure, J.B.; Le Coz, J.; Camenen, B. Estimating and restoring bedload transport through a run-of-river reservoir. *Sci. Total Environ.* **2019**, *654*, 1146–1157. [CrossRef] [PubMed]

8. Isaac, N.; Eldho, T.I. Sediment management studies of a run-of-the-river hydroelectric project using numerical and physical model simulations. *Int. J. River Basin Manag.* **2016**, *14*, 165–175. [CrossRef]

9. Isaac, N.; Eldho, T.I. Sediment removal from run-of-the-river hydropower reservoirs by hydraulic flushing. *Int. J. River Basin Manag.* **2019**, 1–14. [CrossRef]

10. Gallerano, F.; Cannata, G. Compatibility of Reservoir Sediment Flushing and River Protection. *J. Hydraul. Eng.* **2011**, *137*, 1111–1125. [CrossRef]

11. Ateeq-Ur-Rehman, S. *Numerical Modeling of Sediment Transport in Dasu-Tarbela Reservoir Using Neural Networks and TELEMAC Model System*; Technische Universität München: München, Germany, 2019.

12. Chaudhary, H.P.; Isaac, N.; Tayade, S.B.; Bhosekar, V.V. Integrated 1D and 2D numerical model simulations for flushing of sediment from reservoirs. *ISH J. Hydraul. Eng.* **2019**, *25*, 19–27. [CrossRef]

13. Bui, M.D.; Rutschmann, P. Numerical modelling for reservoir sediment management. In Proceedings of the Sixth International Conference on Water Resources and Hydropower Development in Asia, Vientiane, Laos, 1–3 March 2016.

14. Bieri, M.; Müller, M.; Boillat, J.L.; Schleiss, A.J. Modeling of Sediment Management for the Lavey Run-of-River HPP in Switzerland. *J. Hydraul. Eng.* **2012**, *138*, 340–347. [CrossRef]

15. Esmaeili, T.; Sumi, T.; Kantoush, S.A.; Kubota, Y.; Haun, S.; Rüther, N. Three-Dimensional Numerical Study of Free-Flow Sediment Flushing to Increase the Flushing Efficiency: A Case-Study Reservoir in Japan. *Water* **2017**, *9*, 900. [CrossRef]

16. Reisenbüchler, M.; Bui, M.D.; Skublics, D.; Rutschmann, P. Enhancement of a numerical model system for reliably predicting morphological development in the Saalach River. *Int. J. River Basin Manag.* **2019**. [CrossRef]

17. Weiss, F.H. Sediment monitoring, long-term loads, balances and management strategies in southern Bavaria. In *Erosion and Sediment Yield: Global and Regional Perspectives*; Walling, D.E., Webb, B.W., Eds.; IAHS: Wallingford, UK; 1996; Volume 236, pp. 575–582.

18. BMLFUW. *Hydrographisches Jahrbuch von Österreich 2015*; The Austrian Federal Ministry of Agriculture, Forestry, Environment and Water Management: Vienna, Austria, 2015; Volume 123.

19. Olsen, N.R.B.; Haun, S. Numerical modelling of bank failures during reservoir draw-down. *E3S Web Conf.* **2018**, *40*, 03001. [CrossRef]

20. Reisenbüchler, M.; Bui, M.D.; Rutschmann, P. Implementation of a new layer-subroutine for fractional sediment transport in Sisype. In Proceedings of the XXIIIrd Telemac-Mascaret User Conference, Paris, France, 11–13 October 2016; pp. 215–220.

21. Hervouet, J.M. *Hydrodynamics of Free Surface Flows: Modelling with the Finite Element Method*; John Wiley and Sons: Chichester, UK, 2007.

22. Villaret, C.; Hervouet, J.M.; Kopmann, R.; Merkel, U.; Davies, A.G. Morphodynamic modeling using the Telemac finite-element system. *Comput. Geosci.* **2013**, *53*, 105–113. [CrossRef]

23. Ata, R. *Telemac2d User Manual*; Available online: http://www.opentelemac.org/ (accessed on 12 December 2019).

24. Tassi, P.; Villaret, C. *Sisyphe User's Manual*; EDF: Paris, France, 2014; Volume 6.3.

25. Hunziker, R.P. *Fraktionsweiser Geschiebetransport*; Laboratory of Hydraulics, Hydrology and Glaciology (VAW), ETH Zürich: Zürich, Switzerland, 1995; Volume 11037; p. 191.

26. WWA-TS. *Dataset for the Analysis of the Saalach Flood in 2013*; WWA Traunstein: Traunstein, Germany, 2013.

27. Beckers, F.; Sadid, N.; Haun, S.; Noack, M.; Wieprecht, S. Contribution of numerical modelling of sediment transport processes in river engineering: An example of the river Saalach. In Proceedings of the 36th IAHR World Congress 2015, The Hague, The Netherlands, 28 June–3 July 2015.

28. Stephan, U.; Hengl, M. Physical and numerical modelling of sediment transport in river Salzach. In *River Flow 2010*; Dittrich, A., Koll, K., Aberle, J., Geisenhainer, P., Eds.; Federal Waterways Engineering and Resarch Institute: Karlsruhe, Germany, 2010; pp. 1259–1265.

29. Bui, M.D.; Kaveh, K.; Penz, P.; Rutschmann, P. Contraction scour estimation using data-driven methods. *J. Appl. Water Eng. Res.* **2015**, *3*, 143–156. [CrossRef]

30. Ateeq-Ur-Rehman, S.; Bui, M.; Rutschmann, P. Variability and Trend Detection in the Sediment Load of the Upper Indus River. *Water* **2018**, *10*, 16. [CrossRef]

31. Azmathullah, H.M.; Deo, M.C.; Deolalikar, P.B. Neural Networks for Estimation of Scour Downstream of a Ski-Jump Bucket. *J. Hydraul. Eng.* **2005**, *131*, 898–908.:10(898). [CrossRef]

32. Liu, J.; Minami, S.; Otsuki, H.; Liu, B.; Ashida, K. Environmental impacts of coordinated sediment flushing. *J. Hydraul. Res.* **2004**, *42*, 461–472. [CrossRef]

33. Capra, H.; Plichard, L.; Bergé, J.; Pella, H.; Ovidio, M.; McNeil, E.; Lamouroux, N. Fish habitat selection in a large hydropeaking river: Strong individual and temporal variations revealed by telemetry. *Sci. Total Environ.* **2017**, *578*, 109–120. [CrossRef] [PubMed]

34. Kondolf, G.M.; Gao, Y.; Annandale, G.W.; Morris, G.L.; Jiang, E.; Zhang, J.; Cao, Y.; Carling, P.; Fu, K.; Guo, Q.; et al. Sustainable sediment management in reservoirs and regulated rivers: Experiences from five continents. *Earth's Future* **2014**, *2*, 256–280. [CrossRef]

35. Reckendorfer, W.; Badura, H.; Schütz, C. Drawdown flushing in a chain of reservoirs—Effects on grayling populations and implications for sediment management. *Ecol. Evol.* **2019**, *9*, 1437–1451. [CrossRef] [PubMed]

36. Tritthart, M.; Haimann, M.; Habersack, H.; Hauer, C. Spatio-temporal variability of suspended sediments in rivers and ecological implications of reservoir flushing operations. *River Res. Appl.* **2019**, *35*, 918–931. [CrossRef]

Chapter 6

Development of an ANN-based tool for sediment management at run-of-river reservoirs

6.1 Introduction

This thesis has shown the conventional numerical models for modelling sediment transport can and must be improved. However, improvements to the models presented in the previous chapters, cannot answer all the requirements and questions posed by our environment but in combination with other, alternative modelling approaches, offer a way forward.

Artificial intelligence (AI) plays an increasingly important role in science and research these days. In the field of hydrodymorphodynamics, there are various research approaches and aspects in which AI-based inference models, such as artificial neural networks (ANNs) can find clear correlations or patterns in data that help engineers make predictions or understand the processes. [29] shows, for example, that ANN and time series decomposition can be used to reconstruct a reliable and consistent time series of suspended sediment load more accurately than standard rating curve approaches. Such information is crucial when it comes to designing big reservoirs and sediment management approaches. ANNs also work better than existing methods for predicting the maximum abrasion depth, as [30] shows. Furthermore, [31] shows that ANN can even replace conventional numerical morphodynamic models and predict the temporal development of the riverbed. However, this was done under well-defined conditions.

This brief literature review of the use of ANNs in river morphodynamics highlights the broad potential of this methodology. In the following, I combine the results achieved in this thesis (by conventional numerical modelling) with different applications of ANN. Before that, a brief background of ANN is provided with some theoretical considerations.

6.2 Background

An ANN is an information processing paradigm that is inspired by the way human brain processes information. The two major structural constituents of a brain are neurons and synapse. In a ANN, neurons are information processing units and synapses are elementary structural and functional units that mediate the interaction between neurons. This structure can be formulated mathematically as follows:

$$Y = \Theta \left(\sum_{i=1}^{n} X_i w_i + b \right) \qquad 6.1$$

where Y is the output vector of the ANN, Θ is the response characteristic of the neuron, X_i is the input information of to the i-th node and w_i the weight of the node i. In theory, a neuron is a non-linear element with multiple inputs and a single output. In addition to the external inputs X_i, a bias or threshold b is often added for modelling ANNs. The bias is necessary to improve the convergence of the network. Figure 6.1 shows the scheme of a single artificial neuron j.
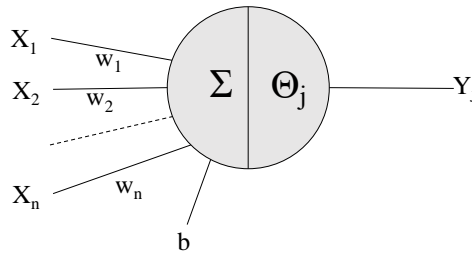

Figure 6.1: Scheme of an artificial neuron.

An ANN consists of three main components, the input layer, one or more hidden layers and the output layer, each of which consists of a certain number of neurons or nodes. The most basic structure of an ANN is a feed-forward network (FFN), in which information is transferred from input to output via the hidden layers. Figure 6.2 shows an example of such a network. Here, three inputs are transferred to one single output through a hidden layer consisting of four neurons. Depending on the problem and complexity, more complex architectures may be necessary. A comprehensive overview of existing and newly developed networks can be found in [32, 33].

Neurons are mapped between different layers using an activation function (AF), sometimes also called a transfer function (TF). This function transfers the input from an unlimited range to an output of a limited range. There is a wide range of different activation or transfer functions in the literature [32, 33]. [34] recommends using the Logistic Sigmoid function as the activation function for the hidden layers that push the information into the range of (0,1). Instead, a linear TF with an infinite range $(-\infty, \infty)$ is used in the
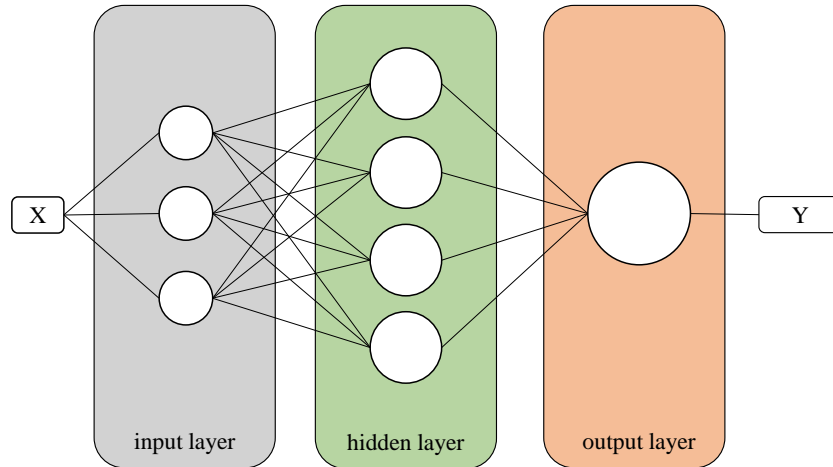
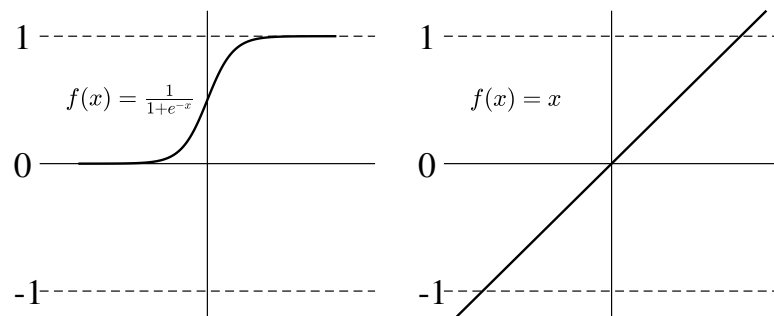Figure 6.2: Scheme of a feed forward network.

Figure 6.3: Logistic sigmoid (left) and linear (right) activation function.

output layer. Figure 6.3 shows these two kinds of TF graphically.

The weights of the neurons are determined during the training phase of the network. Various algorithms can be used for training to adjust the weights [31]. This task is necessary to fit the ANN output to the real output. The classification of a good network is often performed according to statistical performance criteria such as the root-mean-square error (RMSE), e.g. described in [35].

6.3 ANN for sediment management

In this section, two different ANN approaches are presented for sediment management at the study area.

6.3.1 ANN for estimating the volume of flushed sediment

6.3.1.1 Introduction

As mentioned in the discussion in Chapter 1.5.5 (Ref.[4]), the sediment volume flushed out of the reservoir is very important information for the owners of hydropower plants and

to restore a more balanced sediment regime. However, predicting this volume requires the development of a complex conventional morphological model that requires a great deal of data (e.g. bathymetry and granulometry), which is often uncertain and unavailable, and powerful software or hardware. The final numerical model could then, of course, predict the amount of sediment flushed, depending on discharge and weir operation. However, it would be useful if an ANN could only predict the flushed volume using a few discrete input parameters that approximate the process. Some literature can be found on this topic. For instance, [36] uses catchment data such as annual rainfall, annual runoff, and the capacity to predict the reservoir's annual sedimentation. Conversely, [37] applies an ANN to predict the monthly flushed sediment volume based on limited discrete input data and where promising accuracy was achieved. This type of ANN is referred to here as a "steady ANN" as its inputs and outputs are time-independent.

6.3.1.2   Study site and data

The applicability and accuracy of an ANN depends heavily on the data available to train the network. The data must reflect a wide range of possible situations since ANNs can interpolate well but are less suited for extrapolation to data outside of the training range. At the River Saalach study site only sparse documentation was available for this study, consisting of six real flushing events. Each event was described by the peak discharge and the duration of flushing. The volume of flushed sediments is only approximated from annual riverbed measurements. This database is too small to be used in an ANN.

Therefore, the conventionally developed model from Chapter 1.5.5 was used to synthetically generate a broader database. Again, the discharge time series from 1 January 2006 to 31 December 2013 was applied here. In order to obtain a sufficiently large database for training the network, nine different flushing scenarios were generated. Each scenario was based on a clear threshold discharge, at which flushing should be initiated. In the previous study, it was found out that a value of $Q_{f,1}=100\,\mathrm{m^3/s}$ was sufficient to obtain a high sediment output. For the generation of this database, other thresholds were applied: $Q_{f,i=1,9}=[100, 125, 150, 175, 200, 225, 250, 275, 300]$. Moreover, the volume of sediment in the domain, or the riverbed elevation, makes a difference, and thus three different initial bed levels for the simulations were defined: the first representing the highest acceptable riverbed ($V_{b,max}$), the second the design riverbed for flood protection ($V_{b,flood}$), and the third, the riverbed measured in 2005/6 ($V_{b,2005}$).

In total, 27 (9x3) simulations for the time period of eight years were carried out and analysed for the database. Finally, around 600 different flushing events could be extracted from the simulations.

6.3.1.3 Methodology

Based on the literature mentioned, a feed-forward network (FFN) presented a suitable architecture for an ANN to attain the stated objective, of predicting the volume of sediment flushed. In such an FFN the nonlinear relation between input (or more inputs) is learned by the network to fit a certain defined output. In this case, the output or target was the cumulative volume of sediments flushed during a certain event V_f.

According to the results presented in previous chapters of this thesis, the amount of sediment flushed mainly depends on the flow, the operation of the weir, and the initial riverbed before flushing. The flow is parametrised with two variables, the peak discharge (Q_{max}) and the volume of water passing the weir during the flushing (V_{water}). The operation of the weir is also represented twice with the duration of flushing (t_f) and the minimum water level reached during the flushing (Z_f). The last parameter considered is the initial volume of sediments in the domain before flushing ($V_{b,initial}$). However, as $V_{b,initial}$ is hard to estimate and unknown in reality, a normalised variable is here introduced instead. The new parameter is defined as $LoA=(V_{initial}-V_{b,min})/(V_{b,max}-V_{b,min})$ meaning the level of aggregation before a flushing event. At this study site, a maximum acceptable riverbed in the reservoir was defined by the authorities. The volume of this riverbed is calculated as $V_{b,max}$. The lowest riverbed of all simulations is used to estimate the minimum volume $V_{b,min}$. This enables the real use of such a network since the LoA ratio can be estimated.

The variability in the data is visualised in Figure 6.4 using boxplots, where the median as well as the 25% quantiles are highlighted.

6.3.1.4 Results and discussion

Training

Initially, the nodes of the network are connected to each other with random, initial weights. During the training, the network learns the nonlinear relation between input and output, meaning the adjustment of the weights with the help of an algorithm. Here the Levenberg-Marquardt algorithm is applied as it showed good performance in other river engineering applications [38, 34]. Furthermore, the database is divided into three parts, namely training (70%), testing (15%), and validation (15%) to avoid overfitting. It is notable that the division is performed randomly. Moreover, the optimum number of neurons cannot be defined in advance as it is unknown. However, according to [39, 38], we can estimate that the number of neurons in the hidden layer varies from

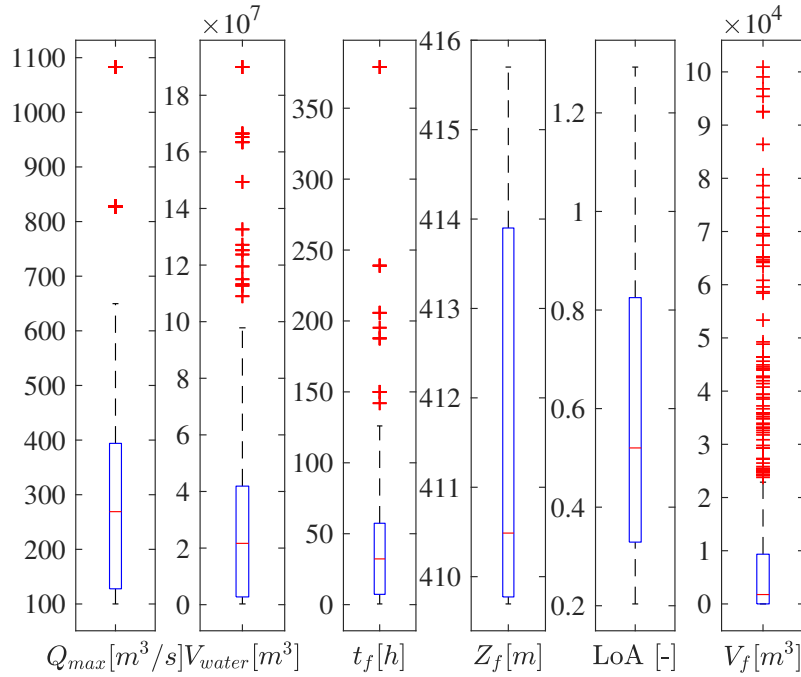$$2\sqrt{N_I} + N_O \quad \text{to} \quad 2N_I + 1 \qquad 6.2$$

Figure 6.4: Analysis of the five input data parameters and the output parameter.

where N_I and N_O represents the number of input and output nodes, respectively. In this case, the number of neurons in the hidden layer is tested iteratively from 4 to 11. The number of neurons is very important since a too small number can lead to underfitting of the network, while too large a number can cause overfitting and unnecessary high computational effort. It is important to mention that the initial weights can also have a major impact on the possible accuracy of a network. In order to avoid this effect, training is conducted several times with new initial weights. In this test, the number of runs for each combination of number of neurons in the hidden layer was conducted done 100 times, resulting in 700 different networks.

The network which showed the best accuracy, i.e. the network with the least error between the measured data and the ANN output can be used for further applications. The root-mean-square error (RMSE) is selected as error criterion to find the best network. This error is not calculated with all data, but only with the data from the test subset.

Of all networks, a network with 10 neurons showed the best accuracy. Figure 6.5 shows the regression of the target data (x-axis) and the corresponding ANN output (y-axis). This illustrates very well that the ANN can learn the relation between the five inputs and the output since the relation is almost linear. Moreover, the mean absolute error in the prediction was only around $1000\,\mathrm{m}^3$ on average per flushing event, which is very low.
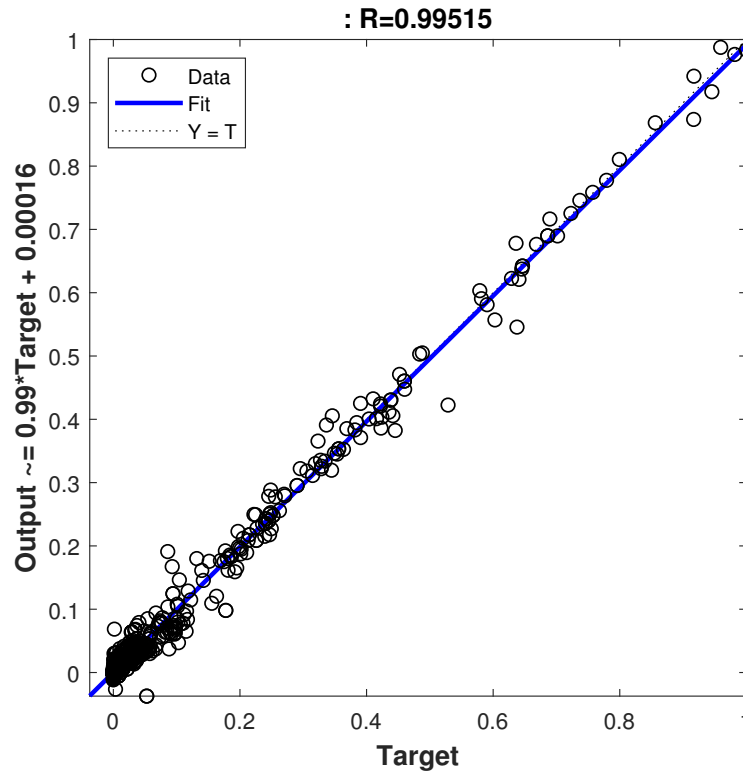
Figure 6.5: Regression of the original data (=Target) and the prediction (=Output).

Discussion

The ANN approach developed as a predictor for reservoir flushing shows promising results. The trained FFN identifies a clear correlation between distinct, measurable input data and the desired mobilised sediment volume. Although this approach has some limitations, the average error is in a range where it can be neglected ($\approx 1000\,\mathrm{m}^3$). Therefore, the developed ANN could be applied at the real-world study area as an estimator for reservoir flushing. For instance, it can be used in some decision support system to efficiently schedule reservoir flushing operations.

The fact that the training data were obtained from a numerical model and not from real measured data limits the applicability of the network to other case studies. However, if the same input data (Q_{max}, V_{water}, t_f, Z_f, and LoA) could be gathered from different hydropower plants, a sufficiently large database could be obtained only with real measurements. The designed network would probably have then to be extended by an additional parameter representing the geometry of the different hydropower plants. Such a parameter was not necessary for this test.

6.3.2 ANN for predicting the bed level change along the river reach

6.3.2.1 Introduction

Artificial neural networks are highly effective at learning the connections between inputs and output - probably better than we understand. In state-of-the-art river morphology, there is no comprehensive formula with which the sediment transport in rivers can be calculated uniformly. Depending on the river type, e.g. sandy/gravel, and the inclination, there are different semi-empirical formulas with different parameters. It could be that an ANN can learn the morphological processes better than these empirical formulas describe. In the previous section, a steady ANN performed well for predicting the total flushed sediment volume. However, information about the local distribution of this sediment during the flushing is lost. This may not be enough to address other, more detailed questions.

This section discusses the development of an unsteady ANN. The unsteady ANN has the task of predicting the development of the riverbed over time in successive steps, similar to a conventional numerical model. The benefit of this would be a tool that requires very little computing effort, no software licenses, and it is easy to use compared to a conventional numerical model. [34] developed an ANN which could be used to replace a conventional numerical model under simplified conditions.

6.3.2.2 Study site and data

The study area is the River Saalach (see Chapter 1, Figure 1.2). At x=5.5 km there is a gauging station at which the discharge is measured every 15 min. Moreover, the water level at the HPP Rott located downstream is determined over time according to the weir regulations. The river bathymetry is measured once a year every 200 m along the river. To simplify the complex domain, a 1D cross-sectional approach was applied in the following. The riverbed is, therefore, discretised into 200 m sections and a mean riverbed is calculated using the methodology in Chapter 1.5.5. With a total river reach length of around 5.6 km, 28 cross-sections were evaluated, the first one being most upstream. However, there are no measurements of the riverbed during flushing, which requires the data from the numerical model as a placeholder for real measurements.

In Chapter 1.5.5, multiple simulations of sediment flushing were conducted and analysed. The simulations include three different discharge conditions (named scenarios) and four different weir operations (named cases) for each scenario. The twelve simulations serve as a database for training the network. The numerical simulation output time step was 15 min, which results in 480 data samples since each simulation spans 120 hours.

6.3.2.3 Methodology

Prediction of the temporal development of the riverbed is no longer possible with a standard FFN. It is clear that the future riverbed depends directly on the previous riverbed, which requires a recurring structure. This means that the predicted output of the ANN is used directly as the input for the next time step. [34] showed that the network may need more past information to understand the processes. In addition to riverbed itself, the external forces on the riverbed should be considered as input. Available information is the upstream discharge measurement and the downstream water level as they are the driving force of the system. However, this information is tied to a particular location and therefore not available in each cross-section. Moreover, processes along with the river change from the free-flowing conditions to reservoir conditions, which can be difficult for only a single ANN. In addition, there are some non-erodible structures in the Saalach such as the step-pool ramp at x=4.6 km and the groundsill below the railway bridge at x=3.0 km. The questions remains, nevertheless, whether an ANN can provide a reliable and solid prediction of the riverbed development despite these challenges.

To answer this question, two different approaches were tested:

Single ANN

First, only one ANN for the entire domain was developed, referred to as 'single ANN' in the following. In addition to the external input (Q^t, Z_f^t), each individual ANN was given the internal input that represents the riverbed sections ($Z_{b,i=1,28}^t$). The advantage of this approach is that only one network predicts the next time step of the riverbed $Z_{b,i=1,28}^{t+1}$ for the entire domain. This approach is based on the assumption that only a single ANN can distinguish the influence of water level and discharge on the different riverbed sections. Moreover, the connection within the cross-sections should also be learned by the single ANN. This means that if there is no erosion upstream, no deposition can take place downstream.
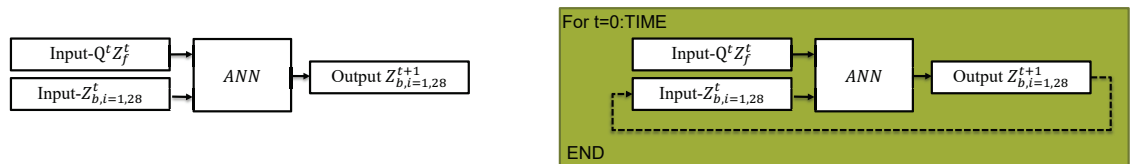

Figure 6.6: Scheme for the single ANN for training (left), and prediction (right).

Figure 6.6 shows the single ANN schematically. For training purposes, the network has a strict feed-forward structure, but for the prediction only the time series of Q^t and

Z_f^t are provided and the initial riverbed $Z_{b,i=1,28}^{t=0}$. The future riverbed is predicted by a time loop.

Multi ANN

The second methodology tested was the combination of multiple ANNs together, i.e., a nested structure of networks each of which is responsible for a specific task in each cross-section (Multi ANN). However, the flow of information must be more preprocessed as the cross-sections are now decoupled. This means that the upstream discharge (Q^t) and downstream water level (Z_f^t) can no longer be used directly as input for each single ANN of a cross-section, but the flow conditions at the specific section (Q_i^t and ($Z_{f,i}^t$) are required. To obtain this information, an additional hydrodynamic ANN (H-ANN) was developed first for each cross-section, which takes into account the riverbed $Z_{b,i}^t$ and the known boundary conditions Q^t and Z_f^t. This H-ANN was then nested with a second, morphological ANN (M-ANN) to predict the future riverbed $Z_{b,i}^{t+1}$ for every section. Figure 6.7 shows the flow of information schematically. Noted that the nested loop of ANNs starts at the most upstream cross-section with i=1.
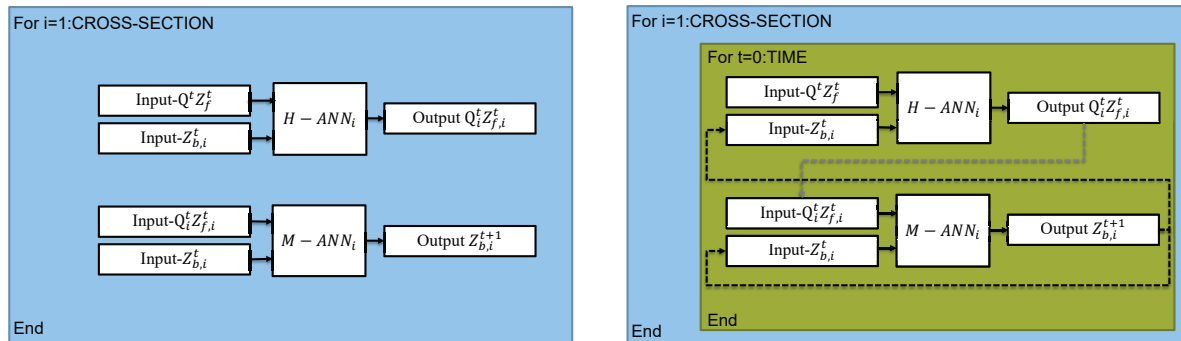

Figure 6.7: Scheme of the Multi-ANN for training (left) and prediction (right)

6.3.2.4 Results and discussion

Training and prediction single ANN

First, the single ANN approach was tested and trained with the data from the twelve simulations. The number of inputs is 30 (Q^t, Z_f^t, and $Z_{b,i}^t$) and if information from a previous time step $Z_{b,i}^{t-1}$, namely a time delay (TD), is also taken into account it increases to 58 (30+28) (TD=1). Using the Equation 6.2, the number of neurons in the hidden layer should be at least 38 to 61 and 43 to 117, respectively. The activation function was selected as Logistic Sigmoidal for the hidden layer and Linear for the output layer. Training was done using the secondary order Levenberg-Marquardt algorithm. The number of neurons was varied in steps of 10 from 38 to 118 to limit the number of training runs to a feasible level. Whether a TD can increase accuracy was also tested. Each combination of the number of neurons in the hidden layer, the TD (0 or 1) was tested 10 times, which led to 180 different networks. A higher number of iterations was limited due to the available computing resources. The training time for one network was on average 1.3 h, which was in total around 10 days. For clarification, in training the network is provided with the knowledge of all data, distributed between training (70%),testing (15%) and validation (15%), and the weights are adjusted so that the output of the network, the riverbed of the next time step, matches the provided data.

According to the RMSE of the testing subset, the best network had an overall error of 0.0026 m between ANN output and target, and consisted of 98 neurons and a time-delay. The best network without a time-delay consisted of 118 neurons and had an RMSE of 0.0029 m, which is quite similar. Using boxplots, Figure 6.8 shows the statistical performance of the networks with respect to their architecture. It is clear that networks with a TD showed better overall performance in training and thus have a lower RMSE. Moreover, increasing the number of neurons from 38 to 68 reduces the error linearly. For higher number of neurons this effect is reduced.
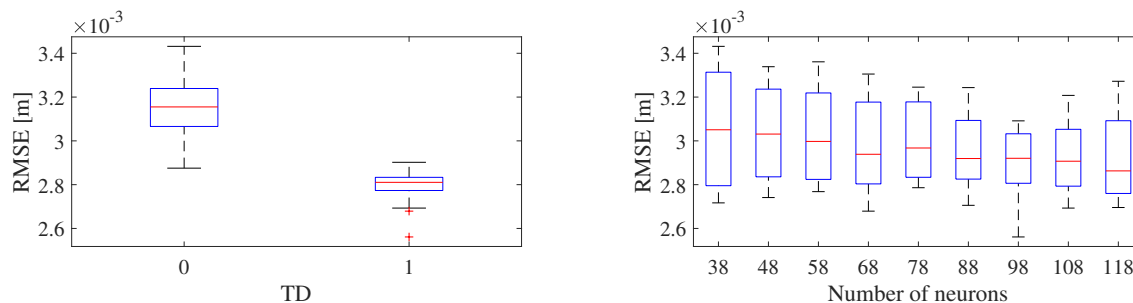

Figure 6.8: Performance of the networks for time-delay (TD) and the number of neurons.

The mode was changed from training to prediction to demonstrate whether the best network could be used for application. Only the initial riverbed and the time series of discharge and water level were provided to the network. All of the following steps are based on the predicted output, as Figure 6.6 shows schematically.

Despite the high accuracy of the network in training, the network could not reproduce entire time series of the riverbed adequately. Figure 6.9, for instance, shows the result of the network for three different cases, and five selected cross-sections. On top of each figure the boundary conditions for each case is shown. The larger network introduces some non-physical oscillations and barely follows the target data for all three cases. Also the network without time-delay and 118 neurons shows a similar pattern of oscillations, which cannot explained.
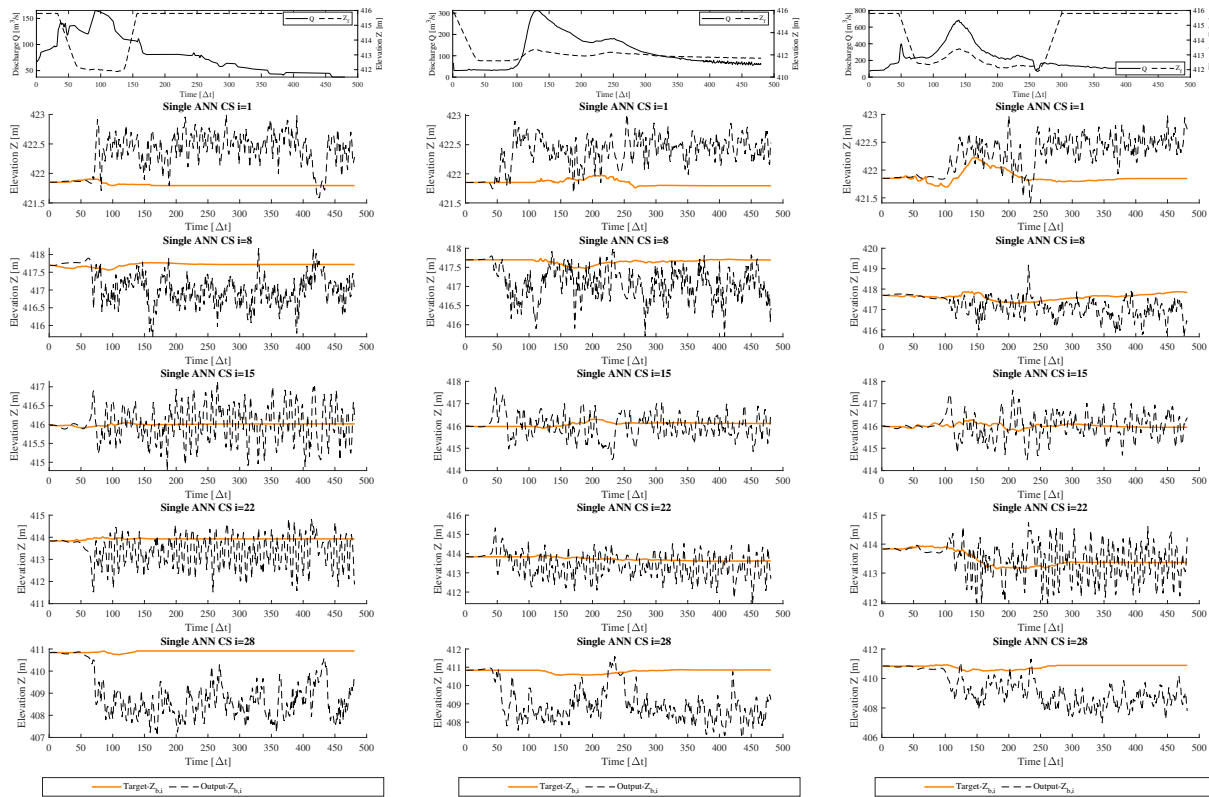

Figure 6.9: Predicted time series of the riverbed $Z_{b,i}^t$ by thesSingle ANN (TD=1, 98-Neurons), for scenario 1, case 4 (left), scenario 2, case 2 (middle), and scenario 3, case 3 (right).

To investigate this issue, smaller networks with less number of neurons were used for prediction, despite being less accurate in training. The result of the same three examples is provided in Figure 6.10. It is clear that although the oscillations vanish, the ANN performs quite badly and fails to predict the riverbed accurately.

Additionally, the best network without time-delay, and a smaller number of neurons
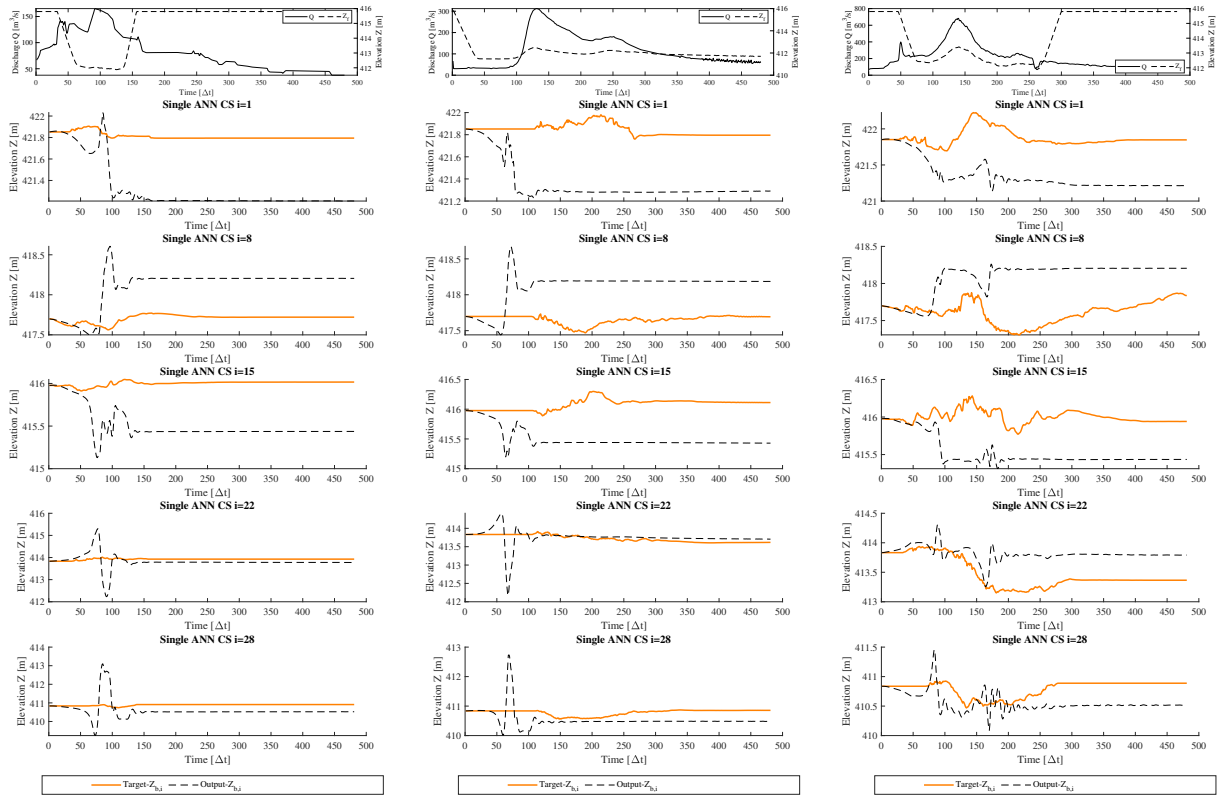
Figure 6.10: Predicted time series of the riverbed $Z_{b,i}^t$ by the Single ANN (TD=1, 43-Neurons), for scenario 1, case 4 (left), scenario 2, case 2 (middle), and scenario 3, case 3 (right).

were tested. The result is provided in Figure 6.11. This visual comparison shows that the time-delay does not play a major role in this application, and there are some bigger problems.

The test of a single unsteady ANN shows that the real-world application tends to be outside the capabilities of a classical feed-forward net. The network cannot grasp the processes adequately and introduces non-physical fluctuations. It appears that a large network that should in theory understand more complex problems will fail in this case because it creates big oscillations. Smaller networks do not show these oscillations, but their prediction is too imprecise for them to be used reliably. It is likely that they cannot compute the extent of the problem and the physical relations between the input data.
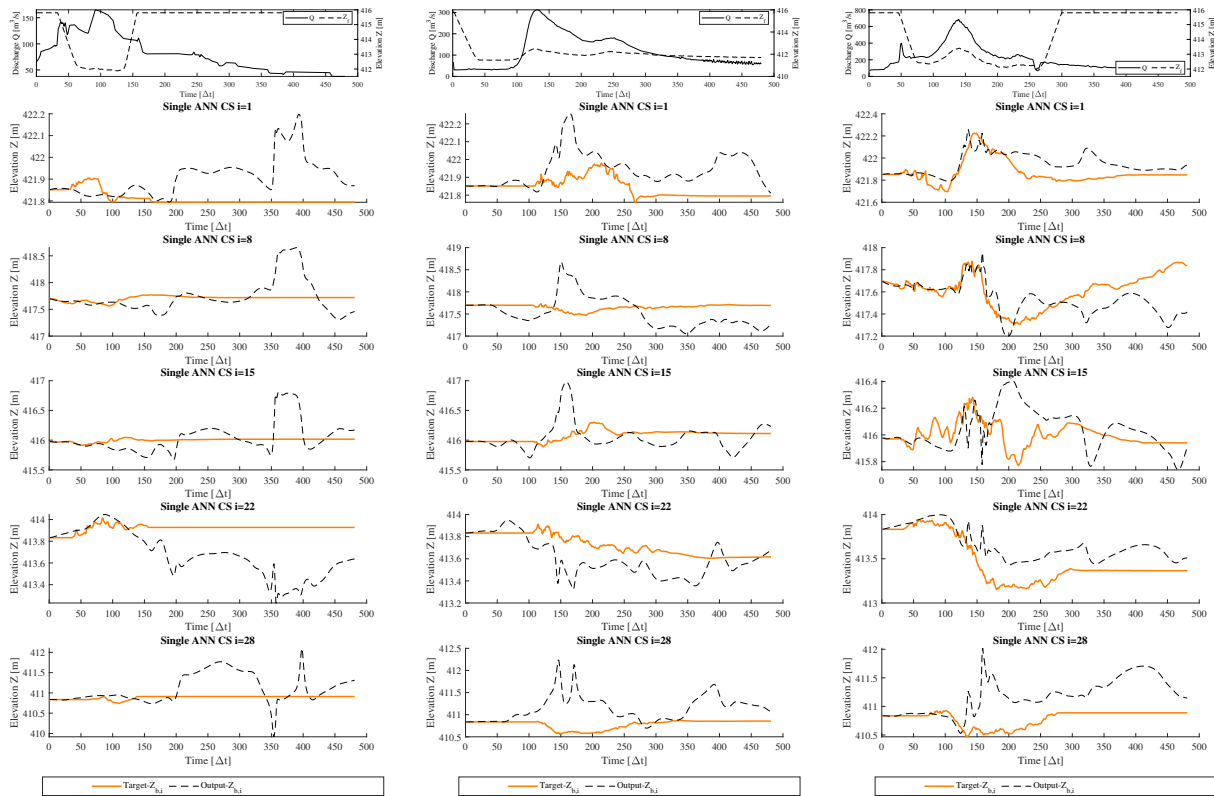
Figure 6.11: Predicted time series of the riverbed $Z_{b,i}^t$ by the Single ANN (TD=0, 48-Neurons), for scenario 1, case 4 (left), scenario 2, case 2 (middle), and scenario 3, case 3 (right).

Training and prediction Multi-ANN

The more complex approach of using several, coupled ANNs requires a different training procedure. First, the 28 hydrodynamic ANNs (H-ANNs) are trained with the time series of the upstream discharge Q^t and downstream water level Z_f^t and the specific riverbed $Z_{b,i}^t$ from the same time step t, and the output is the discharge Q_i^t and water level $Z_{f,i}^t$ at the specific section. Second, each morphological ANN is trained using the following input combinations:

1. $Q_i^t, Z_{f,i}^t, Z_{b,i}^t \rightarrow Z_{b,i}^{t+1}$

2. $Q_i^t, Z_{f,i}^t, Z_{b,i}^t, Z_{b,i}^{t-1} \rightarrow Z_{b,i}^{t+1}$

3. $Q_i^t, Z_{f,i}^t, Z_{b,i}^t, Z_{b,i-1}^t \rightarrow Z_{b,i}^{t+1}$

4. $Q_i^t, Z_{f,i}^t, Z_{b,i}^t, Z_{b,i-1}^t, Z_{b,i}^{t-1} \rightarrow Z_{b,i}^{t+1}$

where i=1:28 and t=1:480. The four combinations of input parameters created not only consists of the spatial and temporal information of the section of interest, i.e. combination 1) but also examines the influence of additional information from the past (t-1) or upstream sections (i-1). Again, the Levenberg-Marquardt training algorithm was applied, and the range for the number of neurons estimated from 4 to 11 applying Equation 6.2. Each combination of the number of neurons for each input parameter configuration was tested 100 times to reduce the influence of the initial weights.

The results of the training are summarised in Table 6.1. It is clear that the difference in the prediction of the discharge increases with the distance from the inlet, which makes sense as the discharge boundary condition is measured at the inlet close to i=1. The water level $Z_{f,i}^t$ prediction does not have this effect;, however, the error is fairly low on average. The overall accuracy of the H-ANN is very good. Each M-ANN performs well and the error is only a few millimeters. It is noteworthy that only the combinations 2 and 4 give the most accurate ANN for each section, which contains information from the past $Z_{b,i}^{t-1}$. No correlation can be observed between the number of neurons and the number of inputs for accuracy, which proves the necessity of the iterative procedure.

The best networks were transferred to the nested structure, which is shown in Figure 6.7 on the right. Despite the fact that the accuracy in training the H-ANNs and the M-ANNs was fairly high, their ability to predict a long time series needs to be tested. In the application process, only the initial riverbed for each section $Z_{b,i}^{t=0}$ is provided together with the entire time series of discharge Q^t and water level Z_f^t at the boundaries. Within a time step, each H-ANN first predicts the flow characteristics of the cross-section at the

Table 6.1: Statistical performance of the Multi-ANN for each cross-section using RMSE.

CROSS-SECTION [i]	Neurons [#]	H-ANN RMSE Q_i [m3/s]	RMSE $Z_{f,i}$ [m]	Combination [/]	M-ANN Neurons [#]	RMSE $Z_{b,i}$ [m]
1	7	0.002	0.031	2	11	0.005
2	7	3.506	0.072	2	10	0.003
3	7	2.339	0.068	4	11	0.003
4	7	2.542	0.060	4	9	0.004
5	7	2.942	0.095	4	10	0.006
6	7	3.268	0.126	4	10	0.006
7	7	3.550	0.092	2	11	0.006
8	6	3.832	0.069	2	11	0.008
9	6	3.873	0.145	2	9	0.004
10	7	4.295	0.059	4	11	0.004
11	7	4.139	0.068	2	8	0.005
12	7	4.380	0.088	2	9	0.004
13	7	5.129	0.072	4	11	0.005
14	7	5.267	0.068	2	9	0.003
15	7	5.333	0.081	2	10	0.006
16	7	5.696	0.073	4	5	0.006
17	7	5.921	0.056	2	9	0.009
18	7	5.433	0.084	2	11	0.007
19	7	6.397	0.118	2	6	0.005
20	7	7.236	0.128	2	10	0.006
21	7	6.102	0.174	2	10	0.007
22	7	7.021	0.177	2	4	0.007
23	7	6.941	0.151	4	7	0.006
24	7	7.132	0.170	4	8	0.007
25	7	7.145	0.271	2	11	0.006
26	7	7.841	0.153	2	11	0.004
27	6	8.303	0.253	2	9	0.004
28	7	8.411	0.108	2	11	0.006

same time step (t), and, second, the M-ANN predicts the riverbed for the next time step (t+1). This output was then used as input for the next time step.

The results of this prediction are visualised in Figures 6.12, 6.13, and 6.14. Only three different cases are visualised here, but the results are representative of the others. Each figure shows the boundary conditions for discharge and flow at the top, and below is the development of five selected sections shown over time (left) and the development of the mean riverbed (right). In the figures, the conventional numerical simulation, the target, is shown as a solid line that is colored in green for the discharge, blue for the water level, and orange for the riverbed. The ANN output is shown as a dashed line. Particular attention is paid to the scaling of the y-axis as this differs from section to section. It can be seen from the three figures that the H-ANN performed very well overall and captured the flow characteristics (free-flowing or ponding). However, the riverbed development differs from the target data. The differences are clearly visible in the figures and do not require any additional statistical performance criteria. It appears that the ANN can reproduce the riverbed development or at least the shape for some cross-sections, but at the same time complete non-physical behavior is observed for others. For example, non-physical means rapid deposition or erosion, even during periods of low flow. There are also some

instabilities and fluctuations for other sections. It is noteworthy, however, that the H-ANN that uses this predicted riverbed as continuous input is still in good agreement with the target flow data.
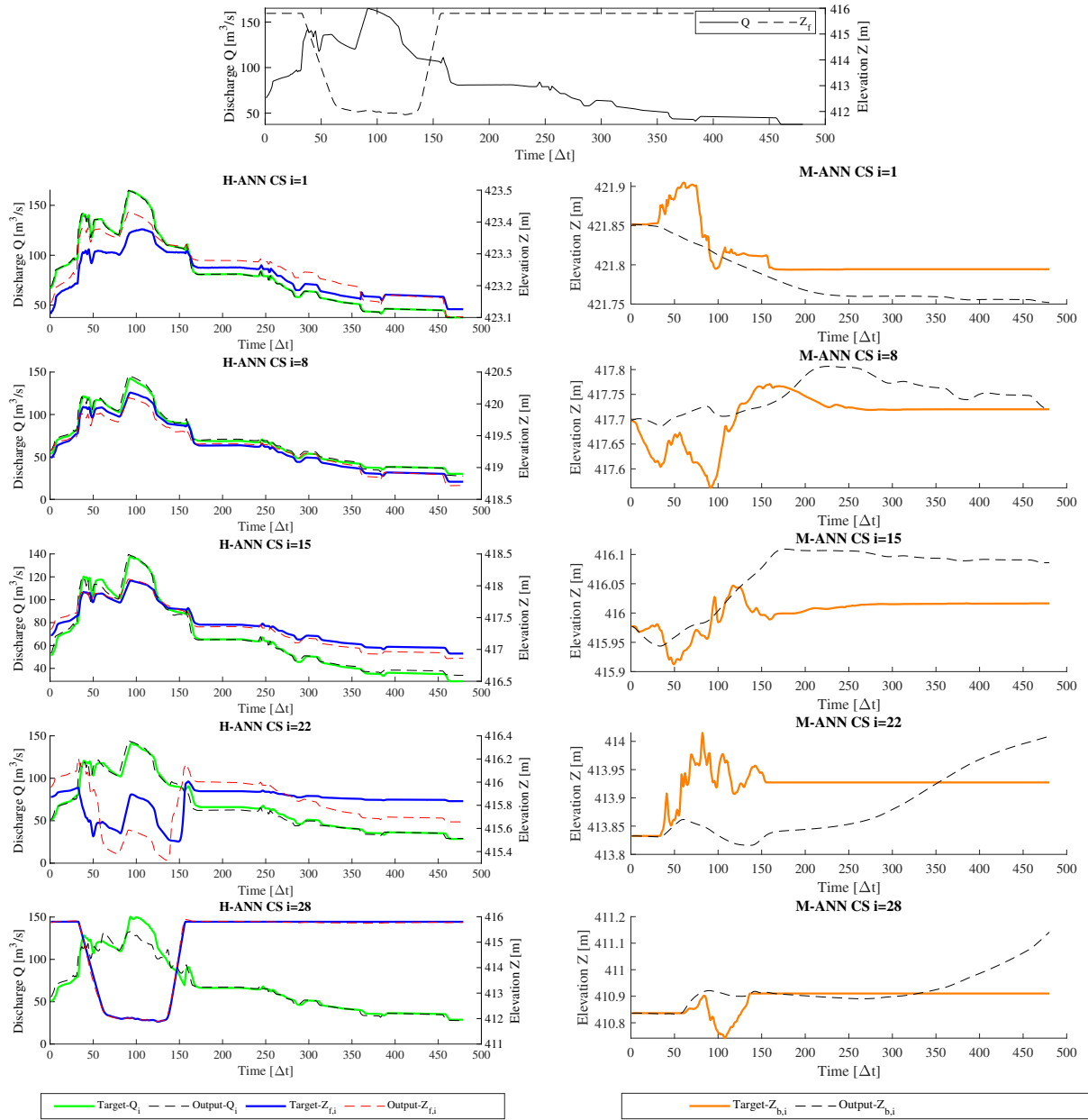
Figure 6.12: Scenario 1, case 4: Predicted time series of Q_i^t and $Z_{f,i}^t$ by the H-ANN (left) and $Z_{b,i}^t$ by the Multi ANN (right).
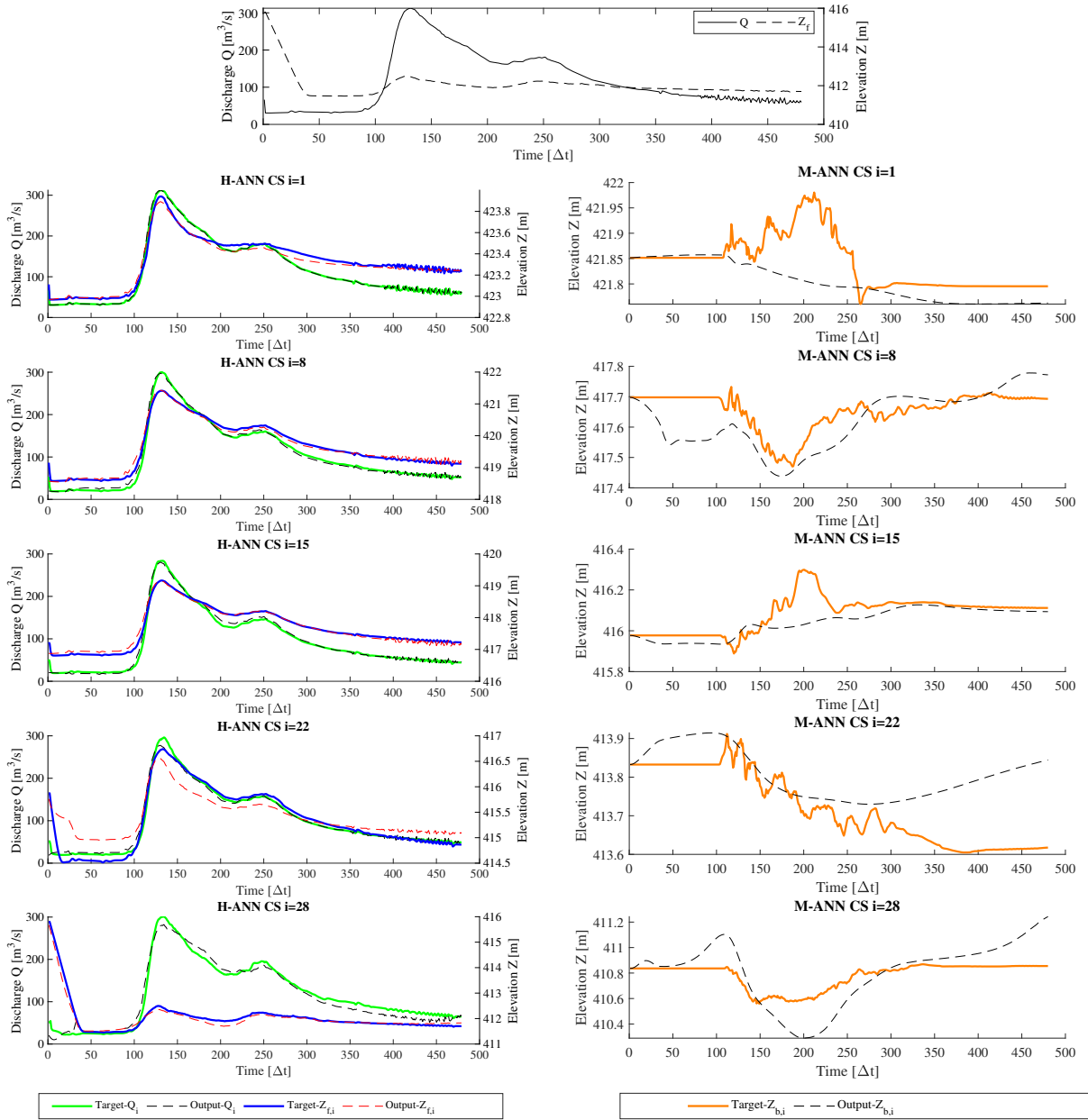
Figure 6.13: Scenario 2, case 2: Predicted time series of Q_i^t and $Z_{f,i}^t$ by the H-ANN (left) and $Z_{b,i}^t$ by the Multi ANN (right).
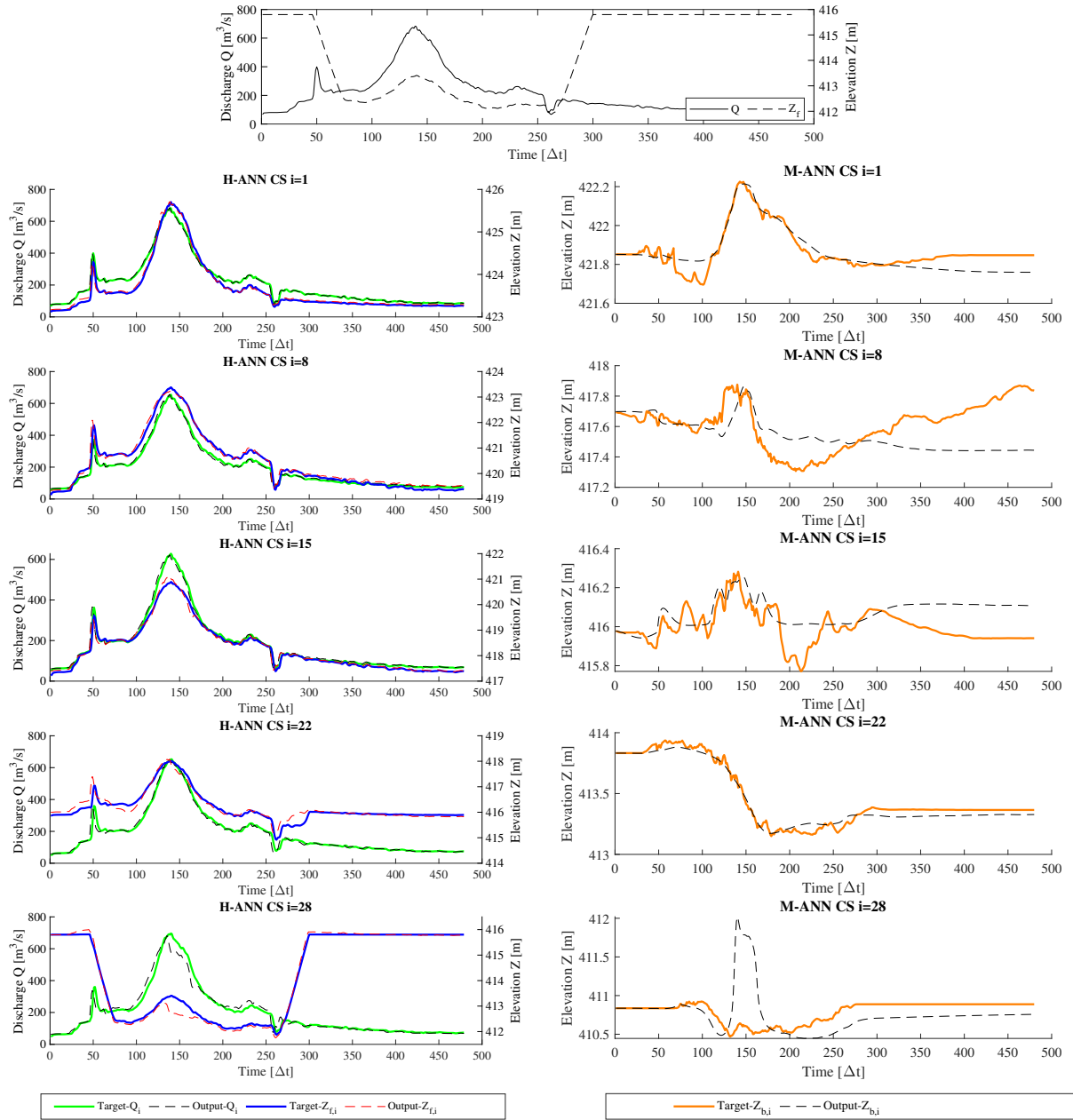
Figure 6.14: Scenario 3, case 3: Predicted time series of Q_i^t and $Z_{f,i}^t$ by the H-ANN (left) and $Z_{b,i}^t$ by the Multi ANN (right).

Discussion

The results show that both approaches - single and multi ANNs - do not provide acceptable results when predicting the riverbed, although the accuracy during training is very high. There may be several reasons for this, which requires further research in this area. One problem is that the error made in predicting one-time step is fed back into the prediction of the next time step and thus accumulates. More complex network architectures such as Long-Short-Term-Memory (LSTM) may be better suited for this type of application. Another critical issue is the conservation of mass, which is not captured in the ANNs. It could be that some important input parameters are missing. It would be worth investigating these issues in future research. One positive aspect of this work is that the prediction of spatial and temporal development of the water level and the discharge along the domain is very good. This might offer valuable information for other tasks or objectives.

6.4   Conclusion

In this chapter, I have presented two different possible applications of ANN for sediment-related issues at the study area. The ANN developed for estimating the volume of flushed sediment provided accurate results. The benefit is clearly in its quick and easy application as only five distinct and measurable inputs are required to approximate the total volume of sediments flushed. The second ANN setup aimed to predict the temporal and spatial development of the riverbed along the study area. The results obtained indicate the direction of this development is promising but needs further improvements before it can be applied in reality.

The first aspects of this work were presented at the 11th RCEM conference and are published in the conference proceedings as:

Reisenbüchler, M.; Bui, M.D.; Rutschmann, P. Development of an ANN-based tool for sediment management at run-of-river reservoirs. 11th River, Coastal and Estuarine Morphodynamics Symposium RCEM 2019; Friedrich, H.; Bryan, K., Eds., 2019, p. 112

Development of an ANN-based tool for sediment management at run-of-river reservoirs

M. Reisenbüchler[1], M.D. Bui[2] and P. Rutschmann[3]

[1] Technical University of Munich, Munich, Germany. markus.reisenbuechler@tum.de
[2] Technical University of Munich, Munich, Germany. bui@tum.de
[3] Technical University of Munich, Munich, Germany. peter.rutschmann@tum.de

1. Introduction

Reservoirs are needed for many fundamental tasks like agriculture, drinking water supply, flood protection, and energy production. For each of the listed demands, sustainable management of the reservoir is of great importance in designing the storage volume of water. However, sedimentation threatens this storage volume worldwide (Schleiss et al., 2016). In addition, a reduced retention volume due to sedimentation might also increase the danger potential of floods (Reisenbüchler et al., 2019).

Numerical models are widely accepted for designing new reservoirs and dams or to develop management strategies at existing dams to counteract sedimentation (Annandale et al., 2016). Such models can accurately represent reality and give reliable predictions. However, accurate and complex (e.g. two- or three-dimensional) models require great computational efforts. Furthermore, achieving an optimal design or evaluating different management strategies requires multiple long-term simulations for different scenarios. In that case, simplified 1D models were still applied. To provide an alternative, our work presents the application of a data-driven method for predicting bed level change along a river section including a hydropower plant.

2. Objective

The study's objective is to develop a data-driven, Artificial-Neural-Network (ANN) to predict future riverbed level changes only based on the available and measurable inputs. This approach can greatly reduce computational cost compared to conventional numerical models, without losing accuracy. Furthermore, the designed network can be considered as an easy-to-use-tool for stakeholders, unlike numerical models.

3. Methodology

This task can be classified as a time series prediction problem, where the future state of a system depends on its previous state and specified input. The training and testing data for the network are obtained from conventional numerical simulations for different flushing operations, see Figure 1. By selecting different, heterogeneous flushing schemes for training, ANN capable of predicting other untrained flushing schemes and the resulting riverbed.

While training the network, a so-called series-parallel or open loop architecture is selected, where the network states are adjusted in a way that the network outputs match the given data, see Figure 2 on the left. Here the external input u(t) contains information regarding the defined flow including the water depth and discharge. The additional input y(t) and output y(t+1) are the riverbed elevation. For further predictions, the best performing network architecture is applied and transferred to a so called
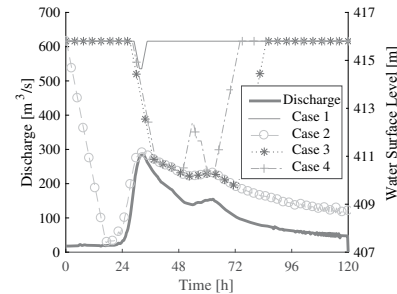

Figure 1. Four tested different flushing schemes during a flood wave.

parallel, or closed loop configuration, on the right side of Figure 2, where the network uses the predicted output y(t+1) as input for the next iteration.
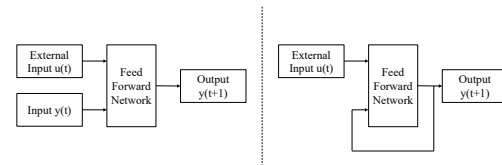

Figure 2. Training in open loop (left) and prediction in closed loop (right) architecture.

4. Conclusions

The proposed ANN-based tool is be a promising alternative to conventional methods for sediment managements at rivers. The advantages of this approach are that it performs with the accuracy of a state-of-the-art 2D hydromorphological model and has low computational requirements, as well as being able to work on standard computers.

References

Annandale, G. W., Morris, G. L., and Karki, P. (2016). *Extending the life of reservoirs : sustainable sediment management for dams and run-of-river hydropower.* Washington, D.C. : World Bank Group.

Reisenbüchler, M., Bui, M. D., Skublics, D., and Rutschmann, P. (2019). An integrative model improves predictive accuracy on floods: Hydromorphological analysis of a flood event in the saalach river. *Science of the Total Environment*, VSI:Effects global change floods.

Schleiss, A. J., Franca, M. J., Juez, C., and De Cesare, G. (2016). Reservoir sedimentation. *Journal of Hydraulic Research*, 54(6):595–614.

Chapter 7

Conclusion and outlook

This thesis reported on efforts to design and improve on existing modelling tools, and proposes methodologies for sustainable sediment management, an issue of global importance. The necessity for sediment modelling was demonstrated in successive steps since there is a deep connection between hydraulics, river engineering, and morphology. In completing this thesis, I would like not only to conclude my findings but also to discuss some possible future research avenues in the field of hydromorphodynamics.

7.1 Conclusion

The thesis and the main findings are summarised in the following:

- Improvement of numerical modelling suite *TELEMAC-SISYPHE*

Fundamental modifications in the open-source morphological module *SISYPHE* provided a more stable, flexible and hence applicable tool for numerical sediment modelling. The suitability and consistency of the modifications were tested against laboratory experiments but also in a complex real case application.

- Analysing the correlation between floods, river engineering works and the morphology

A detailed study on an extraordinary flood event in 2013 in the Alpine Saalach River showed that the morphology had a major impact on the inundation. In addition, the integrative hydromorphological numerical model was able to accurately represent the processes during the flood event, such as reservoir flushing and sedimentation at a structure. This information served as the basis for improved strategy for flood risk and sediment management in this region.

- Integration of a sediment balance approach to a numerical model provides a consistent and accurate modelling approach for real world studies.

Morphological boundary conditions, which are generally uncertain, can be reliable and consistently evaluated using the approach proposed here. The combination of the quantitative sediment balance with a numerical model provides a comprehensive methodology, even in cases with limited data. Finally, a hydromorphological model was precisely calibrated and validated with this approach over a period of several years. The model was able to reproduce measurements of the water level and the riverbed realistically.

- Reservoir flushing could be a suitable management strategy for run-of-river hydropower plants

Sediment management strategies at hydropower plants, and rivers in general, are an important issue worldwide. Using an accurately designed numerical model, reservoir flushing as a management concept was investigated at a run-of-river hydropower plant at the Saalach River. Using this model, an optimised flushing scheme was proposed taking into account flushing duration and intensity. In addition, it was demonstrated that with optimised sediment management offers benefits for flood protection as well.

- Artificial neural network are a powerful extension or alternative to the conventional numerical modelling of morphological processes

It was demonstrated that a simple ANN can accurately predict the total amount of sediment mobilised during a flushing event based on certain discrete inputs. This could be applied as a management tool for reservoir operations. Furthermore, a more complex network, with a time dependent structure, shows promising results in the prediction of riverbed alterations in space and time along a river stretch. A tool such as this could replace conventional numerical models in the future.

7.2   Outlook

The scope of this thesis did not allow the full range of issues involved in sediment modelling to be addressed. In particular, I would like to highlight the following points and research gaps:

- Further extension of *TELEMAC*

Although the *TELEMAC* numerical module is already quite flexible and applicable in research or engineering projects, some important functions are still missing. So far, no sediment transport (suspended or bedload) through or over engineering works (e.g. culverts or weirs) can be modelled. This limits the suitability of the program to section wise

applications, delimited by hydropower plants or dams for instance. A representation of whole river systems at once, therefore, is not possible. Moreover, complex morphological processes such as lateral bank erosion can only be modelled with multiple predefined parameters, which limits the predictive capability.

- Data-driven methods for sediment management

This thesis has shown some of the ways in which ANNs can be combined with conventional numerical models in addressing sediment-related issues. It is clear that there is huge potential in this field, and the results obtained so far could be further improved or extended. It is possible to test alternative network architectures such as Long-Short-Term-Memory (LSTM), which seems more powerful for time-dependent problems such as the prediction of the riverbed development. In addition, the approaches demonstrated concepts could be applied to other river sections to test their overall applicability.

- Reconstruction of an historical river course

Morphological processes have a long response time of several decades. To assess the overall impact of river regulation and the construction of hydropower plants, information on the historical river course is needed, e.g. 100 or even 200 years ago. The reconstruction and study of a river's historical conditions would yield valuable information for the definition of a reference state for floods, morphology, and ecology. There is potential for this within the data from the Bavarian section of the Danube. Historical maps and documentations of floods back to 1800 indicate the river course in natural conditions, with islands and meanders [27]. The first riverbed profiles can be dated back to 1900, with detailed information on the riverbed elevation in some sections. From the construction of the run-of-river hydropower plant chain along the Danube and the tributaries in 1920 onwards, the amount of available data increases. This dataset has a huge potential for detailed analysis and research.

Bibliography

[1] Reisenbüchler, M.; Bui, M.D.; Rutschmann, P. Implementation of a new layer-subroutine for fractional sediment transport in Sisype. Proceedings of the XXIIIrd Telemac-Mascaret User Conference; Bourban, S., Ed.; HR Wallingford Ltd: Wallingford, England, 2016; pp. 215–220.

[2] Reisenbüchler, M.; Bui, M.D.; Skublics, D.; Rutschmann, P. An integrated approach for investigating the correlation between floods and river morphology: A case study of the Saalach River, Germany. *Science of The Total Environment* **2019**, *647*, 814–826, doi:10.1016/j.scitotenv.2018.08.018.

[3] Reisenbüchler, M.; Bui, M.D.; Skublics, D.; Rutschmann, P. Enhancement of a numerical model system for reliably predicting morphological development in the Saalach River. *International Journal of River Basin Management* **2019**, pp. 1–13, doi:10.1080/15715124.2019.1628034.

[4] Reisenbüchler, M.; Bui, M.D.; Skublics, D.; Rutschmann, P. Sediment Management at Run-of-River Reservoirs Using Numerical Modelling. *Water* **2020**, *12*, 249, doi:10.3390/w12010249.

[5] Reisenbüchler, M.; Bui, M.D.; Rutschmann, P. Development of an ANN-based tool for sediment management at run-of-river reservoirs. 11th River, Coastal and Estuarine Morphodynamics Symposium RCEM 2019; Friedrich, H.; Bryan, K., Eds., 2019, p. 112.

[6] Annandale, G.W.; Morris, G.L.; Karki, P. *Extending the life of reservoirs : sustainable sediment management for dams and run-of-river hydropower*; Washington, D.C. : World Bank Group., 2016.

[7] Hervouet, J.M. *Hydrodynamics of Free Surface Flows: Modelling with the finite element method*; John Wiley and Sons: Chichester, England, 2007; pp. 1–341, ISBN. 9780470035580 (ISBN). Cited By :204 Export Date: 30 November 2017 Correspondence Address: Hervouet, J.-M.; Electricité de France (EDF)France.

[8] Ata, R. *Telemac2d User Manual*; Vol. 7.2, EDF: online published, 2017.

[9] Ricci, S.; Piacentini, A.; Weaver, A.; Ata, R.; Goutal, N., Variational data assimilation with telemac. Proof of concept for model state correction on the berre lagoon 3D-model. In *Engineering Geology for Society and Territory*; Lollino G., Manconi A., G.F.C.M.B.P.L.F., Ed.; Springer: Cham, Germany, 2015; Vol. 5, pp. 633–637, ISBN. 9783319090481 (ISBN); 9783319090474 (ISBN). Export Date: 5 December 2017 Correspondence Address: Ricci, S.; Laboratoire National d'Hydraulique et EnvironnementFrance.

[10] Adouin, Y.; Moulinec, C.; Barber, R.; Sunderland, A. Preparing TELEMAC-2D for extremely large simulations. *XVIIIth TELEMAC & MASCARET User Club 2011* **2011**, pp. 41–48.

[11] Moulinec, C.; Andouin, Y.; Sunderland, A. Optimizing TELEMAC-2D for Large-scale Flood Simulations. *Prace Partnership for Advanced Computing in Europe.*

[12] Vittecoq, M.; Gauduin, H.; Oudart, T.; Bertrand, O.; Roche, B.; Guillemain, M.; Boutron, O. Modeling the spread of avian influenza viruses in aquatic reservoirs: A novel hydrodynamic approach applied to the Rhône delta (southern France). *Science of The Total Environment* **2017**, *595*, 787–800, doi:https://doi.org/10.1016/j.scitotenv.2017.03.165.

[13] Capra, H.; Plichard, L.; Bergé, J.; Pella, H.; Ovidio, M.; McNeil, E.; Lamouroux, N. Fish habitat selection in a large hydropeaking river: Strong individual and temporal variations revealed by telemetry. *Sci. Total Environ.* **2017**, *578*, 109–120, doi:https://doi.org/10.1016/j.scitotenv.2016.10.155.

[14] Riesterer, J.; Wenka, T.; Brudy-Zippelius, T.; Nestmann, F. Bed load transport modeling of a secondary flow influenced curved channel with 2D and 3D numerical models. *Journal of Applied Water Engineering and Research* **2016**, *4*, 54–66, doi:10.1080/23249676.2016.1163649.

[15] Wu, W. *Computational river dynamics*; Taylor & Francis: London, 2007; ISBN. 0203938488.

[16] Rijn, L.C.v. Sediment Transport, Part I: Bed Load Transport **1984**. *110*, 1431–1456, doi:doi:10.1061/(ASCE)0733-9429(1984)110:10(1431).

[17] Hunziker, R.P. *Fraktionsweiser Geschiebetransport*; Vol. 11037, Laboratory of Hydraulics, Hydrology and Glaciology (VAW), ETH Zürich: Zürich, Switzerland, 1995; p. 191.

[18] Meyer-Peter, E.; Müller, R. Formulas for bed-load transport. IAHR Congress, Stockholm, appendix 2. IAHR.

[19] Villaret, C.; Hervouet, J.M.; Kopmann, R.; Merkel, U.; Davies, A.G. Morpho-dynamic modeling using the Telemac finite-element system. *Computers & Geosciences* **2013**, *53*, 105–113, doi:https://doi.org/10.1016/j.cageo.2011.10.004.

[20] Janin, J.M.; Lepeintre, F.; Péchon, P., TELEMAC-3D: A Finite Element Code to Solve 3D Free Surface Flow Problems. In *Computer Modelling of Seas and Coastal Regions*; Partridge, P.W., Ed.; Springer Netherlands: Dordrecht, Netherlands, 1992; pp. 489–506, ISBN. 978-94-011-2878-0.

[21] Moulinec, C.; Denis, C.; Pham, C.T.; Rougé, D.; Hervouet, J.M.; Razafindrakoto, E.; Barber, R.W.; Emerson, D.R.; Gu, X.J. TELEMAC: An efficient hydro-dynamics suite for massively parallel architectures. *Computers & Fluids* **2011**, *51*, 30–34, doi:https://doi.org/10.1016/j.compfluid.2011.07.003.

[22] Reisenbüchler, M.; Nguyen, N.D.; Liepert, T.; Bui, M.D.; Rutschmann, P. TELEMAC- A hydrodynamic solver for HPC? *InSiDE* **2018**, *16*, 3.

[23] StMUV. *Hochwasserrisikomanagement-Plan für den bayerischen Anteil der Flussgebietseinheit Donau*; Bavarian State Ministry of the Environment and Consumer Protection: Munich, Germany, 2015; p. 132.

[24] Thieken, A.H.; Kienzler, S.; Kreibich, H.; Kuhlicke, C.; Kunz, M.; Mühr, B.; Müller, M.; Otto, A.; Petrow, T.; Pisi, S.; Schröter, K. Review of the flood risk management system in Germany after the major flood in 2013. *Ecology and Society* **2016**, *21*, 12, doi:http://dx.doi.org/10.5751/ES-08547-210251.

[25] LAWA. *Recommendations for the Establishment of Flood Hazard Maps and Flood Risk Maps*; Vol. 139, German Working Group on Water Issues of the Federal States and the Federal Government: Dresden, Germany, 2010.

[26] LAWA. *Recommendation for the Establishment of Flood Risk Management Plans*; Vol. 139, German Working Group on Water Issues of the Federal States and the Federal Government (LAWA): Dresden, Germany, 2010.

[27] Skublics, D.; Blöschl, G.; Rutschmann, P. Effect of river training on flood reten-
tion of the Bavarian Danube. *Journal of Hydrology and Hydromechanics* **2016**,
64, 349–356, doi:https://doi.org/10.1515/johh-2016-0035.

[28] Günter, A. *Die kritische mittlere Sohlenschubspannung bei Geschiebemischungen
unter Berücksichtigung der Deckschichtbildung und der turbulenzbedingten Sohlen-
schubspannungsschwankungen*; City-Druck AG, Zürich, 1971.

[29] Ateeq-Ur-Rehman, S.; Bui, M.; Rutschmann, P. Variability and Trend Detec-
tion in the Sediment Load of the Upper Indus River. *Water* **2018**, *10*, 16,
doi:https://doi.org/10.3390/w10010016.

[30] Bui, M.D.; Kaveh, K.; Penz, P.; Rutschmann, P. Contraction scour estimation
using data-driven methods. *Journal of Applied Water Engineering and Research*
2015, *3*, 143–156, doi:10.1080/23249676.2015.1051141.

[31] Kaveh, K.; Bui, M.D.; Rutschmann, P. A new approach for morphodynamic
modeling using integrating ensembles of artificial neural networks. Wasserbau –
mehr als Bauen im Wasser. Proceedings of the 18th symposium of TU Munich,
TU Graz and ETH Zurich; Huber, R., Ed. Rutschmann, Peter, Vol. 134, pp.
304–315, ISBN. 978-3-940476-10-3.

[32] Haykin, S.S. *Neural networks : a comprehensive foundation : solutions manual*;
Macmillan College Publishing Company: [New York?], 1994; ISBN. 0023527625
9780023527623.

[33] Haykin, S.; Haykin, S. *Neural Networks and Learning Machines*; Pearson Educa-
tion, Inc, 2009; ISBN. 9780131471399.

[34] Kaveh, K. Development of Data Driven Models for Hydromorphology and Sedi-
ment Transport. Dissertation, Technische Universität München, München, 2019.

[35] Moriasi, D.N.; Arnold, J.G.; Van Liew, M.W.; Bingner, R.L.; Harmel, R.D.; Veith,
T.L. Model evaluation guidelines for systematic quantification of accuracy in wa-
tershed simulations. *Transactions of the American Society of Agricultural and Bi-
ological Engineers* **2007**, *50*, 885–900, doi:http://dx.doi.org/10.13031/2013.23153.

[36] Jothiprakash, V.; Garg, V. Reservoir Sedimentation Estimation Using Artifi-
cial Neural Network. *Journal of Hydrologic Engineering* **2009**, *14*, 1035–1040,
doi:doi:10.1061/(ASCE)HE.1943-5584.0000075.

[37] Li, X.; Qiu, J.; Shang, Q.; Li, F. Simulation of Reservoir Sediment Flushing of the Three Gorges Reservoir Using an Artificial Neural Network **2016**. *6*, 148.

[38] Ateeq-Ur-Rehman, S. *Numerical Modeling of Sediment Transport in Dasu-Tarbela Reservoir using Neural Networks and TELEMAC Model System*; Technische Universität München: München, 2019.

[39] Shahin, M.A.; Maier, H.R.; Jaksa, M.B. Predicting Settlement of Shallow Foundations using Neural Networks. *Journal of Geotechnical and Geoenvironmental Engineering* **2002**, *128*, 785–793, doi:doi:10.1061/(ASCE)1090-0241(2002)128:9(785).